International Journal of Mechanical Sciences

Effect of state-dependent time delay on dynamics of trimming of thin-walled structures

--Manuscript Draft--

Manuscript Number:	SUBMIT2IJMS-D-22-00613R1
Article Type:	Research Paper
Section/Category:	Manufacturing
Keywords:	Milling; Thin-walled workpiece; trimming; state-dependent time delay; Dynamic Stability; bifurcations
Corresponding Author:	Tao Huang, Ph.D Huazhong University of Science and Technology Wuhan, Hubei CHINA
First Author:	Sen-Lin Ma
Order of Authors:	Sen-Lin Ma
	Tao Huang, Ph.D
	Xiao-Ming Zhang
	Marian Wiercigroch
	Ding Chen
	Han Ding
Abstract:	Trimming of cantilever thin-walled structures is commonly seen in aerospace industry, including trimming of blades. Trimming with helix angle tools can cause the vibration of the thin-walled workpiece along the tool-axis, which may disturb the time delay between cutting by the current and previous teeth. The time delay dependent on the vibration state makes the stability analysis of trimming process challenging. This paper is the first attempt to uncover the effect of state-dependent time delay of the trimming process caused by workpiece vibration on chatter stability. Modeling of the cutter-workpiece interactions, state-dependent time delay and the dynamic chip generation mechanism are presented. A time-domain numerical algorithm with an improved stability is constructed to analyze the trimming stability behaviors. We found that the two states exist in the process: period-n instabilities with time-varying time delay and stability status with constant time delay. A focused experimental study was carried out to verify this new finding. This study reveals the way the workpiece vibration affects the time delay and stability in the trimming process, which promotes the understanding of the dynamics of thin-walled workpiece trimming process.
Response to Reviewers:	

Effect of state-dependent time delay on dynamics of trimming of thin-walled structures

Sen-Lin Ma[1, 2], Tao Huang[1 *], Xiao-Ming Zhang[1], Marian Wiercigroch[3], Ding Chen[1], Han Ding[1]

[1]State Key Laboratory of Digital Manufacturing Equipment and Technology, School of Mechanical Science and Engineering, Huazhong University of Science and Technology, Wuhan 430074, China

[2]Institute of Artificial Intelligence, Huazhong University of Science and Technology, Wuhan 430074, China

[3]Centre for Applied Dynamics Research, School of Engineering, University of Aberdeen, Kings College Aberdeen AB24 3UE, Scotland, UK

Abstract: Trimming of cantilever thin-walled structures is commonly seen in aerospace industry, including trimming of blades. Trimming with helix angle tools can cause the vibration of the thin-walled workpiece along the tool-axis, which may disturb the time delay between cutting by the current and previous teeth. The time delay dependent on the vibration state makes the stability analysis of trimming process challenging. This paper is the first attempt to uncover the effect of state-dependent time delay of the trimming process caused by workpiece vibration on chatter stability. Modeling of the cutter-workpiece interactions, state-dependent time delay and the dynamic chip generation mechanism are presented. A time-domain numerical algorithm with an improved stability metrics is constructed to analyze the trimming stability behaviors. We found that the two dominant states can occur, namely, period-n instabilities with time-varying time delay and stability with constant time delay. A focused experimental study was carried out to calibrate this new finding. This study reveals the way the workpiece vibration affects the time delay and stability in the trimming process.

Keywords: milling, thin-walled workpiece, trimming, state-dependent time delay, dynamic stability, bifurcations.

1 Introduction

Trimming of cantilever shape thin-walled workpieces is an important machining operation in aerospace, which has attracted a lot of attention in the recent years, e.g. [1-3]. Trimming is a special kind of milling operation, where a workpiece is clamped at one end forming a cantilever which edge is being milled. Traditional milling of thin-walled structures make walls thinner, while trimming

* Corresponding author: Tao Huang (tao.huang@hust.edu.cn)

make them shorter. Due to large flexibility of thin-walled structures, machining vibration in trimming processes is the key issue affecting machining efficiency and surface finish quality. In typical trimming operations of cantilever shaped thin-walled workpieces, generated vibration are large, which affect nominal cutter-workpiece engagements and they cannot be neglected like in other more traditional milling operations. Before embarking on modeling and analysis of trimming processes, related studies are critically reviewed in this section.

Chatter caused by regenerative effects may result in violent vibration, poor surface finish, lower tool life, and other negative effects. Therefore, it is of a great significance to avoid chatter for achieving high machining quality [4-9]. Constructing stability lobe diagrams is a low-cost way to acquire optimal machining parameters, where the frequency domain analytical methods [10, 11], time-domain semi-analytical methods [12-17] and time-domain numerical simulation methods [18-24] are popular methods. For strongly nonlinear coupling models which cannot be linearized, the time domain simulation method is often the only choice, but its high computational cost is prohibitive.

An accurate dynamic model is the key step for the chatter stability analysis. Classical dynamic models [25-30] consider geometric and kinematic relationships between the tool and the workpiece when describing cutter-workpiece engagement conditions, including start and exit immersion angles, instantaneous rotation angle of cutting element and instantaneous uncut chip thickness. For complex cases with tool runout and irregular geometry tool, although the cutter-workpiece engagement conditions are different for each tooth, cutter-workpiece engagement formulations in these models are still state-independent, which can be calculated without knowing the system vibration state. For example, Yusoff *et al.* [31] analyzed variable helix angle tool and introduced an optimisation algorithm to design variable helix angles to suppress chatter. Dombovari *et al.* [32] summarized cutting performance of non-uniform and harmonically varied helix cutters in case of high and low cutting speed conditions. Based on tooth trochoid motion, Zhang *et al.* [33] analyzed the milling stability by taking cutter runout into account. Niu *et al.* [34] obtained expressions of cutter-workpiece engagement of variable pitch and variable helix tools by taking tool runout into account. Zhan *et al.* [35] presented the dynamic model of five-axis ball-end tool with variable pitches. Recently, the dynamic stability of the serrated milling tool was analyzed by Farahani *et al.* [36] and Bari *et al.* [37]. The geometry of crest cut tool was modeled by Tehranizadeh *et al.* [38] and five-axis bull-nose end milling was modeled by Tang *et al.* [39].

For thin-walled workpiece milling, due to high flexibility and relatively small cutting parameters, the workpiece vibration amplitude is comparable to the nominal chip thickness. Therefore, the effect of cutting system vibration should be taken into account in side milling of thin-walled workpieces. Campomanes *et al.* [23] established a time-domain model to simulate dynamic milling at a very small radial cutting width. In their model, the exact trochoidal motion of the cutter was described by discretized cutter-workpiece kinematics and dynamics expressions, and the effects of changing radial cutting width caused by forced vibrations on chatter stability were investigated. Li *et al.* [40] analyzed the surface form errors caused by vibration of both flexible tool and workpiece in five-axis flank milling of thin-walled parts, where the time-varying stiffness of workpiece caused by material removal was also taken into account. Sun *et al.* [41] analyzed the effects of force-induced deformation calculated by the static stiffness on cutter-workpiece engagement. They found that the actual cutting width and cutting immersion angles deviate from the nominal values a lot and consequently the stability limits are changed. Totis *et al.* [42] developed a new model which considered the coupling relationship between cutting vibrations and cutter-workpiece engagement when the amplitude of steady-state vibrations is comparable to the instantaneous uncut chip thickness, but the linearization method was used to obtain the instantaneous uncut chip thickness rather than establishing the true coupling relationship formulae. Recently, Niu *el al.* [43] obtained the implicit cutter-workpiece engagement formulae by analyzing the teeth trajectories which are composed of cutting vibration, tool rotation and feed movement. In these literatures, the focuses are on the influence of cutting vibration along the tool radial direction on cutter-workpiece engagement. However, in trimming process of thin-walled parts, the engagement of cutter-workpiece is affected by the workpiece vibration along the tool axis. Therefore, not only the time delay but also the instantaneous rotation angle become state-dependent. This problem is yet to be investigated.

In addition to cutter-workpiece engagement, time delay in milling process plays a crucial role in dynamical stability, many studies have been conducted on variable time delay dynamic models. Song et al. [44] proposed an approach to design variable pitch tools with high milling stability based on a generalized expression of tooth engagement factor. Sellmeier and Denkena [45] observed the stable islands in the stability charts of unequally pitched end mills. Wan *et al.* [46] analyzed the characteristics of multiple delays in milling process by considering the effects of variable tooth pitch angle and tool runout. Comak and Budak [47] proposed an accurate design method for optimal selection of pitch angles to maximize chatter free material removal rate of variable pitch tools. Hayasaka *et al.* [48] presented a generalized design method for selection of highly-varied-helix end mills to suppress the regenerative chatter. Otto *et al.* [49] studied mechanical vibration in milling with non-uniform pitch and variable helix tools considering different factors (e.g., the nonlinear cutting force behaviour, the effect of runout et al.). Recently, Jiang *et al.* [50] analyzed the variable-pitch/helix milling process considering axially varying dynamics by taking cutter runout offset and tilt into account. These studies were conducted based on changing tool geometric parameters, time delay is generally proportional to the flute angles of milling tools and keeps discrete constant under a fixed spindle speed. For variable spindle speed milling, triangle-wave [51], sine-wave [52, 53], random [54, 55], and saw-tooth [56] are used to modulate spindle speed. Seguy *et al.* [51] analyzed the effect of spindle speed variation in the high spindle speeds domain and found that a variable spindle speed can effectively suppress period-doubling bifurcations and have no effect on Hopf bifurcations. Sastry *et al.* [52] analyzed the stability of the variable speed face milling based on the Floquent theory, and the milling chatter was effectively suppressed at low spindle speeds. Different methods, such as frequency-domain and time-domain discretization, were used to analyze the effect of variable speed on milling stability [55-57]. Wang *et al.* [58] adopted a multi-harmonic spindle speed variation to suppress milling chatter and the genetic algorithm is used to select optimal parameters. Although time delay is variable in the above models, it is regarded as a state-independent parameter. Even for trochoid tool path [59, 60] or the turn-milling operations [61], time delay is periodic time-varying, but not related to the system state. Few studies have been covered on state-dependent dynamic models. For example, Insperger *et al.* [62] modeled the state-dependent regenerative time delay in two degrees of freedom milling process. Latter, Bachrathy *et al.* [63] further proposed a comprehensive model which considers the effect of self-excited vibration of the milling tool and trochoidal path of the cutting edges on time delay, and they used a shooting method to analyze the nonlinear dynamic equations. Recently, Niu *et al.* [43] used numerical algorithms to analyze the stability and surface location error of milling thin-walled workpieces considering effects of cutting vibration, feed movement, tool rotation and tool runout on time delay.

Due to vibration induced time delay, dynamics of trimming is very different from dynamics of traditional milling processes. Time delay becomes state-dependent and is related to the workpiece vibration directly. In addition, the existing literature on trimming thin-walled workpiece mainly focuses on reducing the workpiece vibration amplitude. For example, Liu *et al.* [2] optimized the tool inclination angle based on an analytical 3D forces model to decrease the machined surface roughness and the vibration amplification in the side tilt milling of edges of thin-walled workpieces. They experimentally investigated the influence of tool helix angle and tilt angle on surface quality on the workpiece in trimming process [3]. Wan *et al.* [1] suppressed the vibration in trimming process of the plate-like workpiece by additional dynamic vibration absorbers (DVA) and they also optimized the location of DVA on the workpiece.

Simultaneous effects of state-dependent and time delays caused by workpiece vibration have not been yet comprehensively modelled and analyzed, which is the main aim of this work. Specifically, we develop here a novel dynamic model of trimming thin-walled cantilever plates by considering the effect of workpiece vibration along the tool axis on time delay and instantaneous rotation angle. Mechanisms explaining tool-workpiece interactions, state-dependent time delay and the dynamic chip generation will be discussed. Trimming stability will be investigated by computing and comparing stability lobe diagrams for mathematical models having various degree of complexity and fidelity including the developed here time-domain numerical algorithm with an improved stability metrics.

The remainder of the paper is structured as follows. In Section 2, a novel mathematical model to describe dynamics of thin-walled workpiece trimming is developed. Then in Section 3, the effects of state-dependent instantaneous rotation angle and time delay on trimming stability are modelled, where time delay is calculated by an iterative method and the time-domain numerical algorithm with improved stability metrics is proposed to analyze the trimming stability behaviors. In Section 4, simulation results and experimental validations are presented. Finally, some conclusions are drawn in Section 5.

2 State-dependent dynamic model of trimming

Trimming with helix angle tools can cause vibration of the thin-walled workpiece along the tool-axis, which may disturb the time delay between cutting by the current and previous teeth. In this section, we aim to construct the state-dependent dynamic model of trimming of thin-walled structures for further investigations of the effect of state-dependent time delay. First, the dynamic interactions between the tool and the workpiece are analyzed. Then, the expressions of state-dependent parameters such as instantaneous rotation angle, chip thickness and time delay are obtained. Last, the stability prediction method with an improved metrics in time-domain is proposed to investigate stability lobes.

A typical example of trimming is a compressor blade top cutting as shown in Figure 1 together with its physical model. For convenience of analysis, the structure is simplified to a cantilever thin-walled plate, which is depicted in Figure 1(b). To mathematically describe the process, a Cartesian coordinate system is used where X-axis and Z-axis are in the directions of feed and tool-axis, respectively, and Y-axis satisfies the right-hand rule. Four simplifying assumptions are adopted in the modelling:

(i) Only dynamics of the tool in X and Y-directions and the workpiece in Z-direction are considered as other directions are significantly stiffer.

(ii) Interactions during the cutting process are strongly nonlinear especially when the tool makes intermittent contacts with the workpiece. In this study we assume that the tool does not loose contact with the workpiece.

(iii) Effects of material removal on modal parameters are neglected hence the modal parameters of the dynamic system are assumed to be constant during cutting.

(iv) In trimming the width of cut is constant.

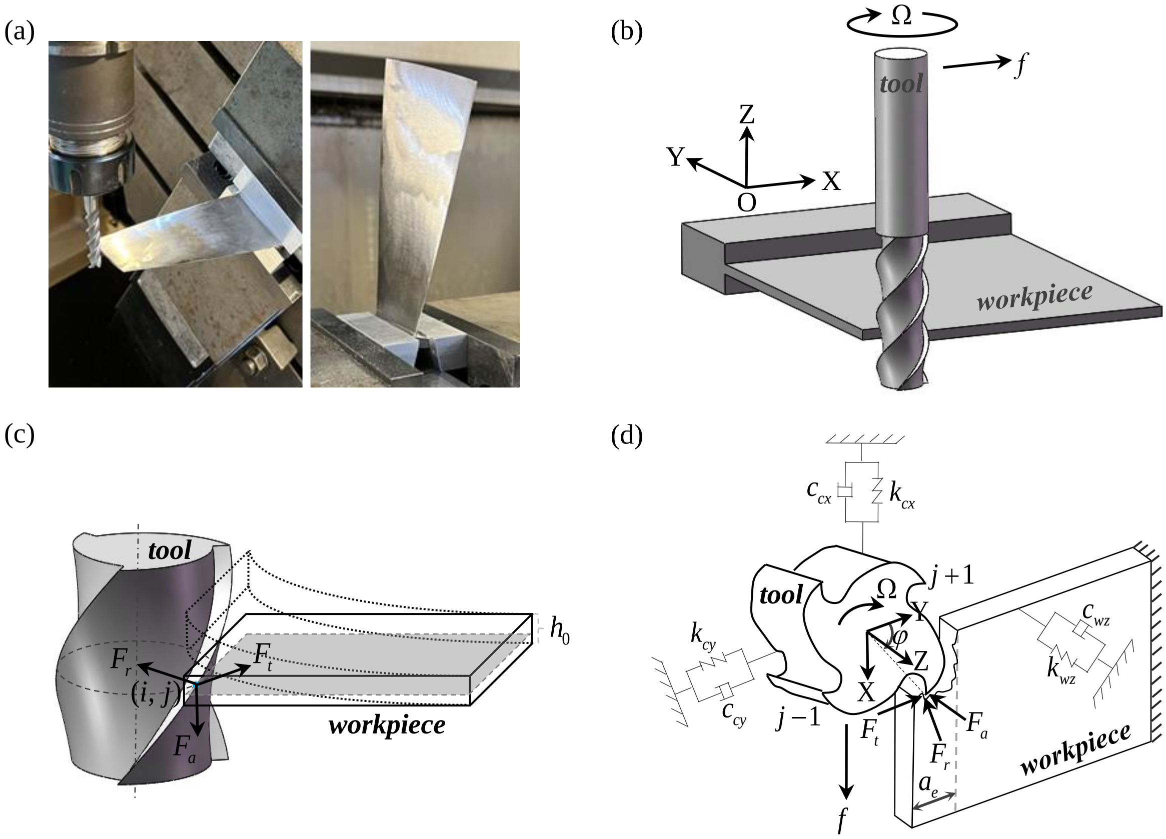

Figure 1. Dynamic interactions between the tool and the workpiece in trimming of thin-walled structures; (a) a typical example of trimming a compressor blade; (b) kinematics of the process; (c) cutting forces generated during the process; (d) physical model of the process where the tool and the workpiece supported three Kelvin-Voight pairs in *X*, *Y* and *Z* directions. To analyze the cutting forces of the tool, the workpiece is discretized into N_A number of slices along the *Z*-direction and the ***i***-th element of the workpiece is depicted by shaded area. The direction of the cutting forces on the tool, i.e. tangential F_t, radial F_r and axial F_a, components (i, j) are shown, where (i, j) represents the contact parts of the ***j***-th tooth and the ***i***-th element of the workpiece. One state of the workpiece vibration along the *Z*-direction is described by dashed lines.

The dynamic interactions occurring during the process can be derived from the Newton's second law, which in the fully nonlinear case can be represented in the matrix form using the generalized co-ordinates $\mathbf{q}$ as

$$\mathbf{M}(\mathbf{q})\ddot{\mathbf{q}}+\mathbf{C}(\mathbf{q})\dot{\mathbf{q}}+\mathbf{K}(\mathbf{q})\mathbf{q}=\mathbf{F}(\mathbf{q},\dot{\mathbf{q}}), \tag{1}$$

which after applying the simplifying assumptions (i) – (iv) can be reduced to its linearized matrix form given below:

$$\mathbf{M}\ddot{\mathbf{q}}+\mathbf{C}\dot{\mathbf{q}}+\mathbf{K}\mathbf{q}=\mathbf{F}(\mathbf{q},\dot{\mathbf{q}}). \tag{2}$$

Assuming that the nonlinear force, $\mathbf{F}(\mathbf{q},\dot{\mathbf{q}})$, for the steady state milling is a periodic function of time, $\mathbf{F}(t)=\mathbf{F}(t+T_r)$, is governed by the rotation speed of the tool with period T_r, the dynamics of the trimming process can be described in the familiar form for the manufacturing community by Eq. (3)

$$\mathbf{M}\ddot{\mathbf{q}}(t)+\mathbf{C}\dot{\mathbf{q}}(t)+\mathbf{K}\mathbf{q}(t)=\mathbf{F}(t), \tag{3}$$

where $\mathbf{M}=diag(m_{cx} \quad m_{cy} \quad m_{wz})$, $\mathbf{C}=diag(c_{cx} \quad c_{cy} \quad c_{wz})$ and $\mathbf{K}=diag\left(k_{cx} \quad k_{cy} \quad k_{wz}\right)$ are modal mass, damping and stiffness matrices, respectively, where the subscript c and w represent tool and workpiece, respectively. $\ddot{\mathbf{q}}(t)=[\ddot{x}_c(t) \quad \ddot{y}_c(t) \quad \ddot{z}_w(t)]^T$, $\dot{\mathbf{q}}(t)=[\dot{x}_c(t) \quad \dot{y}_c(t) \quad \dot{z}_w(t)]^T$ and $\mathbf{q}(t)=[x_c(t) \quad y_c(t) \quad z_w(t)-z_0-h_0/2]^T$ are the relative acceleration, velocity and displacement vectors between the tool and the workpiece at the time t, and $x_c(0)=0$, $y_c(0)=0$, $z_w(0)=z_0+h_0/2$, where z_0 is the distance between the workpiece bottom and the tool bottom at the initial time and h_0 is the thickness of the workpiece. $\mathbf{F}(t)=[F_x(t) \quad F_y(t) \quad -F_z(t)]^T$ is the force vector at the time t, $F_x(t)$, $F_y(t)$ and $F_z(t)$ are the cutting forces acting on the tool. Eq. (3) is nonlinear due to the cutting force and will be modeled in detail later on.

According to [64, 65], the milling process with helical angle cutters can be modeled as the simultaneous processes of cutting with a number of single-point cuts. In Figure 1(c), the workpiece is discretized into N_A number of slices along the *Z*-axis. Each slice are treated as single point oblique cutting which has an inclination angle of β (helix angle of the tool). The tangential force $F_t(t,i,j)$, radial force $F_r(t,i,j)$ and axial force $F_a(t,i,j)$ on cutting element ($i=1$, $j=1$) at time t are calculated as follow:

$$\begin{bmatrix} F_t(t,i,j) \\ F_r(t,i,j) \\ F_a(t,i,j) \end{bmatrix} = \left\{ \begin{bmatrix} K_t \\ K_r \\ K_a \end{bmatrix} h(t,i,j) + \begin{bmatrix} K_{te} \\ K_{re} \\ K_{ae} \end{bmatrix} \right\} \Delta a, \tag{4}$$

where $\Delta a = h_0 / N_A$ is the cutting depth of each slice; N_A denotes the number of axial discretization slices of the contact parts ($i=1,\cdots,N_A$) and N denotes the number of teeth ($j=1,\cdots,N$); $h(t,i,j)$ is the chip thickness of cutting element (i, j) at time t; and K_t, K_{te}, K_r, K_{re}, K_a, K_{ae} are the cutting force coefficients and edge force coefficients of tangential, radial and axial, respectively.

As shown in Figure 1(d), the milling resultant force in the *X*, *Y*, and *Z*-directions at time *t* can be expressed from the tangential, radial, and axial elemental forces and is shown as follow:

$$\begin{bmatrix} F_x(t) \\ F_y(t) \\ F_z(t) \end{bmatrix} = \sum_{i=1}^{N_A}\sum_{j=1}^{N} \left\{ g\left(\varphi_{t,i,j}\right) \begin{bmatrix} -\cos\left(\varphi_{t,i,j}\right) & -\sin\left(\varphi_{t,i,j}\right) & 0 \\ \sin\left(\varphi_{t,i,j}\right) & -\cos\left(\varphi_{t,i,j}\right) & 0 \\ 0 & 0 & 1 \end{bmatrix} \begin{bmatrix} F_t(t,i,j) \\ F_r(t,i,j) \\ F_a(t,i,j) \end{bmatrix} \right\}, \tag{5}$$

$$g\left(\varphi_{t,i,j}\right) = \begin{cases} 1 & \left(\text{if } \varphi_{st} < \operatorname{mod}\left(\varphi_{t,i,j},\ 2\pi\right) < \varphi_{ex}\right) \\ 0 & (\text{otherwise}) \end{cases}, \tag{6}$$

$$\begin{cases} \varphi_{st} = \arccos\left(\frac{2a_e}{D} - 1\right),\ \varphi_{ex} = \pi\ (down\ milling) \\ \varphi_{st} = 0,\ \varphi_{ex} = \arccos\left(1 - \frac{2a_e}{D}\right)\ (up\ milling) \end{cases}, \quad (7)$$

where the $g\left(\varphi_{t,i,j}\right)$ is a switch function to determine whether the infinitesimal cutting flute is involved in cutting or not. $\varphi_{t,i,j}$ is the instantaneous rotation angle of the cutting element (i, j) at time t. The start angle and the exit angle are φ_{st}, φ_{ex} respectively. a_e is width of cut, and D is the diameter of the tool.

3 Instantaneous rotation angle, chip thickness and time delay

Due to the large overhang of the workpiece, the stiffness of the workpiece is very low (refer to Table 1). Compared with the common vibration magnitude ranging from a few micrometers to tens of micrometers, the vibration amplitude of the workpiece in such trimming process could reach several millimeters, which is comparable to the workpiece thickness. In such case, the effect of workpiece vibration on the cutter-workpiece engagement needs to be taken into consideration.

In Figure 2(a), the motion track of the workpiece along the *Z*-direction at different times is illustrated where the positions of the workpiece at time t_0, t_1 and t_2 are also depicted. The location of the workpiece along the *Z*-direction is changing over time so that the cutter-workpiece engagement area becomes state-dependent. For a milling tool with N number of tooth rotating at spindle speed Ω rpm (revolution per minute), the instantaneous rotation angle of cutting element (i, j) at time t can be expressed as follow:

$$\varphi_{t,i,j} = \frac{2\pi\Omega}{60}t + \frac{(j-1)2\pi}{N} - \frac{2\tan\beta}{D}\left(z_w(t) - \frac{h_0}{2} + (i-1)\Delta a\right). \quad (8)$$

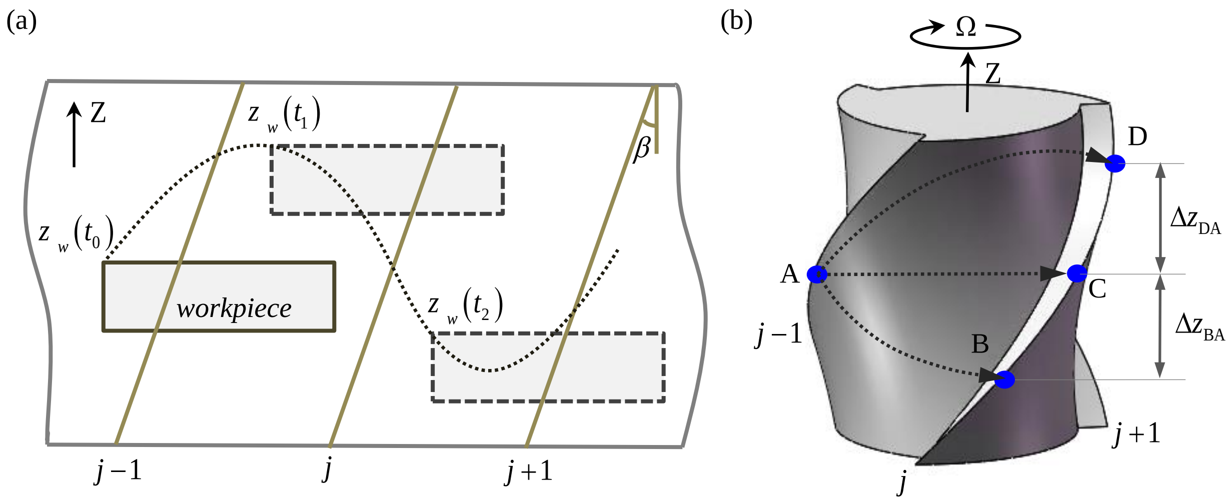

Figure 2. State-dependent instantaneous rotation angle $\varphi_{t,i,j}$ and time delay $\tau(t)$; (a) The tool circumference is expanded where a schematic diagram showing the vibration track of the workpiece along the *Z*-direction and the positions of the workpiece at three different times is presented. Due to the workpiece vibration, the contact parts of workpiece and tool along the *Z*-direction is time-varying. (b) Set point A as the cutting element (i, $j-1$), due to the workpiece vibration, the corresponding cutting element (i, j) may be point B, C or D. Thus, the time interval between the current and previous teeth is changed, which means time delay is state-dependent and time-varying.

The instantaneous uncut chip thickness at the time t consists of two parts, i.e., the static part contributed by the feed motion and the dynamic part by the vibration of the tool, respectively. The variable uncut chip thickness can be expressed as follow:

$$h(t,i,j) = f\tau(t)\sin(\varphi_{t,i,j}) + \begin{bmatrix}\sin(\varphi_{t,i,j}) & \cos(\varphi_{t,i,j})\end{bmatrix}\begin{bmatrix} x_c(t) - x_c(t-\tau(t)) \\ y_c(t) - y_c(t-\tau(t))\end{bmatrix}, \quad (9)$$

where f is the feed rate, $\tau(t)$ is the time delay between the current and previous teeth at time t; $x_c(t-\tau(t))$, $y_c(t-\tau(t))$ are the tool vibrations in *X*, *Y*-directions at time $t-\tau(t)$, respectively.

Although the expression of the chip thickness $h(t,i,j)$ has been obtained from Eq. (9), the time delay $\tau(t)$ remains undetermined. In Figure 2(b), set point A as the cutting element (i, j−1), if the vibration of the workpiece in *Z*-direction is neglected, the cutting element (i, j) is C, and the time delay is equal to tooth period T. However, when the workpiece vibration in *Z*-direction is considered, the cutting element (i, j) may be B, C or D, and the time interval between the current and previous teeth is changed. Thus, the time delay $\tau(t)$ may decrease, increase or remain unchanged. The state-dependent time delay can be modeled by Eq. (10) as shown below:

$$\begin{cases} \Delta z_w(t) = z_w(t) - z_w(t-\tau(t)) \\ \Delta\varphi(t) = \dfrac{2\tan\beta}{D}\Delta z_w(t) \\ \tau(t) = T + \dfrac{\Delta\varphi(t)}{2\pi}TN \end{cases}, \tag{10}$$

where $\Delta z_w(t)$ is the regenerative vibration of the workpiece, $\Delta\varphi(t)$ is the rotation angle variation between previous and current teeth caused by the workpiece vibration. According to Eq. (10), the time delay $\tau(t)$ can be rewritten as follow:

$$\tau(t) = T + \frac{2\tan\beta}{D}\left(z_w(t) - z_w(t-\tau(t))\right)\frac{TN}{2\pi}. \tag{11}$$

Substituting Eq. (11) into Eq. (9), the expression of chip thickness $h(t,i,j)$ can be rewritten as follow:

$$\begin{cases} f_t' = f_t\left(1 + \left(z_w(t) - z_w(t-\tau(t))\right)\dfrac{N\tan\beta}{\pi D}\right) \\ h(t,i,j) = f_t'\sin(\varphi_{t,i,j}) + \left[\sin(\varphi_{t,i,j}) \quad \cos(\varphi_{t,i,j})\right]\begin{bmatrix} x_c(t) - x_c(t-\tau(t)) \\ y_c(t) - y_c(t-\tau(t)) \end{bmatrix} \end{cases}, \tag{12}$$

where f_t is the nominal feed per tooth, f_t' is the actual feed per tooth. From Eq. (11), we can conclude that time delay depends not only on process parameters and tool geometry, but also on the vibration state. Moreover, time delay in trimming model is related to the regenerate effect of the workpiece vibration. The expression of the time delay, Eq. (11), is implicit so that we propose to calculate it by an iterative method. And from Eq. (12), due to the effect of time-varying time delay, the actual feed per tooth is not equal to the nominal feed per tooth f_t, and it is also changing due to the regenerate effect of the workpiece vibration.

To compute complex and interwoven nonlinear relationships between chip thicknesses and generated cutting forces, dynamical responses and time delay need to be evaluated in the sequence shown in Figure 3. This demonstrates that time delay is state-dependent, and can also affect the dynamic response.

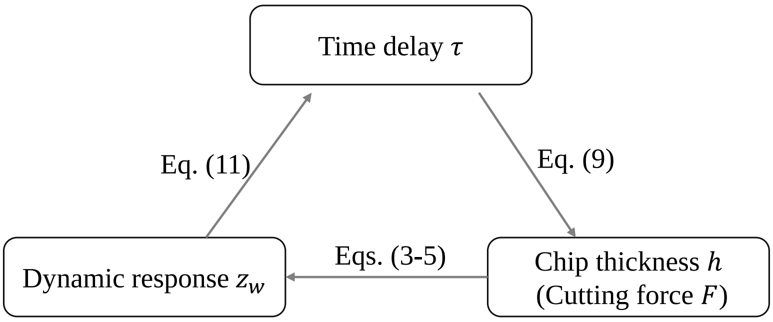

Figure 3. Sequential relationships between time delay, dynamic response and chip thickness. Dynamic response z_w affects time delay τ as described in Eq. (11), time delay affects uncut chip thickness h captured by Eq. (9) and uncut chip thickness affects dynamic response by Eqs (3-5).

The dynamic model of trimming process has a strong nonlinearity hence no suitable linearization method is readily available to analyze its stability efficiently, so that the time-domain numerical simulation method is adopted. The time-domain simulation process is based on the scheme proposed in [19]. For a given spindle speed and width of cut, the simulation time duration t_{end} is equal to the time 120 revolutions. Time increment Δt is calculated from Eq. (13) to ensure that the tooth period is divided into integer interval.

$$\Delta t = T / \mathrm{ceil}\left(T / \Delta t_0\right), \tag{13}$$

where 'ceil(λ)' is the function that takes as input a real number λ and gives as output the nearest integer greater than or equal to λ, and $\Delta t_0 = 1 \times 10^{-6}$ s.

Time delay $\tau(t)$ is calculated by an iterative search method and the procedure is explained in Appendix A. The milling forces are calculated by Eq. (5) and the dynamic displacements of the tool in *X* and *Y*-directions and the workpiece in *Z*-direction can be obtained by using the explicit Euler method by integrating the Eq (3). Subharmonic sampling strategy proposed by Schmitz et al. [20] combined with a new stability metrics Eq. (14) is used to detect different milling states, e.g., stability and milling bifurcation phenomenon.

$$M_n = \frac{\sum_{i=2}^{N_s} \left| z_{sn}(i) - z_{sn}(i-1) \right|}{N_s}, \tag{14}$$

where z_{sn} is the vector of z_w displacements sampled once every n tooth period, and N_s is the length of the z_{sn} vector. In order to avoid the effect of free vibration, we have truncated the output signals z_w to remove the first 67%.

When compared with the conventional stiffness of the milling systems, the stiffness of the workpiece in this study is very low (refer to Table 1), hence the vibration amplitude of the workpiece in trimming process can reach 1~2 millimeters rather than a few micrometers or tens of micrometers.

Therefore, the improved stability metrics is proposed, the order of magnitude of the vibration displacements z_w is changed by $z_s = z_w / 10^{\eta}$ before calculating M_n, where η is a positive integer, and η is set to 2 in this study. The flow chart of the algorithm for constructing the stability lobe diagram is shown in the **Appendix B**, where $\Delta\Omega$ and a_e are the interval value of spindle speed and width of cut, respectively.

4 Numerical simulation and experimental validation

The proposed state-dependent dynamic model of trimming and numerical algorithm with improved stability metrics will be validated with simulations and experiments in this section. The workpiece is made of Aluminum Alloy 7075 and as 100 mm × 60 mm × 2 mm thin-walled plate with 80 mm overhang. The stiffness is low in *Z*-direction while strong enough in *X* and *Y*-direction. To focus on the effect of state-dependent time delay and instantaneous rotation angle caused by workpiece vibration, a single tooth ($N = 1$) tool is adopted with diameter $D = 8$ mm, helix angle $\beta = 45^{\circ}$ and overhang $L = 20$ mm to ensure enough stiffness of the tool. The tool originally had two teeth but one of the teeth is removed by grinding wheel to avoid disturbances, e.g., tool runout.

4.1 Identification of dynamic parameters

The identification experiment of cutting force coefficients was carried out similar to that in Ref [66]. In order to avoid the effect of cutting vibration and bottom edge cutting on cutting force, the thin-walled plate with 4 mm overhanging length was cut by side milling with 3.5 mm width of cut. The cutting forces were measured by a dynamometer with the sampling frequency was set to 20 kHz. The identified cutting coefficients parameters are K_a=481 N/mm^2 and K_{ae}=2.0 N/mm.

The experimental modal test was performed on the workpiece with impact hammer, accelerometer, and data acquisition system. Two different points on the workpiece are measured. The distance between the two points along the *X*-direction is 10mm and the connecting line between the two points is parallel to the *X*-direction. Modal parameters including modal mass, natural frequency, damping ratio and stiffness calculated by rational fraction polynomial fitting algorithm are shown in Table 1, and the measured and fitted FRFs are compared in Figure 4. It is seen that the modal curves of the two points are almost the same, which indicates that the modal parameters of the two positions are basically the same. The data of Measurement-1 is used to calculate the stability lobe diagram. As the stiffness along the *X*-direction of the thin-walled structure changes gradually, we used a narrow area of the workpiece to carry out the simulations and experiments so that the stiffness variation along the workpiece edge is small. This is confirmed by the modal data of Measurement-1 and of Measurement -2, which are almost the same as can be see in Figure 4 and Table 1.

Table 1. Identified modal parameters of the experimental milling system.

Mode	Order	Frequency (Hz)	Mass (kg)	Damping ratio (%)	Stiffness (N/m)
Measurement-1	1st	243.12	0.0084	0.8720	1.9707×10^4
	2nd	755.75	0.0138	0.2187	3.1093×10^5
Measurement-2	1st	243.05	0.0086	1.0249	2.007×10^4
	2nd	755.79	0.0174	0.2445	3.9161×10^5

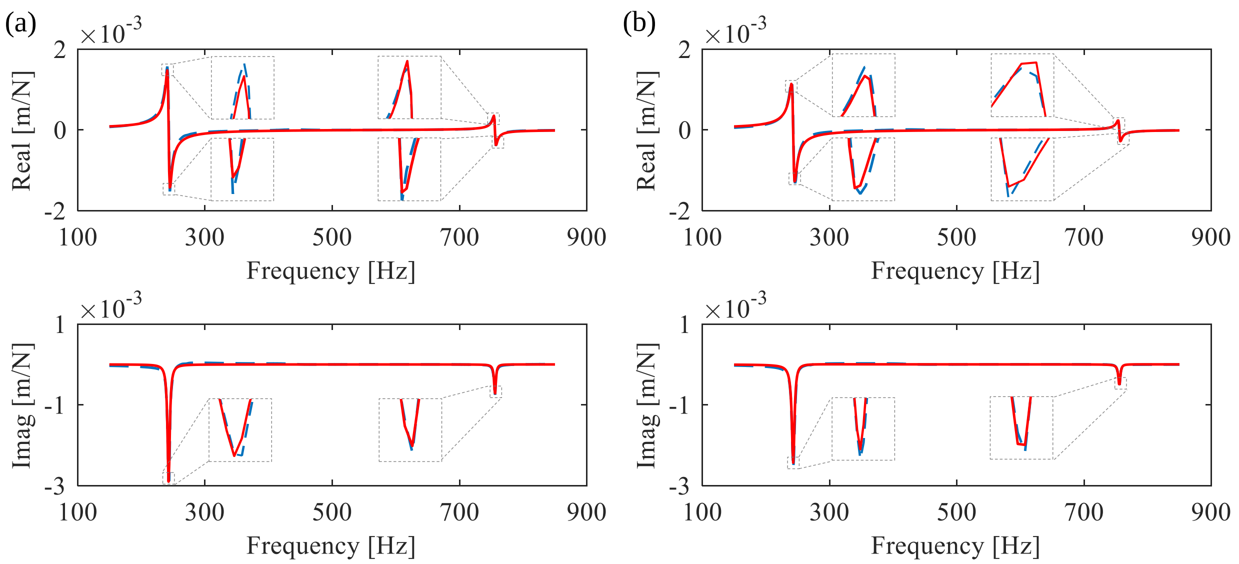

Figure 4. FRF of the workpiece in *Z*-direction. The blue dash lines and red solid lines represent the measured and fitted results, respectively. Data of two different points on the workpiece is shown in (a) and (b). The distance between the two points along the *X*-direction is 10mm and the connecting line between the two points is parallel to the *X*-direction. The modal curves of the two points are almost the same, which indicates that the modal parameters of the two positions are basically the same. The experimental modal tests are conducted 3 times on each point and the set of data of measured frequency response have been averaged in ModalView software.

4.2 Prediction of stability charts

Since the dynamic response z_w depends on uncut chip thickness, uncut chip thickness depends on time delay and time delay depends on dynamic response, the dynamic model of trimming process exists complex nonlinear coupling relationships. In order to analyze the stability property of the trimming process, we set cutting conditions with up milling, $f_t = 0.03$ mm to draw the stability lobe diagram. The range of spindle speed is 3000 to 6300 rpm with the step of 100 rpm and radial width is 1.0 to 5.0 mm with the step of 0.1 mm. Stability solution presented in the last part of Section 3 is used to predict stability and bifurcation types. First, the simulation time duration t_{end} is divided equally with time increment Δt. Then, time delay, cutting forces and vibration displacements are calculated by Eq. (11), Eq. (5) and Eq. (3) for each time step, respectively. The vibration displacement of the workpiece z_w is selected to calculate the stability metrics M_n by Eq. (14). Last, the subharmonic sampling strategy is used to analyze the dynamic behaviors of milling process. This procedure is carried out for every combination of spindle speed and width of cut within the given range, specifically from 3000 to 6300 rpm and from 1.0 to 5.0 mm. The computed stability lobe diagram is shown in Figure 5(a), where blank and blue areas indicate stable and chatter regions respectively. Hopf bifurcations are marked by red dot and period-2 bifurcations by blue circles. The peak-to-peak (PTP) diagram proposed by Smith and Tlusty [21] is also plotted in Figure 5(b). The boundaries of the two-lobe diagrams are roughly the same, which shows the validity of the improved stability metrics.

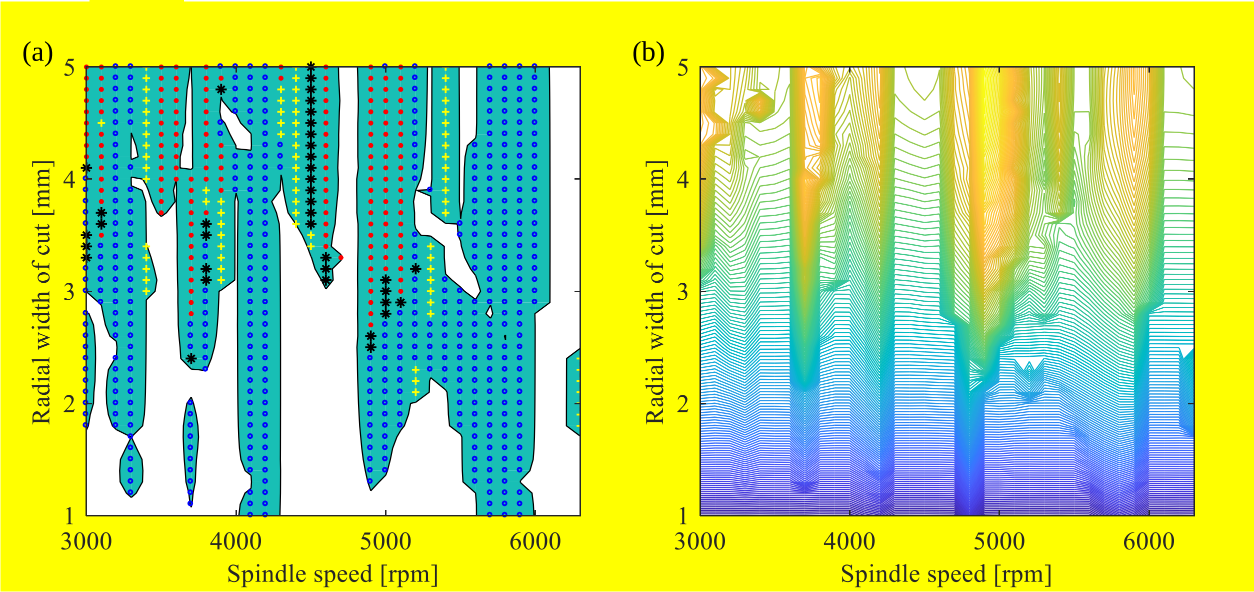

Figure 5. Example results of dynamic stability for the trimming process; (a) stability lobe diagram plotted using time-domain numerical simulation with the improved stability metrics; (b) Peak-Po-Peak (PTP) diagram plotted using the cutting force in *Z*-direction.; In the panel (a), the blank area is the stable area and the blue area is the chatter area. Some unstable points such as Period-2 (blue circle ‘o’), period-3 (yellow plus sign ‘+’), period-4 (black asterisk ‘*’), and secondary Hopf or high order period-n (red dot ‘.’) are marked with different symbols and colors. The stable boundaries of the two-lobe diagrams calculated by different methods are roughly the same, which shows the validity of the improved stability metrics.

For stable trimming process (such as $\Omega = 6100\,\text{rpm}$, $a_e = 3.0\,\text{mm}$), the workpiece vibration is periodic with tooth period (forced vibration only), the motion trajectories of the workpiece as well as the corresponding 1/revolution-sampled points (‘.’ pitch-label) is plotted in Figure 6(a). Only a single group of points is observed in the Poincaré map for once per tooth sampling which is shown in Figure 6(b). Figure 6 indicates that the axial height difference of the workpiece vibration between current and previous teeth is zero so that time delay calculated by Eq. (11) converges to a constant value, which is seen in Figure 7.

Instantaneous rotation angle $\varphi_{t,i,j}$ is a linear function of time if the workpiece vibration are neglected. However, in this study, the instantaneous rotation angle $\varphi_{t,i,j}$ depends on the vibration displacement of workpiece which is time-varying so that the instantaneous rotation angle changes nonlinearly. As the chip thickness and cutting force are closely related to the instantaneous rotation angle, these values are also changed at different time rather than phase shifts. In Figure 8, the instantaneous rotation angle $\varphi_{t,i,j}$ of the cutting element $(i=1, j=1)$ and the Z-direction cutting force of the tool at different time are plotted. Comparing with the case that workpiece is rigid, the cutting force with considering the workpiece vibration changes at different time. The start and end time of the engagement between the cutter and the workpiece is different and t_1 is less than t_2 (t_1 and t_2 are the cutting time when the workpiece is regarded rigid and flexible, respectively.), which indicates that the state-dependent rotation angle $\varphi_{t,i,j}$ caused by the workpiece vibration changes the actual engagement time in each tooth period.

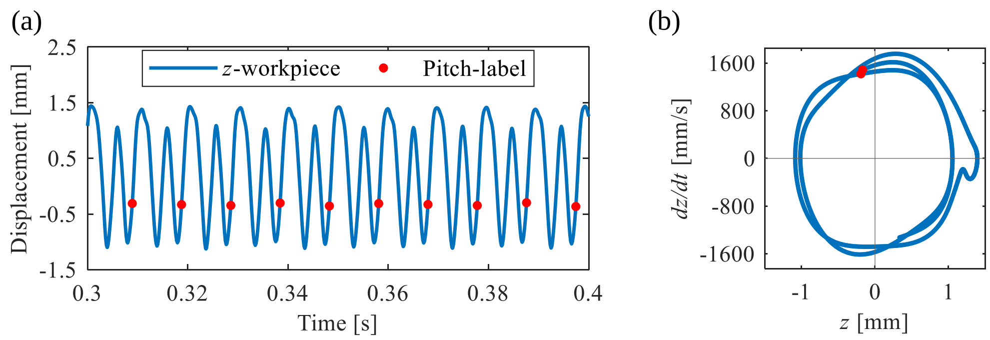

Figure 6. Stable trimming behaviour obtained for $\Omega = 6100$ rpm and $a_e = 3.0$ mm; (a) time history of workpiece vibration displacement in Z-direction and pitch label displacement 1/rev; (b) phase portrait and Poincaré map (red point).

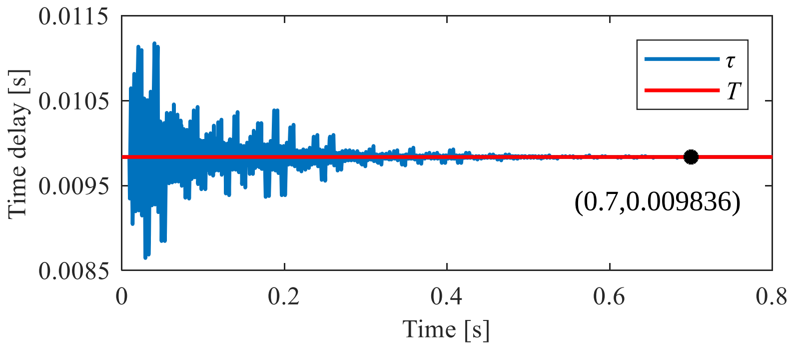

Figure 7. Simulated time delay and tooth period for $\Omega = 6100$ rpm and $a_e = 3.0$ mm. For stable trimming, the time delay converges to the tooth period $T = 0.009836$ s.

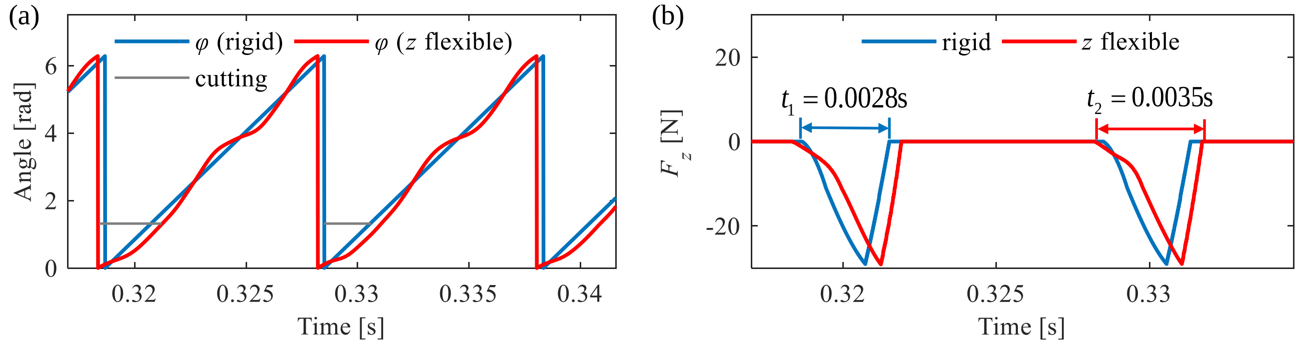

Figure 8. Comparison of the instantaneous rotation angle and cutting force between flexible and rigid workpieces with $\Omega = 6100$ rpm and $a_e = 3.0$ mm; (a) the instantaneous rotation angle φ of the cutting element $(i = 1, j = 1)$ at different time. When workpiece vibration is considered, φ changes nonlinearly, and the engagment time of tool-workpiece is also shown by 'cutting'; (b) the cutting force of the tool in *Z*-direction at different time. t_1 and t_2 are the cutting duration when workpiece is regarded rigid or flexible, respectively, where t_2 is 25% longer than t_1 .

For the period-*n* bifurcation, the motion trajectories of the workpiece vibration repeat every *n* tooth periods, and the sampled points appear at n distinct locations in the Poincaré map. Taking period-2 bifurcation trimming (such as $\Omega = 4100$ rpm, $a_e = 3.5$ mm) as an example, the cutting force of the tool in *Z*-direction as well as the corresponding 1/revolution-sampled points ('•' pitch-label) is plotted in Figure 9(a). The Poincaré map of the workpiece vibration displacement for once per tooth period sampling is shown in Figure 9(b), which indicates that period-2 bifurcation occurs.

In order to analyze the characteristics of period-2 bifurcation in the proposed model, the state-dependent time delay is shown in Figure 10, the instantaneous rotation angle and chip thickness of the cutting element ($i = 1, j = 1$) at different time are plotted in Figure 11. In period-2 bifurcation trimming, the time delay is time-varying and its maximum change is nearly 8% compared with the tooth period. The variation period of the time delay is consistent with the vibration period of the workpiece. Similarly to the stable trimming, the instantaneous rotation angle changes nonlinearly in period-2 bifurcation trimming, but its period has changed. Comparing the uncut chip thicknesses with (h_2) and without (h_1) considering the workpiece vibration, we find that the phase of h_1 and h_2 is different, and the cutting thickness h_1 does not change completely smoothly in one of the tooth periods. It is noted that the sharp change of h_2 in Figure 11(b) is reasonable because of the sudden change of the time delay at the corresponding time node.

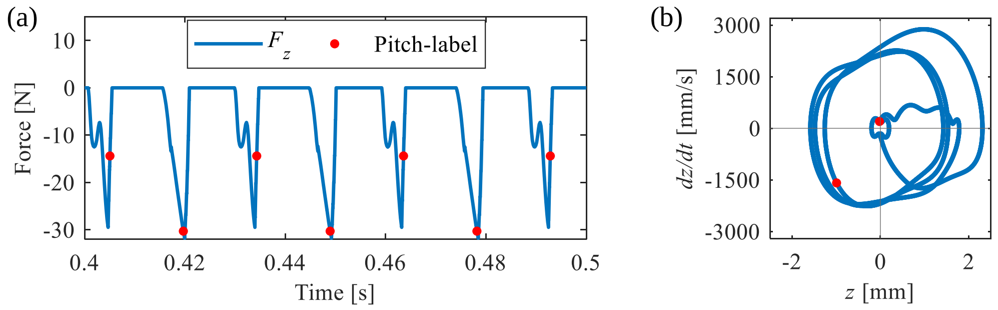

Figure 9. Period-2 bifurcation with $\Omega = 4100$ rpm and $a_e = 3.5$ mm; (a) the cutting force of tool in *Z*-direction and pitch label cutting force 1/rev; (b) phase portrait and Poincaré map (red point).

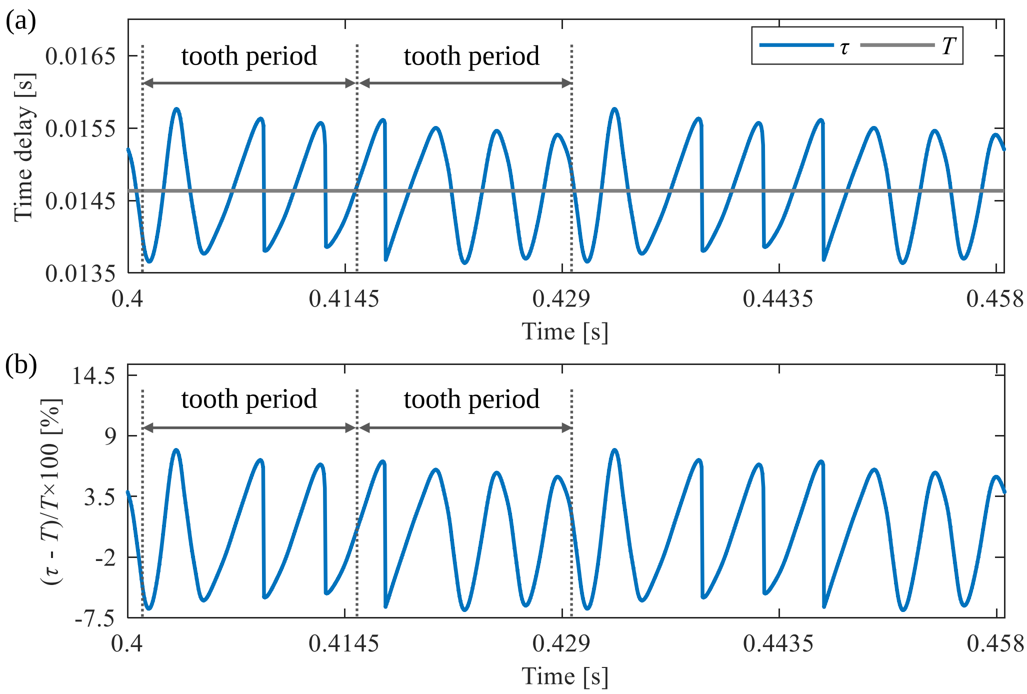

Figure 10. Simulated time histories for time delay, tooth period and change rate with $\Omega = 4100$ rpm and $a_e = 3.5$ mm; (a) For period-2 bifurcation trimming, the time delay is time-varying, and the maximum and minimum values are 0.01578 s and 0.01356 s, respectively. The tooth period is 0.01463 s. (b) Use the equation $(\tau - T)/T \times 100$ to calculate the change rate, and the maximum value is nearly 8%.

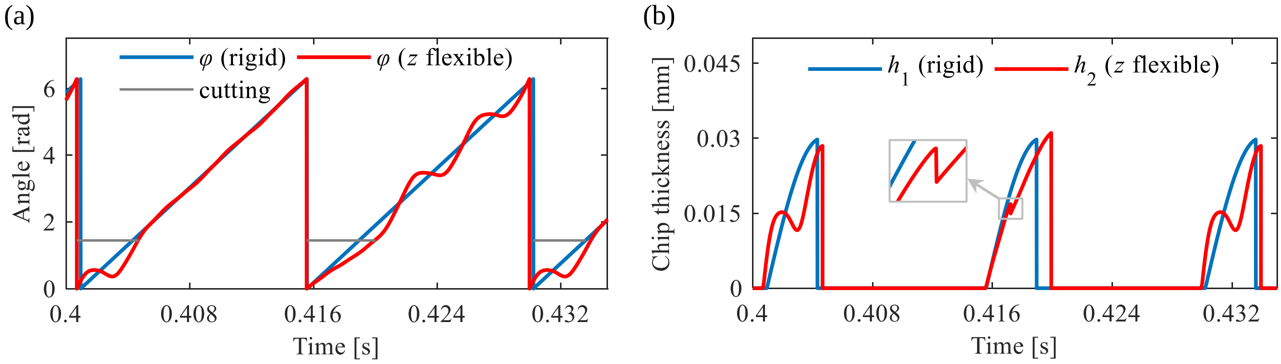

Figure 11. Comparisons between state-dependent and independent dynamics for $\Omega = 4100$ rpm and $a_e = 3.5$ mm; (a) the instantaneous rotation angle φ of the cutting element (i=1, j=1) at different time; (b) the instantaneous chip thickness of the cutting element (i=1, j=1) at different time. When the workpiece vibration is considered, φ changes nonlinearly, and the engagement duration of tool-workpiece is also shown by 'cutting'. h_1 is the static cutting thickness without considering the workpiece vibration, h_2 is the dynamic cutting thickness.

4.3 Discussion on engagement conditions and stability analysis

As explained in Section 3.2, the actual cutting duration will be changed at stable trimming process when workpiece vibration is taken into account. In order to further investigate this phenomenon, we have analyzed the change rate trend of cutting duration at the same spindle speed and different width of cut or at different spindle speeds and the same width of cut. The results are shown in Figure 12(a) and (b). In Figure 12(a), for low spindle speeds (such as $\Omega = 3500$ rpm, $\Omega = 4500$ rpm), with the increase of width of cut, the change rate of cutting duration decreases. However, for high spindle speeds such as $\Omega = 6100$ rpm, $\Omega = 6200$ rpm, with the increase of width of cut, the change rate of cutting duration increases first and then decreases. In Figure 12(b), when width of cut a_e is set to 1.5 mm, with the increase of spindle speed, the change rate of cutting duration also increases. And when the width of cut a_e is set to 2.0 or 2.5 mm, with the increase of spindle speed, the change rate of cutting duration only fluctuates slightly, which indicates that the change of spindle speed has little effect on cutting duration at these widths of cut.

The same strategy is adopted to analyze the variation trend of the change rate of time delay at period-2 bifurcation trimming process and the results are shown in Figure 12(c) and (d). In Figure 12(c), with the increase of width of cut, the maximum change rate of time delay also increases for spindle speeds $\Omega = 4100$ rpm and $\Omega = 5900$ rpm. However, for the spindle speeds, $\Omega = 4200$ rpm and $\Omega = 5800$ rpm, the maximum change rate of time delay remains basically unchanged with the increase of width of cut. These four curves are far apart from each other along the vertical axis, which shows that the spindle speed has a relatively big effect on the maximum change of time delay. In Figure 12(d), when the width of cut a_e is set to 1.7, 2.1 or 2.5 mm, with the increase of spindle speed, the maximum change rate of time delay also increases. These three curves are relatively steep, which also shows that the spindle speed has a relatively big effect on the maximum change of time delay. Since these three curves are almost close to each other along the vertical axis excepting the cutting parameter ($\Omega = 5500$ rpm, $a_e = 1.7$ mm), it shows that the width of cut has little effect on the maximum change of time delay within the spindle speed range of 5500 to 5900 rpm.

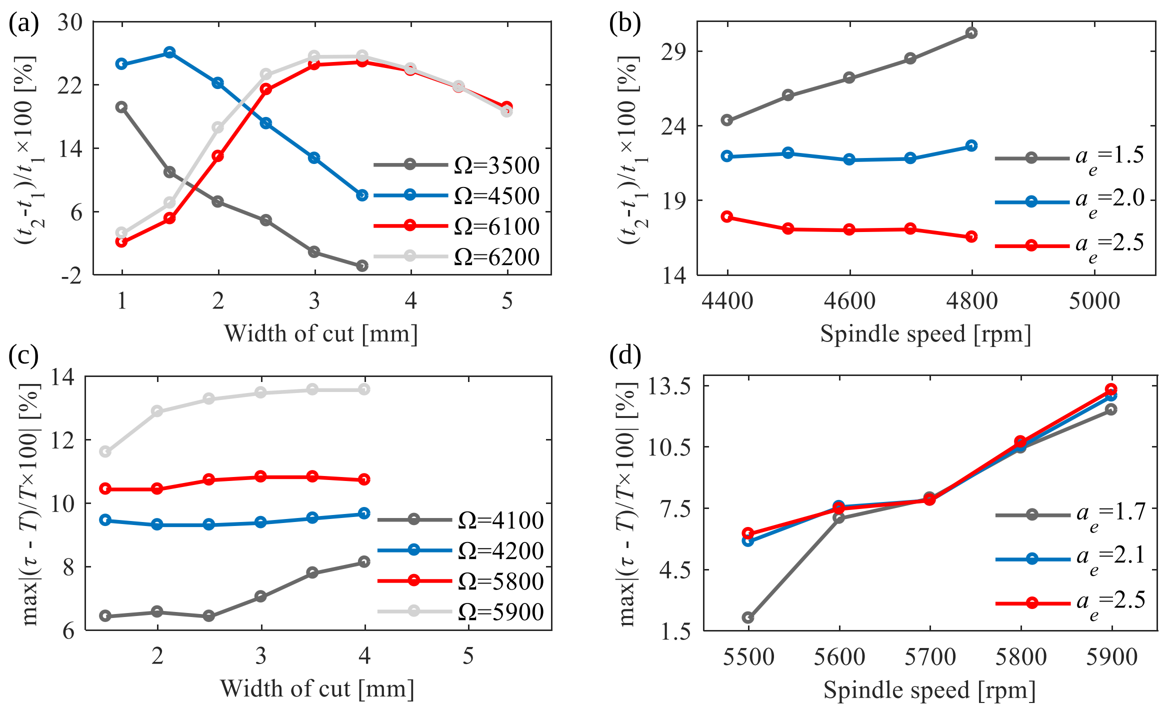

Figure 12. Change rate of cutting time and time delay under different cutting parameters. t_1 and t_2 are the cutting time when the workpiece is regarded as rigid and flexible respectively. τ and T are the time delay and tooth period respectively. (a) The change rate of cutting time at the same spindle speed and different width of cut. (b) The change rate of cutting time at the same width of cut and different spindle speed. (c) The maximum change rate of time delay at the same spindle speed and different width of cut. (d) The maximum change rate of time delay at the same width of cut and different spindle speed.

As has been explained at the beginning of Section 4, to focus more on the effect of state-dependent and time-varying time delays caused by workpiece vibration, the stiffness of the tool in our experiment is designed to be very high. This effectively changes the problem from 3 DOF (three degrees-of-freedom) to 1 DOF (one degree-of-freedom), where only flexibility of the workpiece is in the *Z*-direction. In another words, when state-dependent and time-varying time delays are not considered, vibration in *Z*-direction can be neglected as the system stiffness becomes high resulting that all the cutting parameters in the stability lobe diagram are stable.

Let us examine now the stability lobe diagram corresponding to the following set of cutting parameter represented by points A(6100 rpm, 2.5 mm), B(6100 rpm, 3.5 mm), C(6200 rpm, 2.5 mm), D(6200 rpm, 3.0 mm) E(4100 rpm, 3.3 mm), F(4200 rpm, 3.0 mm), G(4200 rpm, 3.5 mm), as shown in Figure 13(a). And the related experimental results are presented in Section 4.4.

In order to assess a difference between the stability lobe diagrams calculated with the classic approach without considering the state dependent time delay, we superimposed these two lobe diagrams, which is shown in Figure 13(b). The red curve represents the classic lobe diagram with 2 DOF (two degrees-of-freedom), where the dynamics of the tool in *X* and *Y*-directions are considered. The black curve marks the stability borders for our approach having 3 DOF with the state-dependent and time-varying time delay, where the dynamics of the tool in *X* and *Y*-directions and the workpiece in *Z*-direction are considered. Four simulated results, marked as points P1 (4600 rpm, 3.5 mm), P2 (5900 rpm, 1.5 mm), P3 (6300 rpm, 1.6 mm), P4 (7100 rpm, 2.1 mm), were used to probe the computed stability lobe diagrams. In Figure 13(b), P1, P2 and P3 are in the chatter area for 3 DOF model but they are stable according to 2 DOF model. In contrast, P4 is a stable point for 3 DOF model but it exhibits chatter in 2 DOF prediction. The simulated displacement time histories for points P1 to P4 are presented in **Appendix C**.

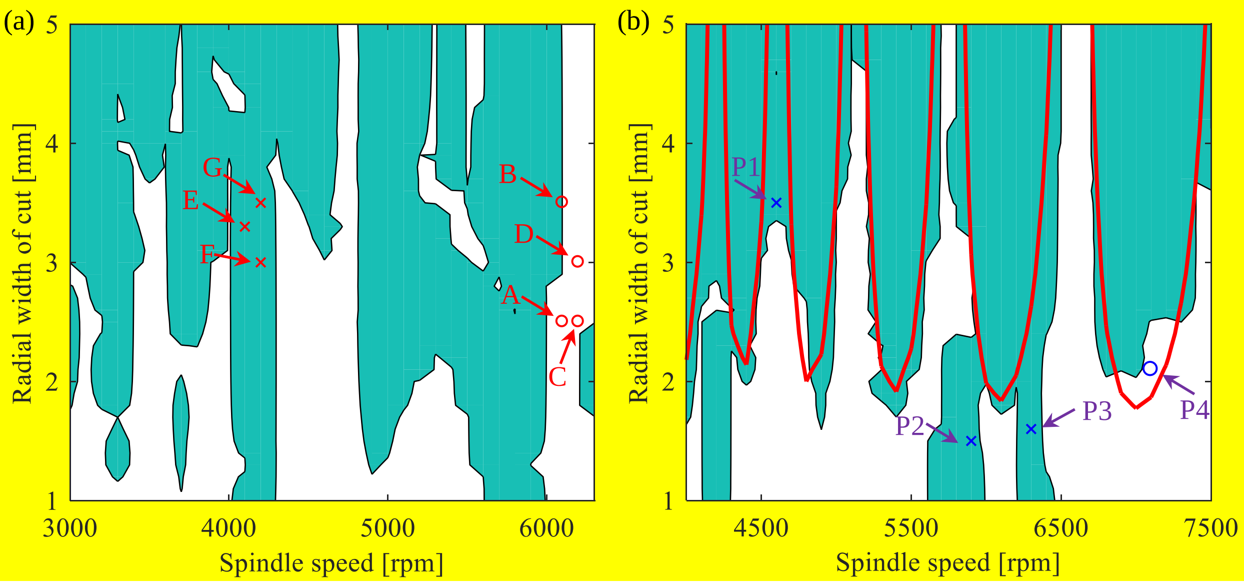

Figure 13. Stability lobe diagrams for three different models and test points obtained for a chosen set of cutting parameters given in brackets; (a) 1 DOF with state-dependent and time-varying time delay marking important points A(6100 rpm, 2.5 mm), B(6100 rpm, 3.5 mm), C(6200 rpm, 2.5 mm), D(6200 rpm, 3.0 mm), E(4100 rpm, 3.3 mm), F(4200 rpm, 3.0 mm) and G(4200 rpm, 3.5 mm); Points E, F, G are period-2 bifurcations; (b) classic 2 DOF (red curves) and the 3 DOF with state-dependent and time-varying time delay (color areas). The blank and color areas mark stable and chatter regions respectively. Four typical points P1 (4600 rpm, 3.5 mm), P2 (5900 rpm, 1.5 mm), P3 (6300 rpm, 1.6 mm), P4 (7100 rpm, 2.1 mm) are also shown.

4.4 Experimental studies

In this work the experiments were conducted to calibrate the developed mathematical model and provide some insight into its validation. The trimming tests are carried out on the five-axis machining center (Mikron UCP800) and the experimental setup is shown in Figure 14. A rotating dynamometer is used to record the dynamic milling force and an accelerometer is attached on the workpiece to measure the vibration acceleration signal. The Keyence laser displacement sensor is used to measure the vibration amplitude of the workpiece.

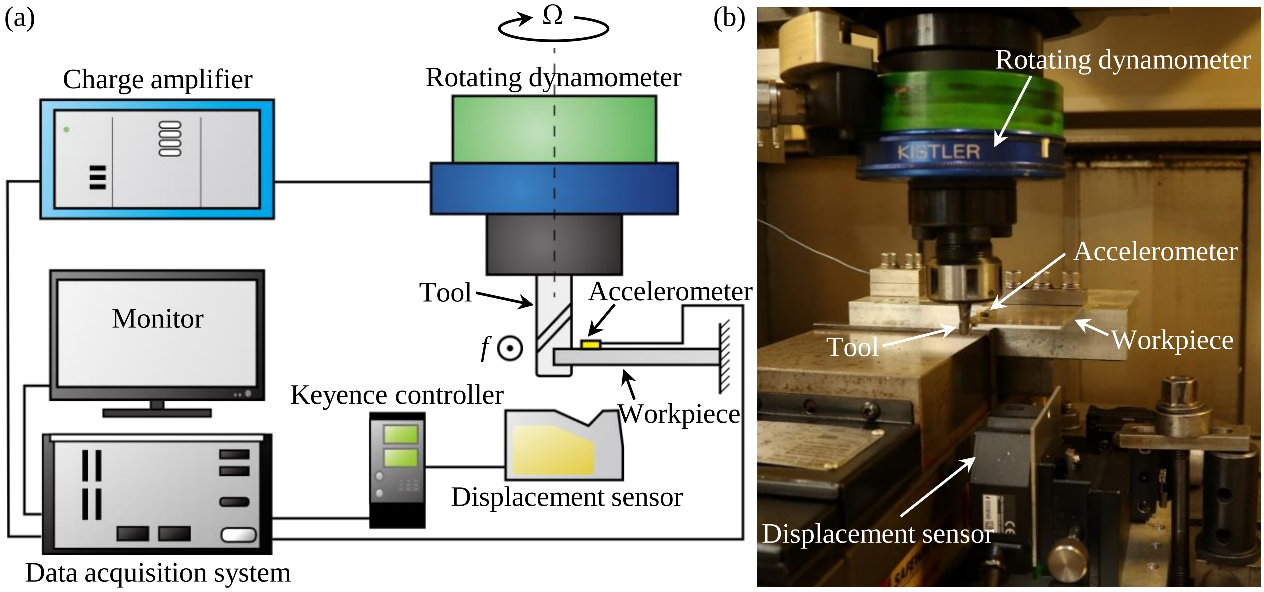

Figure 14. Experimental set-up for investigating the dynamics of trimming thin-walled structures; (a) schematic diagram of experimental set-up; (b) photograph showing sensor locations. A rotating dynamometer is used to record the dynamic milling force of tool. Accelerometer and Keyence laser displacement sensors are used to measure the acceleration and displacement of the workpiece respectively.

For stable trimming ($\Omega = 6100$ rpm, $a_e = 3.0$ mm, we used the same stable parameters as in the simulation), the acceleration of the workpiece vibration as well as the corresponding 1/revolution-sampled points ('.' pitch-label) is plotted in Figure 15(a), and the corresponding FFT spectrum is shown in Figure 15(b). It can be seen that the signal in stable state only has the tooth passing frequency and its harmonics, and the dominant frequencies 915 Hz, 508.4 Hz are 9, 5 multiplication of the tool passing frequency, respectively. A comparison of the measured and simulated displacements is shown in Figure 16, where a good agreement of the main waveforms is evident but there is a space for a better correlation. Specifically, higher harmonics in time histories obtained from simulation and experiment results differ, which may be attributed to identification errors of cutting force coefficients and modal parameters.

The FFT spectra of measured displacement in points A (6100 rpm, 2.5 mm), B (6100 rpm, 3.5 mm), C (6200 rpm, 2.5 mm), D (6200 rpm, 3.0 mm) are shown in Figure 17. Since the frequencies are multiples of the tooth passing frequency, these points are all stable.

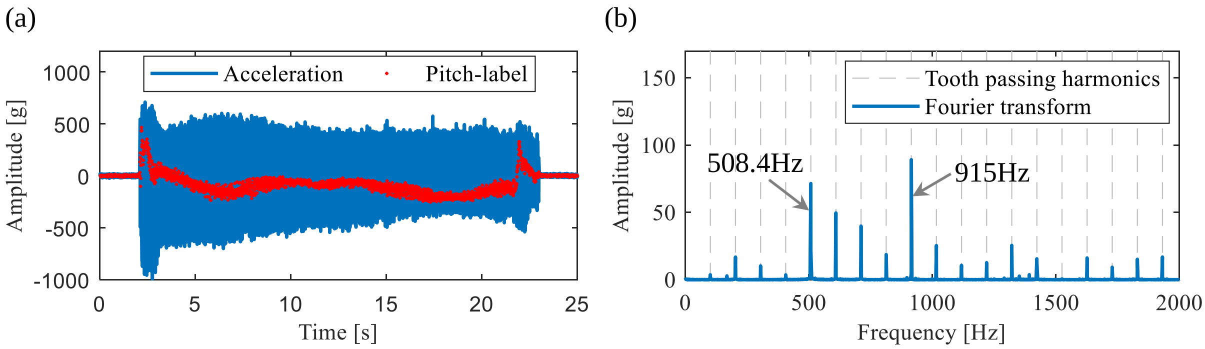

Figure 15. Measured acceleration for $\Omega = 6100$ rpm and $a_e = 3.0$ mm; (a) time histories of the acceleration and the corresponding 1/revolution-sampled points ('•' pitch-label); (b) FFT spectrum of the acceleration signal and the frequencies are integral multiplication of the tooth passing frequency. These results show that the trimming process under this cutting parameters is stable.

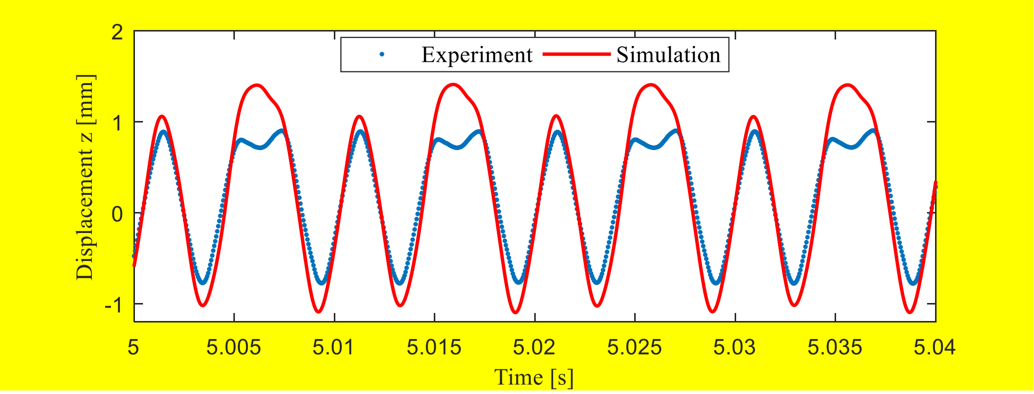

Figure 16. Experimental and simulated workpiece displacement time histories for $\Omega = 6100$ rpm and $a_e = 3.0$ mm. A good agreement is clearly visible for the fundamental waveform with some discrepancies for the higher harmonics. Possible reasons for the difference are potential errors in identification of cutting force coefficients and modal parameters.

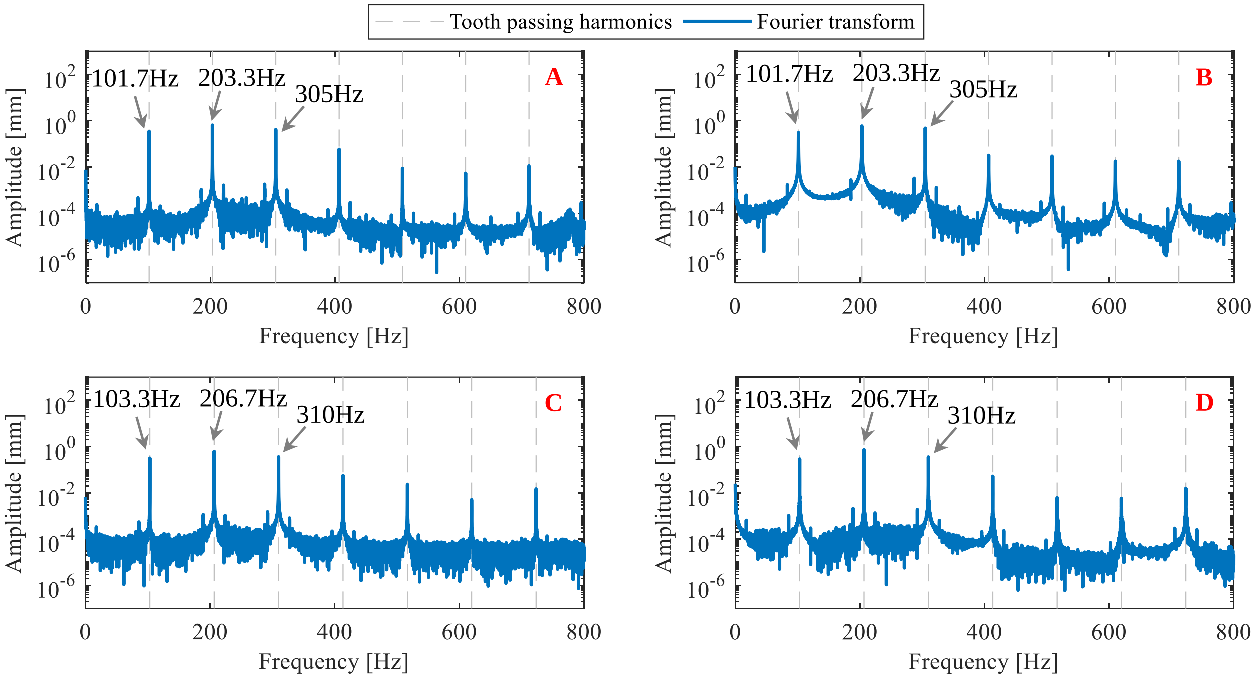

Figure 17. FFT spectra of the measured displacements at different stable points A(6100 rpm, 2.5 mm), B(6100 rpm, 3.5 mm), C(6200 rpm, 2.5 mm), D(6200 rpm, 3.0 mm) in logarithmic scale. These frequencies are multiples of the tooth frequency, indicating that these points are stable.

Taking the cutting parameters $\Omega = 4100$ rpm and $a_e = 3.5$ mm, which is unstable in the simulation, the FFT spectrum of the measured displacement shown in Figure 18(a) indicates that the fundamental frequency 34.17 Hz is a half of the tooth passing frequency 68.33 Hz. The dominant frequencies 205 Hz is 3 multiple of the tool passing frequency, and the frequencies 102.5 Hz and 239.2 Hz are 3 and 7 multiplication, respectively, of the fundamental frequency. The FFT spectrum of the measured acceleration is demonstrated in Figure 18(b), where the dominant frequencies 273.3 Hz is 4 multiplication of the tool passing frequency. The frequencies 102.5 Hz, 307.5 Hz and 512.5 Hz are 3, 9 and 15 multiples, respectively, of the fundamental frequency 34.17 Hz. Due to half of the tooth passing frequency has been discovered in these experimental results, period-2 bifurcation is verified.

The FFT spectra of the measured displacements of points E(4100 rpm, 3.3 mm), F(4200 rpm, 3.0 mm), G(4200 rpm, 3.5 mm) are shown in Figure 19. When $\Omega = 4200$ rpm, the fundamental frequency 35 Hz is a half of the tooth passing frequency 70 Hz, other frequencies are multiplication of 35 Hz.

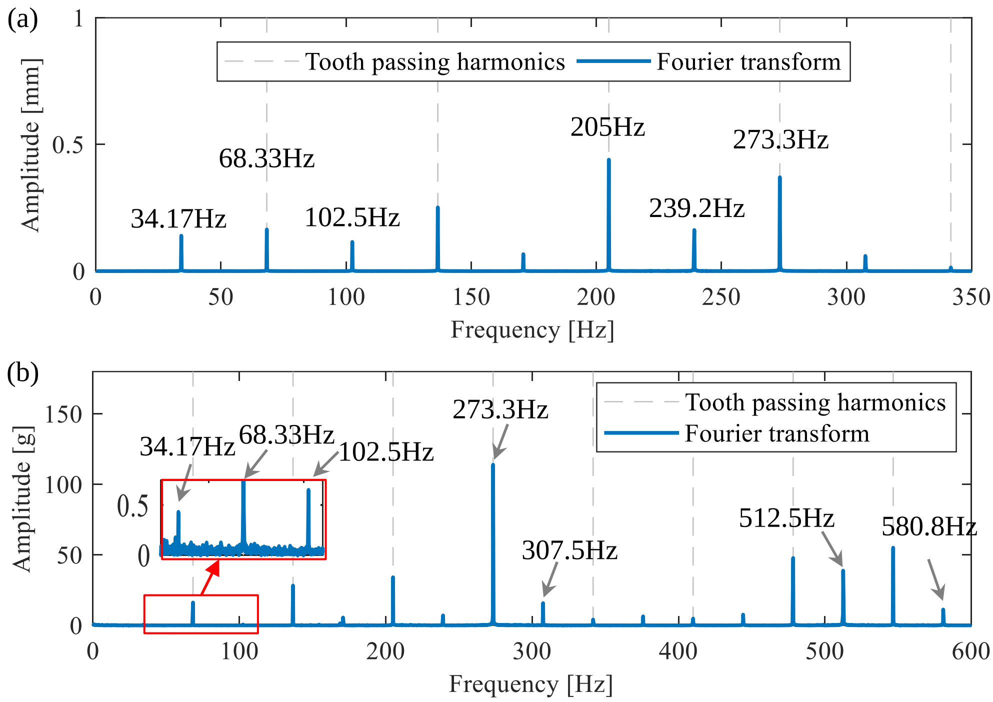

Figure 18. Spectra of workpiece displacement (a) and acceleration (b) for $\Omega = 4100$ rpm and $a_e = 3.5$ mm. The fundamental frequency 34.17 Hz is half of the tooth passing frequency 68.33 Hz and other frequency (such as 102.5 Hz, 239.2 Hz, 307.5 Hz, 512.5 Hz, 580.8 Hz) are integral multiples of the fundamental frequency 34.17 Hz.

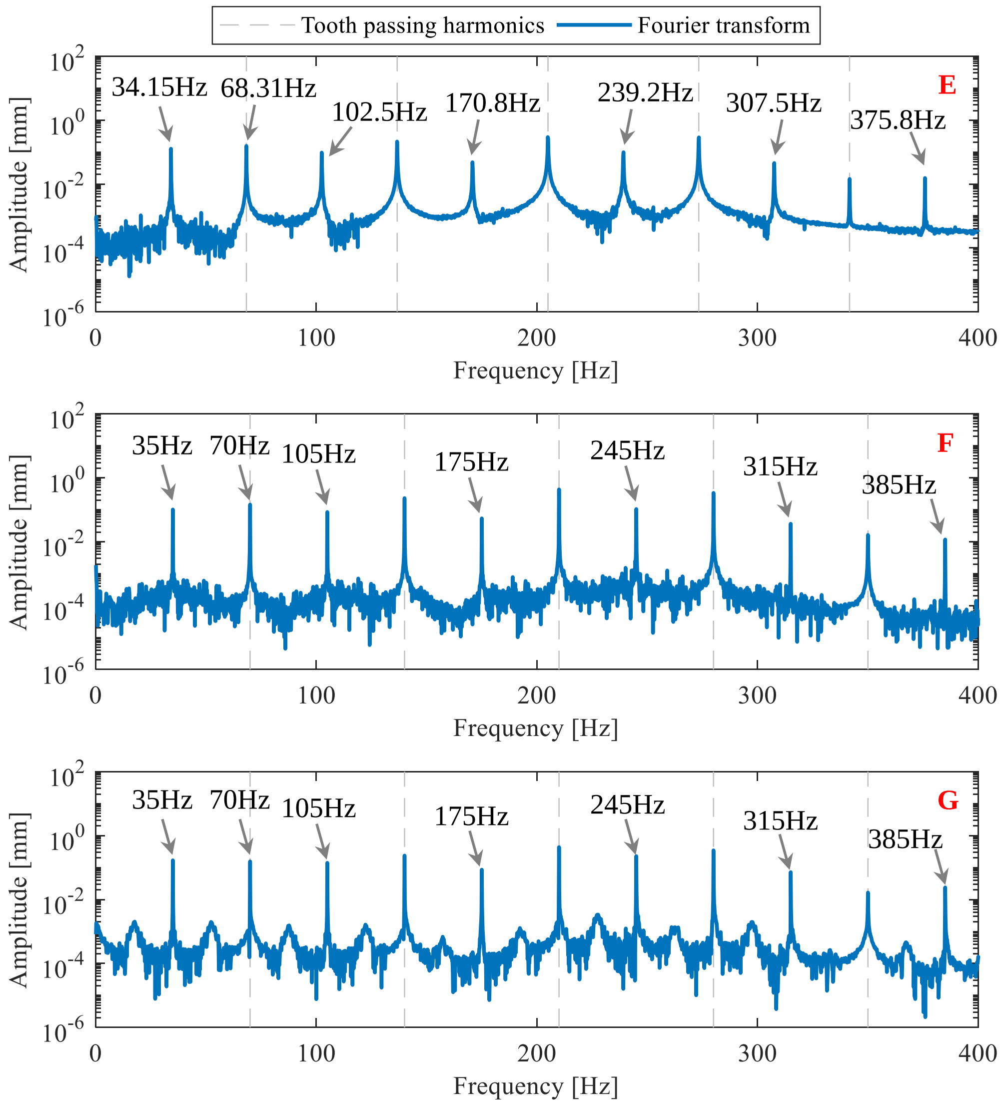

Figure 19. FFT spectra of the measured displacements at different period-2 bifurcation points E(4100 rpm, 3.3 mm), F(4200 rpm, 3.0 mm), G(4200 rpm, 3.5 mm) in logarithmic scale. The fundamental frequency is a half of the tooth passing frequency.

5 Conclusions

This study presents a development of the mathematical model of trimming a thin-walled cantilever workpiece by considering the effect of workpiece vibration along the tool-axis on time delay and instantaneous rotation angle when the helix angle cutters are used. A novel dynamic model accurately describing the dynamics of thin-walled workpiece trimming process is established, where the relay relationship of state-dependent time delay, uncut chip thickness (cutting forces) and dynamic response is clearly figured out. To solve the strongly nonlinear dynamic problem, an iterative method for calculation of the state-dependent time delay and a time-domain numerical algorithm with an improved stability metrics for the prediction of trimming stability are presented.

Simulation results comparing with those of the traditional model show the efficiency of the proposed model. Moreover, the mechanism of period-n instability phenomenon observed in trimming process is fully explained. Both of the simulation and experiment results verified that two states, i.e., period-n instabilities with time-varying time delay and stability states with constant time delay, exist in the thin-walled workpiece trimming process.

Our investigations reveal how the large amplitude vibration of workpiece affects the time delay and stability in the trimming process. The new findings of this study can enhance our understanding of the thin-walled workpiece trimming process. It is expected to help the research community and industry in programming of parameters and even in development of new equipment, such as trimming robot, to improve productivity. For future work, the following questions about thin-walled workpiece trimming may be further explored: high order period-n phenomenon in trimming process by considering the tool runout when multi-tooth milling tool is used; optimization the helix angle of the tool and feed rate, as these factors have a relatively large effect on workpiece vibration amplitude.

CRediT authorship contribution statement

Sen-Lin Ma: Investigation, Methodology, Formal analysis, software, Data Curation, Writing - original draft, Writing - review & editing.

Tao Huang: Investigation, Methodology, Formal analysis, Supervision, Writing - review & editing, Funding acquisition.

Xiao-Ming Zhang: Investigation, Formal analysis, Supervision, Writing - review & editing, Funding acquisition.

Marian Wiercigroch: Investigation, Formal analysis, Writing - review & editing.

Ding Chen: Investigation, Methodology.

Han Ding: Supervision, Project administration, Funding acquisition.

Declaration of Competing Interest

The authors declare that they have no known competing financial interests or personal relationships that could have appeared to influence the work reported in this paper.

Acknowledgments

This work was supported by the National Natural Science Foundation of China (52075205, 92160207, 52090054), National Key R&D Program of China (2020YFA0714900) and Natural Science Foundation of Hubei Province, China (2020CFA077).

Appendixes

A. Algorithm for calculating time delay

Time delay $\tau(t)$ is calculated by an iterative search method and the detailed procedure is shown in Table A1. The input parameters include tooth period T, time node t, time increment Δt, displacement $z_w(t)$, time delay of previous time node $\tau(t-\Delta t)$, tool geometric parameters β D N, and error threshold ε. And the output parameter is Time delay τ. The iterative error τ_{error} and its derivative $d\tau_{error}/d\tau$ is used to judge the iterative direction. Due to the strong nonlinearity of the model, the solution result of the time delay may have multiple solutions. For this, we adopt multiple initial values τ_0 for iterative search, and then compare the obtained results $\tau(t)$ with $\tau(t-\Delta t)$. According to the continuity of the physical process, we select the value closest to $\tau(t-\Delta t)$ as the final value. For the selection of the initial value τ_0, we first set the change range of time delay to be ±20% of the tooth period T ($0.8T \sim 1.2T$), then divide this range into five equal parts, and select the middle four values as the initial values.

Table A1. Algorithm for calculating time delay

Input: tooth period T; time node t; time increment Δt; displacement $z_w(t)$; time delay of previous time node $\tau(t-\Delta t)$; tool geometric parameters β D N; error threshold ε, initial values τ_0.

Output: Time delay τ

Step I:

(0) Set $\tau_{error} = \tau - \left(T + \frac{TN\tan\beta}{\pi D}\left(z_w(t) - z_w(t-\tau)\right)\right)$, $\frac{d\tau_{error}}{d\tau} = 1 + \frac{TN\tan\beta}{\pi D\Delta t}\left(z_w(t-\tau) - z_w(t-\tau+\Delta t)\right)$;

(1) If first tooth period, let $\tau = t$, exit and output τ; Else let $\tau = \tau_0$;

(2) If $t - \tau < 0$, let $\tau = t$; Elseif $\tau <= 0$, let $\tau = \Delta t$;

(3) Calculate τ_{error} and $\frac{d\tau_{error}}{d\tau}$, let $\tau_{error0} = \tau_{error}$; If $\tau_{error}\frac{d\tau_{error}}{d\tau} < 0$, let flag = 1; Else let flag = -1;

(4) If $|\tau_{error}| < \varepsilon$ or $\tau_{error0}\tau_{error} <= 0$, exit and output τ;

(5) If flag = = -1, let $\tau = \tau - \Delta t$; Elseif flag = = 1, let $\tau = \tau + \Delta t$;

(6) If $t - \tau < 0$, let $\tau = t$; Elseif $\tau <= 0$, let $\tau = \Delta t$;

(7) let $\tau_{error0} = \tau_{error}$ and Calculate τ_{error}, and go to **Step**:4.

Step II:

(0) Set $\Delta\tau = \left|\tau - \tau(t-\Delta t)\right|$;

(1) Calculate $\Delta\tau$ for each iterative search result τ with different initial values τ_0;

(2) Select time delay τ corresponding to the minimum $\Delta\tau$.

B. Flow chart of the algorithm for constructing the stability lobe diagrams

The flow chart of the algorithm for constructing the stability lobe diagram is shown in Figure A1. The input parameters include tool parameters (D, β, N), system modal parameters ($\mathbf{M}$, $\mathbf{C}$, $\mathbf{K}$), cutting force coefficients (K_t, K_{te}, K_r, K_{re}, K_a, K_{ae}) and cutting conditions (Ω, f_t, a_e, h_0, up or down milling). And the output of the algorithm is a stability lobe diagram with different bifurcation types. The procedure of the algorithm is described as follows:

For current given spindle speed and width of cut, time delay, the cutting forces and vibration displacements are calculated by Eq. (9), Eq. (3) and Eq. (1), respectively, in simulation time duration t_{end}. Then, the stability metrics M_n is calculated by Eq. (12) and the stability of the milling process behaviors mapped as stable, period-n bifurcation and Hopf bifurcation. This process needs to be carried out for every spindle speed and width of cut. At the end, the stability lobe diagram is constructed.

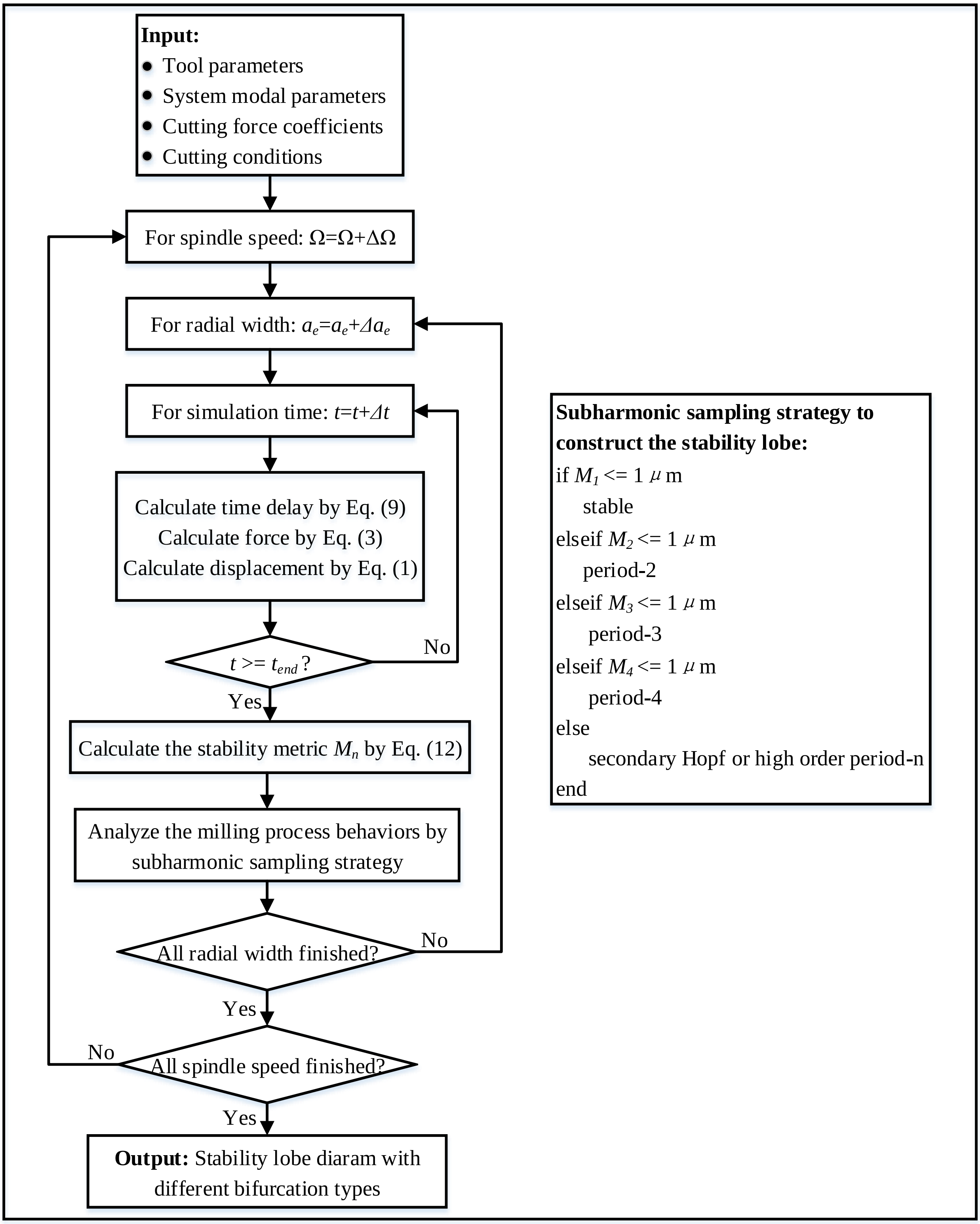

Figure A1. Flow chart of the numerical algorithm to construct the stability lobe diagram. The input parameters include tool parameters, system modal parameters, cutting force coefficients and cutting conditions. And the output result is a stability lobe diagram with different bifurcation types. For given spindle speed and width of cut, we calculate time delay, cutting forces and vibration displacements by Eq. (9), Eq. (3) and Eq. (1), respectively, in the set simulation time duration t_{end}. Then, the stability metrics M_n can be calculated by Eq. (12), and the milling process behaviors can be analyzed by subharmonic sampling strategy.

C. Simulation parameters of stability lobe diagram (Figure 13(b)) and corresponding simulated vibration displacement time histories for P1 to P4

The simulation parameters of the stability lobe diagram shown in Figure 13(b) are assigned as follows: A single tooth ($N=1$) tool with diameter $D=8$ mm, helix angle $\beta=45^{\circ}$ is used. The thickness of the plate is 2 mm which is equal to the cutting depth. The modal parameters of the tool and workpiece are listed in Table A2 and the cutting coefficients parameters are listed in Table A3. Up milling with feed per tooth $f_t=0.03$ mm. The range of spindle speed is 4000 to 7500 rpm with the step of 100 rpm and radial width is 1.0 to 5.0 mm with the step of 0.1mm.

Table A2. Modal parameters of the milling system.

Mode	Frequency (Hz)	Mass (kg)	Damping ratio (%)	Stiffness (N/m)
Workpiece (Z)	243.12	0.0084	0.8720	1.9707×10^4
Tool (X)	768.90	0.6859	0.6823	1.6009×10^7
Tool (Y)	775.33	0.6526	0.9137	1.5576×10^7

Table A3. Cutting coefficients parameters.

K_t (MPa)	K_r (MPa)	K_a (MPa)	K_{te} (N/mm)	K_{re} (N/mm)	K_{ae} (N/mm)
1128	395	195	26.3	39.1	4.3

The simulated displacement time histories of four typical points P1 (4600 rpm, 3.5 mm), P2 (5900 rpm, 1.5 mm), P3 (6300 rpm, 1.6 mm), P4 (7100 rpm, 2.1 mm) of Figure 13(b) are shown in Figure A2 to Figure A5, respectively. P1, P2 and P3 are chatter points in 3 DOF, but stable points in 2 DOF, P4 is a stable point in 3 DOF, but chatter point in 2 DOF.

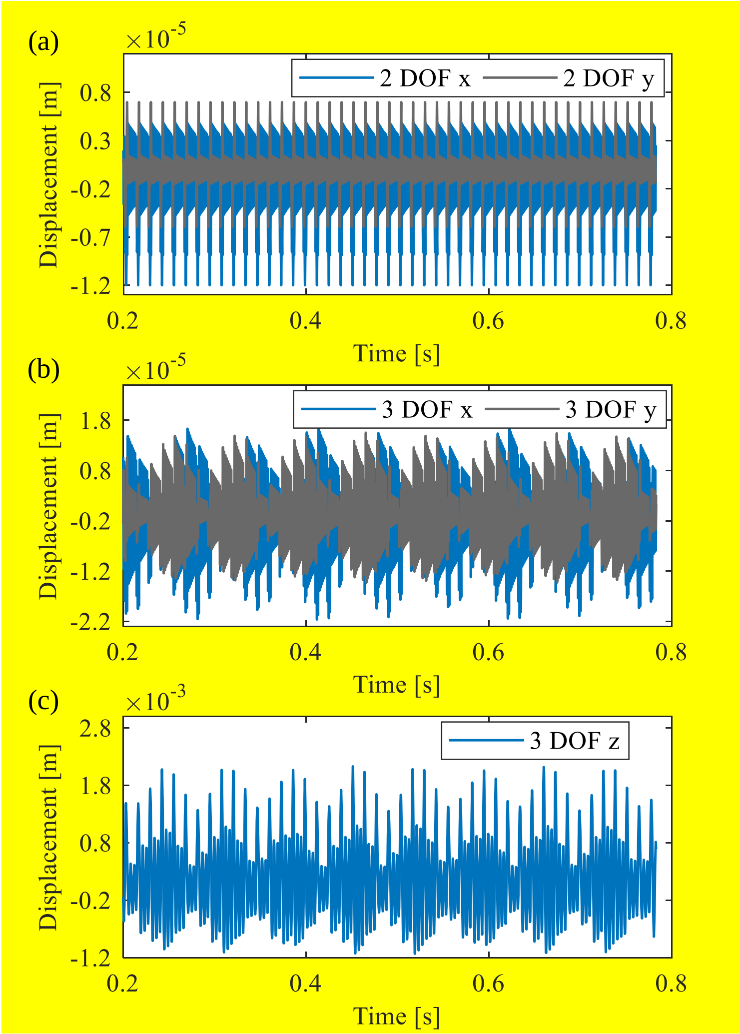

Figure A2. Simulated displacement time histories for P1 (4600 rpm, 3.5 mm), which is a stable point in 2 DOF, but chatter point in 3 DOF.

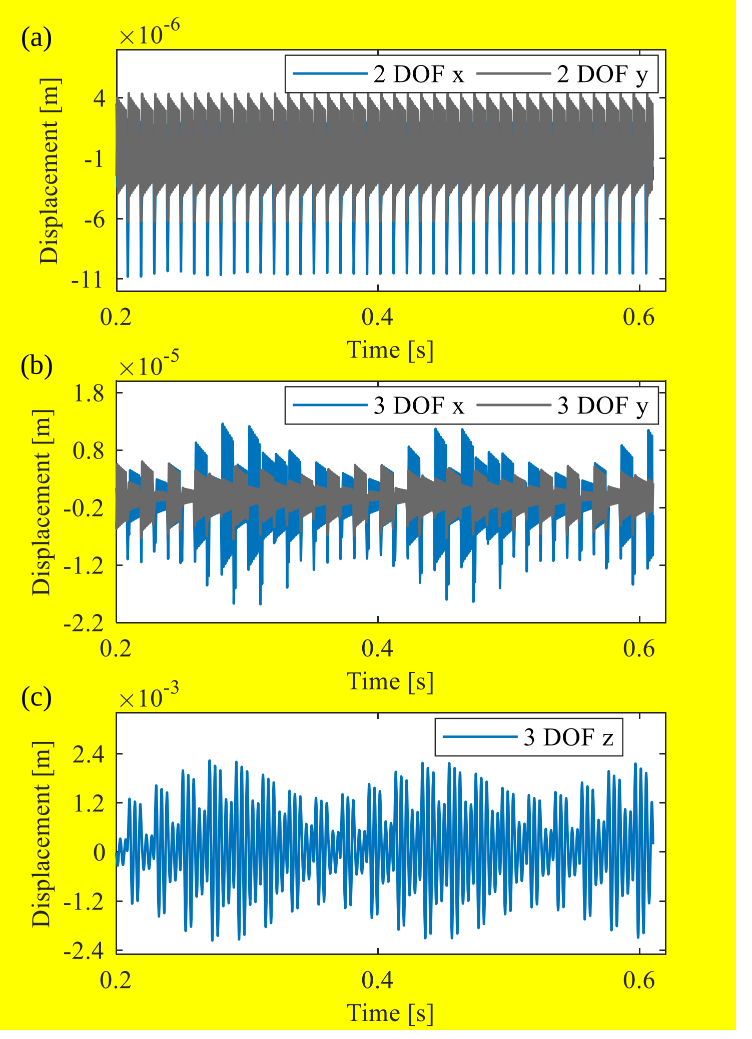

Figure A3. Simulated displacement time histories for P2 (5900 rpm, 1.5 mm), which is a stable point in 2 DOF, but chatter point in 3 DOF.

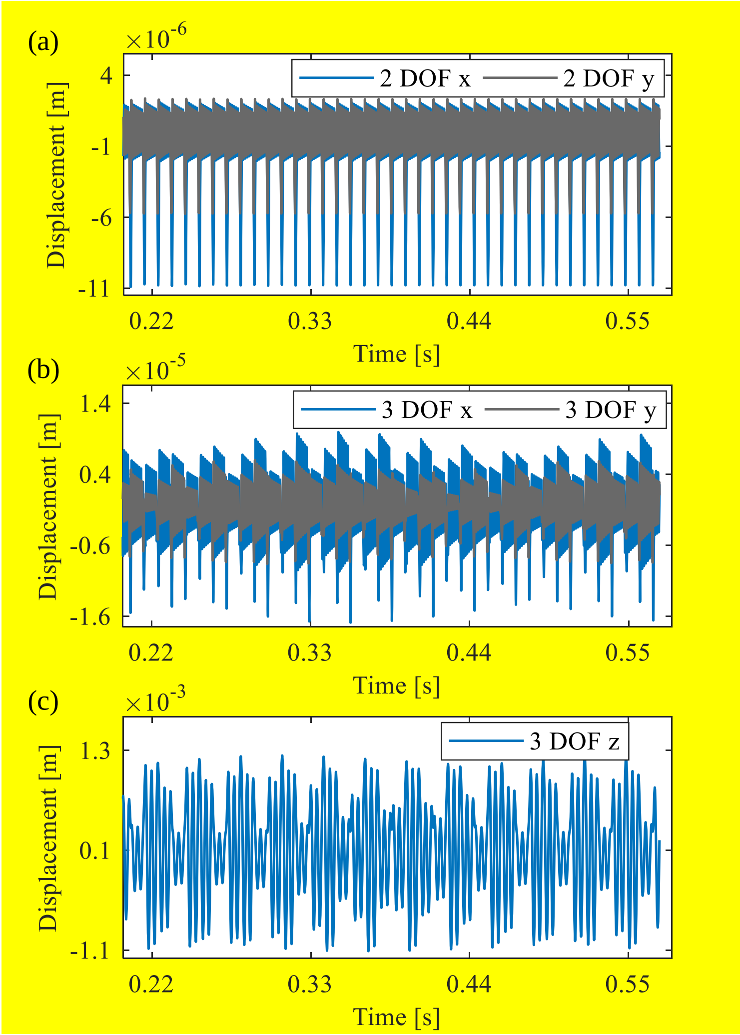

Figure A4. Simulated displacement time histories for P3 (6300 rpm, 1.6 mm), which is a stable point in 2 DOF, but chatter point in 3 DOF.

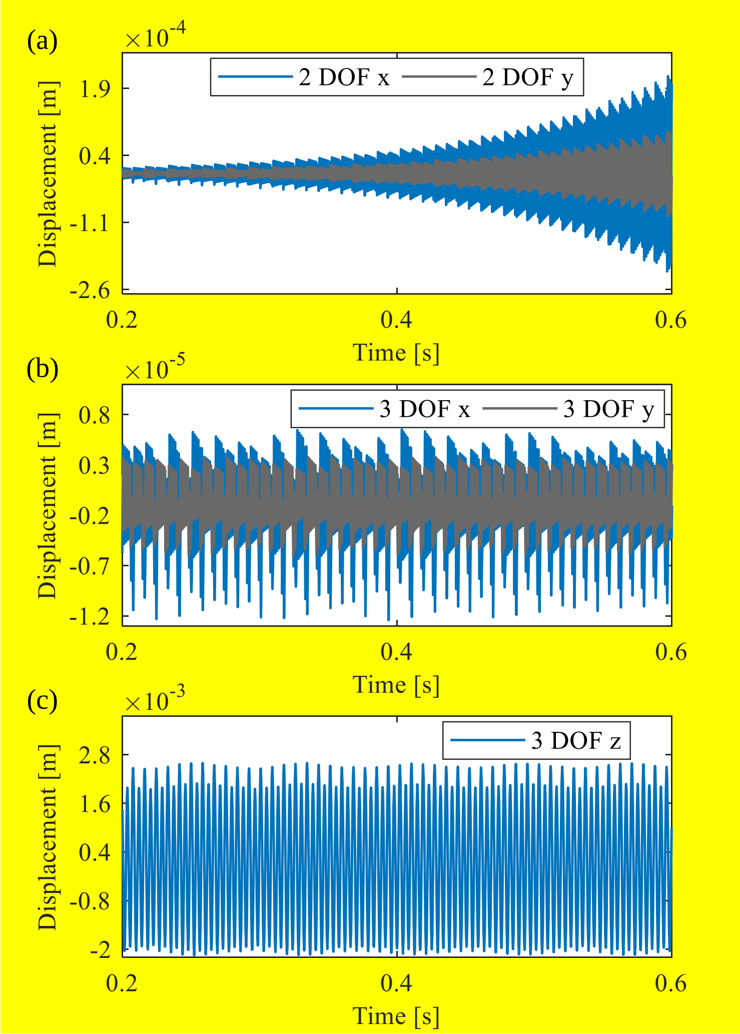

Figure A5. Simulated displacement time histories for P4 (7100 rpm, 2.1 mm), which is a chatter point in 2 DOF, but stable point in 3 DOF.

References

[1] M. Wan, X. Liang, Y. Yang, W. Zhang, Suppressing vibrations in milling-trimming process of the plate-like workpiece by optimizing the location of vibration absorber, Journal of Materials Processing Technology 278 (2020) 116499.

[2] G. Liu, J. Dang, W. Ming, Q. An, M. Chen, H. Li, High-quality machining of edges of thin-walled plates by tilt side milling based on an analytical force-based model, Journal of Manufacturing Science and Engineering 141 (2019) 61008.

[3] G. Liu, J. Dang, C. Li, W. Ming, Q. An, M. Chen, Investigation on the vibration and machined surface quality in tilt side milling of thin-walled plates, The International Journal of Advanced Manufacturing Technology 103 (2019) 2287-2300.

[4] J. Qiu, R. Ge, An improved stability lobe and turning chatter characteristic investigation, International Journal of Mechanical Sciences 149 (2018) 338-348.

[5] Y. Liu, Z. Liu, Q. Song, B. Wang, Development of constrained layer damping toolholder to improve chatter stability in end milling, International Journal of Mechanical Sciences 117 (2016) 299-308.

[6] Z. Fu, X. Zhang, X. Wang, W. Yang, Analytical modeling of chatter vibration in orthogonal cutting using a predictive force model, International Journal of Mechanical Sciences 88 (2014) 145-153.

[7] M. Wiercigroch, E. Budak, Sources of nonlinearities, chatter generation and suppression in metal cutting, Philosophical Transactions of the Royal Society of London. Series A: Mathematical, Physical and Engineering Sciences 359 (2001) 663-693.

[8] Y. Yan, J. Xu, M. Wiercigroch, Regenerative chatter in a plunge grinding process with workpiece imbalance, The International Journal of Advanced Manufacturing Technology 89 (2017) 2845-2862.

[9] Y. Yan, J. Xu, M. Wiercigroch, Regenerative and frictional chatter in plunge grinding, Nonlinear Dynamics 86 (2016) 283-307.

[10] S.D. Merdol, Y. Altintas, Multi frequency solution of chatter stability for low immersion milling, Journal of Manufacturing Science and Engineering 126 (2004) 459-466.

[11] Y. Altintas, E. Budak, Analytical prediction of stability lobes in milling, CIRP annals 44 (1995) 357-362.

[12] L. Cao, X.M. Zhang, T. Huang, H. Ding, Derived nodes approach for improving accuracy of machining stability prediction, Journal of Vibration and Acoustics 140 (2018) 31017.

[13] T. Huang, X.M. Zhang, H. Ding, A novel approach with smallest transition matrix for milling stability prediction, Nonlinear Dynamics 90 (2017) 95-104.

[14] T. Huang, X.M. Zhang, X.J. Zhang, H. Ding, An efficient linear approximation of acceleration method for milling stability prediction, International Journal of Machine Tools and Manufacture 74 (2013) 56-64.

[15] Y. Ding, L. Zhu, X. Zhang, H. Ding, A full-discretization method for prediction of milling stability, International Journal of Machine Tools and Manufacture 50 (2010) 502-509.

[16] J. Niu, Y. Ding, L. Zhu, H. Ding, Runge – Kutta methods for a semi-analytical prediction of milling stability, Nonlinear Dynamics 76 (2014) 289-304.

[17] W. Li, L. Wang, G. Yu, An accurate and fast milling stability prediction approach based on the Newton-Cotes rules,

International Journal of Mechanical Sciences 177 (2020) 105469.

[18] N.D. Sims, The self-excitation damping ratio: a chatter criterion for time-domain milling simulations, Journal of Manufacturing Science and Engineering 127 (2005) 433-445.

[19] A. Honeycutt, T.L. Schmitz, A new metrics for automated stability identification in time domain milling simulation, Journal of Manufacturing Science and Engineering 138 (2016) 74501.

[20] A. Honeycutt, T.L. Schmitz, Milling stability interrogation by subharmonic sampling, Journal of Manufacturing Science and Engineering 139 (2017) 41009.

[21] S. Smith, J. Tlusty, Efficient simulation programs for chatter in milling, CIRP Annals Manufacturing Technology 42 (1993) 463-466.

[22] H.Z. Li, X.P. Li, X.Q. Chen, A novel chatter stability criterion for the modelling and simulation of the dynamic milling process in the time domain, The International Journal of Advanced Manufacturing Technology 22 (2003) 619-625.

[23] M.L. Campomanes, Y. Altintas, An improved time domain simulation for dynamic milling at small radial immersions, Journal of Manufacturing Science and Engineering 125 (2003) 416-422.

[24] L. Zhongqun, L. Qiang, Solution and analysis of chatter stability for end milling in the time-domain, Chinese Journal of Aeronautics 21 (2008) 169-178.

[25] Y. Yan, J. Xu, M. Wiercigroch, Estimation and improvement of cutting safety, Nonlinear Dynamics 98 (2019) 2975-2988.

[26] Y. Yan, M. Wiercigroch, Dynamics of rotary drilling with non-uniformly distributed blades, International Journal of Mechanical Sciences 160 (2019) 270-281.

[27] Y. Yan, J. Xu, M. Wiercigroch, Modelling of regenerative and frictional cutting dynamics, International Journal of Mechanical Sciences 156 (2019) 86-93.

[28] Z. Zhang, H. Li, X. Liu, W. Zhang, G. Meng, Chatter mitigation for the milling of thin-walled workpiece, International Journal of Mechanical Sciences 138-139 (2018) 262-271.

[29] D. Wang, M. Löser, S. Ihlenfeldt, X. Wang, Z. Liu, Milling stability analysis with considering process damping and mode shapes of in-process thin-walled workpiece, International Journal of Mechanical Sciences 159 (2019) 382-397.

[30] X. Dang, M. Wan, W. Zhang, Y. Yang, Chatter analysis and mitigation of milling of the pocket-shaped thin-walled workpieces with viscous fluid, International Journal of Mechanical Sciences 194 (2021) 106214.

[31] A.R. Yusoff, N.D. Sims, Optimisation of variable helix tool geometry for regenerative chatter mitigation, International Journal of Machine Tools and Manufacture 51 (2011) 133-141.

[32] Z. Dombovari, G. Stepan, The effect of helix angle variation on milling stability, Journal of Manufacturing Science and Engineering 134 (2012) 51015.

[33] X. Zhang, J. Zhang, B. Pang, D. Wu, X. Zheng, W. Zhao, An efficient approach for milling dynamics modeling and analysis with varying time delay and cutter runout effect, The International Journal of Advanced Manufacturing Technology 87 (2016) 3373-3388.

[34] J. Niu, Y. Ding, L. Zhu, H. Ding, Mechanics and multi-regenerative stability of variable pitch and variable helix milling tools considering runout, International Journal of Machine Tools and Manufacture 123 (2017) 129-145.

[35] D. Zhan, S. Jiang, J. Niu, Y. Sun, Dynamics modeling and stability analysis of five-axis ball-end milling system with variable pitch tools, International Journal of Mechanical Sciences 182 (2020) 105774.

[36] N.D. Farahani, Y. Altintas, Chatter stability of serrated milling tools in frequency domain, Journal of Manufacturing Science and Engineering 144 (2021) 31013.

[37] P. Bari, Z.M. Kilic, M. Law, P. Wahi, Rapid stability analysis of serrated end mills using graphical-frequency domain methods, International Journal of Machine Tools and Manufacture 171 (2021) 103805.

[38] F. Tehranizadeh, K. Rahimzadeh Berenji, E. Budak, Dynamics and chatter stability of crest-cut end mills, International Journal of Machine Tools and Manufacture 171 (2021) 103813.

[39] X. Tang, F. Peng, R. Yan, Z. Zhu, Z. Li, S. Xin, Nonlinear process damping identification using finite amplitude stability and the influence analysis on five-axis milling stability, International Journal of Mechanical Sciences 190 (2021) 106008.

[40] Z. Li, O. Tuysuz, L. Zhu, Y. Altintas, Surface form error prediction in five-axis flank milling of thin-walled parts, International Journal of Machine Tools and Manufacture 128 (2018) 21-32.

[41] Y. Sun, S. Jiang, Predictive modeling of chatter stability considering force-induced deformation effect in milling thin-walled parts, International Journal of Machine Tools and Manufacture 135 (2018) 38-52.

[42] G. Totis, T. Insperger, M. Sortino, G. Stépán, Symmetry breaking in milling dynamics, International Journal of Machine Tools and Manufacture 139 (2019) 37-59.

[43] J. Niu, J. Jia, R. Wang, J. Xu, Y. Sun, D. Guo, State dependent regenerative stability and surface location error in peripheral milling of thin-walled parts, International Journal of Mechanical Sciences 196 (2021) 106294.

[44] Q. Song, X. Ai, J. Zhao, Design for variable pitch end mills with high milling stability, The International Journal of Advanced Manufacturing Technology 55 (2011) 891-903.

[45] V. Sellmeier, B. Denkena, Stable islands in the stability chart of milling processes due to unequal tooth pitch, International Journal of Machine Tools and Manufacture 51 (2011) 152-164.

[46] M. Wan, W. Zhang, J. Dang, Y. Yang, A unified stability prediction method for milling process with multiple delays, International Journal of Machine Tools and Manufacture 50 (2010) 29-41.

[47] A. Comak, E. Budak, Modeling dynamics and stability of variable pitch and helix milling tools for development of a design method to maximize chatter stability, Precision Engineering 47 (2017) 459-468.

[48] T. Hayasaka, A. Ito, E. Shamoto, Generalized design method of highly-varied-helix end mills for suppression of regenerative chatter in peripheral milling, Precision Engineering 48 (2017) 45-59.

[49] A. Otto, S. Rauh, S. Ihlenfeldt, G. Radons, Stability of milling with non-uniform pitch and variable helix Tools, The International Journal of Advanced Manufacturing Technology 89 (2017) 2613-2625.

[50] S. Jiang, D. Zhan, Y. Liu, Y. Sun, J. Xu, Modeling of variable-pitch/helix milling system considering axially varying dynamics with cutter runout offset and tilt effects, MECHANICAL SYSTEMS AND SIGNAL PROCESSING 168 (2022) 108674.

[51] S. Seguy, T. Insperger, L. Arnaud, G. Dessein, G. Peigné, On the stability of high-speed milling with spindle speed variation, The International Journal of Advanced Manufacturing Technology 48 (2010) 883-895.

[52] S. Sastry, S.G. Kapoor, R.E. DeVor, Floquet theory based approach for stability analysis of the variable speed face-

milling process, Journal of Manufacturing Science and Engineering 124 (2002) 10-17.

[53] E. Al-Regib, J. Ni, S. Lee, Programming spindle speed variation for machine tool chatter suppression, International Journal of Machine Tools and Manufacture 43 (2003) 1229-1240.

[54] A. Yilmaz, R.E. AL, J. Ni, Machine tool chatter suppression by multi-level random spindle speed variation, Journal of Manufacturing Science and Engineering 124 (2002) 208-216.

[55] M. Zatarain, I. Bediaga, J. Muñoa, R. Lizarralde, Stability of milling processes with continuous spindle speed variation: Analysis in the frequency and time domains, and experimental correlation, CIRP Annals 57 (2008) 379-384.

[56] S. Sébastien, D. Gilles, A. Lionel, I. Tamás, Control of chatter by spindle speed variation in high-speed milling, Advanced Materials Research 112 (2010) 179-186.

[57] G. Jin, H. Qi, Z. Li, J. Han, Dynamic modeling and stability analysis for the combined milling system with variable pitch cutter and spindle speed variation, Communications in Nonlinear Science and Numerical Simulation 63 (2018) 38-56.

[58] C. Wang, X. Zhang, R. Yan, X. Chen, H. Cao, Multi harmonic spindle speed variation for milling chatter suppression and parameters optimization, Precision Engineering 55 (2019) 268-274.

[59] X.H. Long, B. Balachandran, B.P. Mann, Dynamics of milling processes with variable time delays, Nonlinear Dynamics 47 (2006) 49-63.

[60] B. Pritam, L. Mohit, W. Pankaj, Improved chip thickness model for serrated end milling, CIRP Journal of Manufacturing Science and Technology 25 (2019) 36-49.

[61] A. Comak, Y. Altintas, Dynamics and stability of turn-milling operations with varying time delay in discrete time domain, Journal of Manufacturing Science and Engineering 140 (2018) 101013.

[62] T. Insperger, G. Stepan, F. Hartung, J. Turi, State dependent regenerative delay in milling processes., Long Beach, California USA, 2005, pp. 5138-5147.

[63] D. Bachrathy, G. Stépán, J. Turi, State dependent regenerative effect in milling processes, Journal of Computational and Nonlinear Dynamics 6 (2011) 41002.

[64] H.Z. Li, W.B. Zhang, X.P. Li, Modelling of cutting forces in helical end milling using a predictive machining theory, International Journal of Mechanical Sciences 43 (2001) 1711-1730.

[65] H. Li, X. Li, Modelling and simulation of chatter in milling using a predictive force model, International Journal of Machine Tools and Manufacture 40 (2000) 2047-2071.

[66] M.Y. Tsai, S.Y. Chang, J.P. Hung, C.C. Wang, Investigation of milling cutting forces and cutting coefficient for aluminum 6060-T6, Computers and Electrical Engineering 51 (2016) 320-330.

Declaration of interests

☒ The authors declare that they have no known competing financial interests or personal relationships that could have appeared to influence the work reported in this paper.

☐The authors declare the following financial interests/personal relationships which may be considered as potential competing interests:

Author statement

Sen-Lin Ma: Investigation, Methodology, Formal analysis, software, Data Curation, Writing - original draft, Writing - review & editing.

Tao Huang: Investigation, Methodology, Formal analysis, Supervision, Writing - review & editing, Funding acquisition.

Xiao-Ming Zhang: Investigation, Formal analysis, Supervision, Writing - review & editing, Funding acquisition.

Marian Wiercigroch: Investigation, Formal analysis, Writing - review & editing.

Ding Chen: Investigation, Methodology.

Han Ding: Supervision, Project administration, Funding acquisition.

Effect of state-dependent time delay on dynamics of trimming of thin-walled structures

Sen-Lin Ma[1, 2], Tao Huang[1 *], Xiao-Ming Zhang[1], Marian Wiercigroch[3], Ding Chen[1], Han Ding[1]

[1]State Key Laboratory of Digital Manufacturing Equipment and Technology, School of Mechanical Science and Engineering, Huazhong University of Science and Technology, Wuhan 430074, China

[2]Institute of Artificial Intelligence, Huazhong University of Science and Technology, Wuhan 430074, China

[3]Centre for Applied Dynamics Research, School of Engineering, University of Aberdeen, Kings College Aberdeen AB24 3UE, Scotland, UK

Abstract: Trimming of cantilever thin-walled structures is commonly seen in aerospace industry, including trimming of blades. Trimming with helix angle tools can cause the vibration of the thin-walled workpiece along the tool-axis, which may disturb the time delay between cutting by the current and previous teeth. The time delay dependent on the vibration state makes the stability analysis of trimming process challenging. This paper is the first attempt to uncover the effect of state-dependent time delay of the trimming process caused by workpiece vibration on chatter stability. Modeling of the cutter-workpiece interactions, state-dependent time delay and the dynamic chip generation mechanism are presented. A time-domain numerical algorithm with an improved stability metrics is constructed to analyze the trimming stability behaviors. We found that the two dominant states can occur, namely, period-n instabilities with time-varying time delay and stability with constant time delay. A focused experimental study was carried out to calibrate this new finding. This study reveals the way the workpiece vibration affects the time delay and stability in the trimming process.

Keywords: milling, thin-walled workpiece, trimming, state-dependent time delay, dynamic stability, bifurcations.

1 Introduction

Trimming of cantilever shape thin-walled workpieces is an important machining operation in aerospace, which has attracted a lot of attention in the recent years, e.g. [1-3]. Trimming is a special kind of milling operation, where a workpiece is clamped at one end forming a cantilever which edge is being milled. Traditional milling of thin-walled structures make walls thinner, while trimming

[*] Corresponding author: Tao Huang (tao.huang@hust.edu.cn)

make them shorter. Due to large flexibility of thin-walled structures, machining vibration in trimming processes is the key issue affecting machining efficiency and surface finish quality. In typical trimming operations of cantilever shaped thin-walled workpieces, generated vibration are large, which affect nominal cutter-workpiece engagements and they cannot be neglected like in other more traditional milling operations. Before embarking on modeling and analysis of trimming processes, related studies are critically reviewed in this section.

Chatter caused by regenerative effects may result in violent vibration, poor surface finish, lower tool life, and other negative effects. Therefore, it is of a great significance to avoid chatter for achieving high machining quality [4-9]. Constructing stability lobe diagrams is a low-cost way to acquire optimal machining parameters, where the frequency domain analytical methods [10, 11], time-domain semi-analytical methods [12-17] and time-domain numerical simulation methods [18-24] are popular methods. For strongly nonlinear coupling models which cannot be linearized, the time domain simulation method is often the only choice, but its high computational cost is prohibitive.

An accurate dynamic model is the key step for the chatter stability analysis. Classical dynamic models [25-30] consider geometric and kinematic relationships between the tool and the workpiece when describing cutter-workpiece engagement conditions, including start and exit immersion angles, instantaneous rotation angle of cutting element and instantaneous uncut chip thickness. For complex cases with tool runout and irregular geometry tool, although the cutter-workpiece engagement conditions are different for each tooth, cutter-workpiece engagement formulations in these models are still state-independent, which can be calculated without knowing the system vibration state. For example, Yusoff *et al.* [31] analyzed variable helix angle tool and introduced an optimisation algorithm to design variable helix angles to suppress chatter. Dombovari *et al.* [32] summarized cutting performance of non-uniform and harmonically varied helix cutters in case of high and low cutting speed conditions. Based on tooth trochoid motion, Zhang *et al.* [33] analyzed the milling stability by taking cutter runout into account. Niu *et al.* [34] obtained expressions of cutter-workpiece engagement of variable pitch and variable helix tools by taking tool runout into account. Zhan *et al.* [35] presented the dynamic model of five-axis ball-end tool with variable pitches. Recently, the dynamic stability of the serrated milling tool was analyzed by Farahani *et al.* [36] and Bari *et al.* [37]. The geometry of crest cut tool was modeled by Tehranizadeh *et al.* [38] and five-axis bull-nose end milling was modeled by Tang *et al.* [39].

For thin-walled workpiece milling, due to high flexibility and relatively small cutting parameters, the workpiece vibration amplitude is comparable to the nominal chip thickness. Therefore, the effect of cutting system vibration should be taken into account in side milling of thin-walled workpieces. Campomanes *et al.* [23] established a time-domain model to simulate dynamic milling at a very small radial cutting width. In their model, the exact trochoidal motion of the cutter was described by discretized cutter-workpiece kinematics and dynamics expressions, and the effects of changing radial cutting width caused by forced vibrations on chatter stability were investigated. Li *et al.* [40] analyzed the surface form errors caused by vibration of both flexible tool and workpiece in five-axis flank milling of thin-walled parts, where the time-varying stiffness of workpiece caused by material removal was also taken into account. Sun *et al.* [41] analyzed the effects of force-induced deformation calculated by the static stiffness on cutter-workpiece engagement. They found that the actual cutting width and cutting immersion angles deviate from the nominal values a lot and consequently the stability limits are changed. Totis *et al.* [42] developed a new model which considered the coupling relationship between cutting vibrations and cutter-workpiece engagement when the amplitude of steady-state vibrations is comparable to the instantaneous uncut chip thickness, but the linearization method was used to obtain the instantaneous uncut chip thickness rather than establishing the true coupling relationship formulae. Recently, Niu *el al.* [43] obtained the implicit cutter-workpiece engagement formulae by analyzing the teeth trajectories which are composed of cutting vibration, tool rotation and feed movement. In these literatures, the focuses are on the influence of cutting vibration along the tool radial direction on cutter-workpiece engagement. However, in trimming process of thin-walled parts, the engagement of cutter-workpiece is affected by the workpiece vibration along the tool axis. Therefore, not only the time delay but also the instantaneous rotation angle become state-dependent. This problem is yet to be investigated.

In addition to cutter-workpiece engagement, time delay in milling process plays a crucial role in dynamical stability, many studies have been conducted on variable time delay dynamic models. Song et al. [44] proposed an approach to design variable pitch tools with high milling stability based on a generalized expression of tooth engagement factor. Sellmeier and Denkena [45] observed the stable islands in the stability charts of unequally pitched end mills. Wan *et al.* [46] analyzed the characteristics of multiple delays in milling process by considering the effects of variable tooth pitch angle and tool runout. Comak and Budak [47] proposed an accurate design method for optimal selection of pitch angles to maximize chatter free material removal rate of variable pitch tools. Hayasaka *et al.* [48] presented a generalized design method for selection of highly-varied-helix end mills to suppress the regenerative chatter. Otto *et al.* [49] studied mechanical vibration in milling with non-uniform pitch and variable helix tools considering different factors (e.g., the nonlinear cutting force behaviour, the effect of runout et al.). Recently, Jiang *et al.* [50] analyzed the variable-pitch/helix milling process considering axially varying dynamics by taking cutter runout offset and tilt into account. These studies were conducted based on changing tool geometric parameters, time delay is generally proportional to the flute angles of milling tools and keeps discrete constant under a fixed spindle speed. For variable spindle speed milling, triangle-wave [51], sine-wave [52, 53], random [54, 55], and saw-tooth [56] are used to modulate spindle speed. Seguy *et al.* [51] analyzed the effect of spindle speed variation in the high spindle speeds domain and found that a variable spindle speed can effectively suppress period-doubling bifurcations and have no effect on Hopf bifurcations. Sastry *et al.* [52] analyzed the stability of the variable speed face milling based on the Floquent theory, and the milling chatter was effectively suppressed at low spindle speeds. Different methods, such as frequency-domain and time-domain discretization, were used to analyze the effect of variable speed on milling stability [55-57]. Wang *et al.* [58] adopted a multi-harmonic spindle speed variation to suppress milling chatter and the genetic algorithm is used to select optimal parameters. Although time delay is variable in the above models, it is regarded as a state-independent parameter. Even for trochoid tool path [59, 60] or the turn-milling operations [61], time delay is periodic time-varying, but not related to the system state. Few studies have been covered on state-dependent dynamic models. For example, Insperger *et al.* [62] modeled the state-dependent regenerative time delay in two degrees of freedom milling process. Latter, Bachrathy *et al.* [63] further proposed a comprehensive model which considers the effect of self-excited vibration of the milling tool and trochoidal path of the cutting edges on time delay, and they used a shooting method to analyze the nonlinear dynamic equations. Recently, Niu *et al.* [43] used numerical algorithms to analyze the stability and surface location error of milling thin-walled workpieces considering effects of cutting vibration, feed movement, tool rotation and tool runout on time delay.

Due to vibration induced time delay, dynamics of trimming is very different from dynamics of traditional milling processes. Time delay becomes state-dependent and is related to the workpiece vibration directly. In addition, the existing literature on trimming thin-walled workpiece mainly focuses on reducing the workpiece vibration amplitude. For example, Liu *et al.* [2] optimized the tool inclination angle based on an analytical 3D forces model to decrease the machined surface roughness and the vibration amplification in the side tilt milling of edges of thin-walled workpieces. They experimentally investigated the influence of tool helix angle and tilt angle on surface quality on the workpiece in trimming process [3]. Wan *et al.* [1] suppressed the vibration in trimming process of the plate-like workpiece by additional dynamic vibration absorbers (DVA) and they also optimized the location of DVA on the workpiece.

Simultaneous effects of state-dependent and time delays caused by workpiece vibration have not been yet comprehensively modelled and analyzed, which is the main aim of this work. Specifically, we develop here a novel dynamic model of trimming thin-walled cantilever plates by considering the effect of workpiece vibration along the tool axis on time delay and instantaneous rotation angle. Mechanisms explaining tool-workpiece interactions, state-dependent time delay and the dynamic chip generation will be discussed. Trimming stability will be investigated by computing and comparing stability lobe diagrams for mathematical models having various degree of complexity and fidelity including the developed here time-domain numerical algorithm with an improved stability metrics.

The remainder of the paper is structured as follows. In Section 2, a novel mathematical model to describe dynamics of thin-walled workpiece trimming is developed. Then in Section 3, the effects of state-dependent instantaneous rotation angle and time delay on trimming stability are modelled, where time delay is calculated by an iterative method and the time-domain numerical algorithm with improved stability metrics is proposed to analyze the trimming stability behaviors. In Section 4, simulation results and experimental validations are presented. Finally, some conclusions are drawn in Section 5.

2 State-dependent dynamic model of trimming

Trimming with helix angle tools can cause vibration of the thin-walled workpiece along the tool-axis, which may disturb the time delay between cutting by the current and previous teeth. In this section, we aim to construct the state-dependent dynamic model of trimming of thin-walled structures for further investigations of the effect of state-dependent time delay. First, the dynamic interactions between the tool and the workpiece are analyzed. Then, the expressions of state-dependent parameters such as instantaneous rotation angle, chip thickness and time delay are obtained. Last, the stability prediction method with an improved metrics in time-domain is proposed to investigate stability lobes.

A typical example of trimming is a compressor blade top cutting as shown in Figure 1 together with its physical model. For convenience of analysis, the structure is simplified to a cantilever thin-walled plate, which is depicted in Figure 1(b). To mathematically describe the process, a Cartesian coordinate system is used where X-axis and Z-axis are in the directions of feed and tool-axis, respectively, and Y-axis satisfies the right-hand rule. Four simplifying assumptions are adopted in the modelling:

(i) Only dynamics of the tool in X and Y-directions and the workpiece in Z-direction are considered as other directions are significantly stiffer.

(ii) Interactions during the cutting process are strongly nonlinear especially when the tool makes intermittent contacts with the workpiece. In this study we assume that the tool does not loose contact with the workpiece.

(iii) Effects of material removal on modal parameters are neglected hence the modal parameters of the dynamic system are assumed to be constant during cutting.

(iv) In trimming the width of cut is constant.

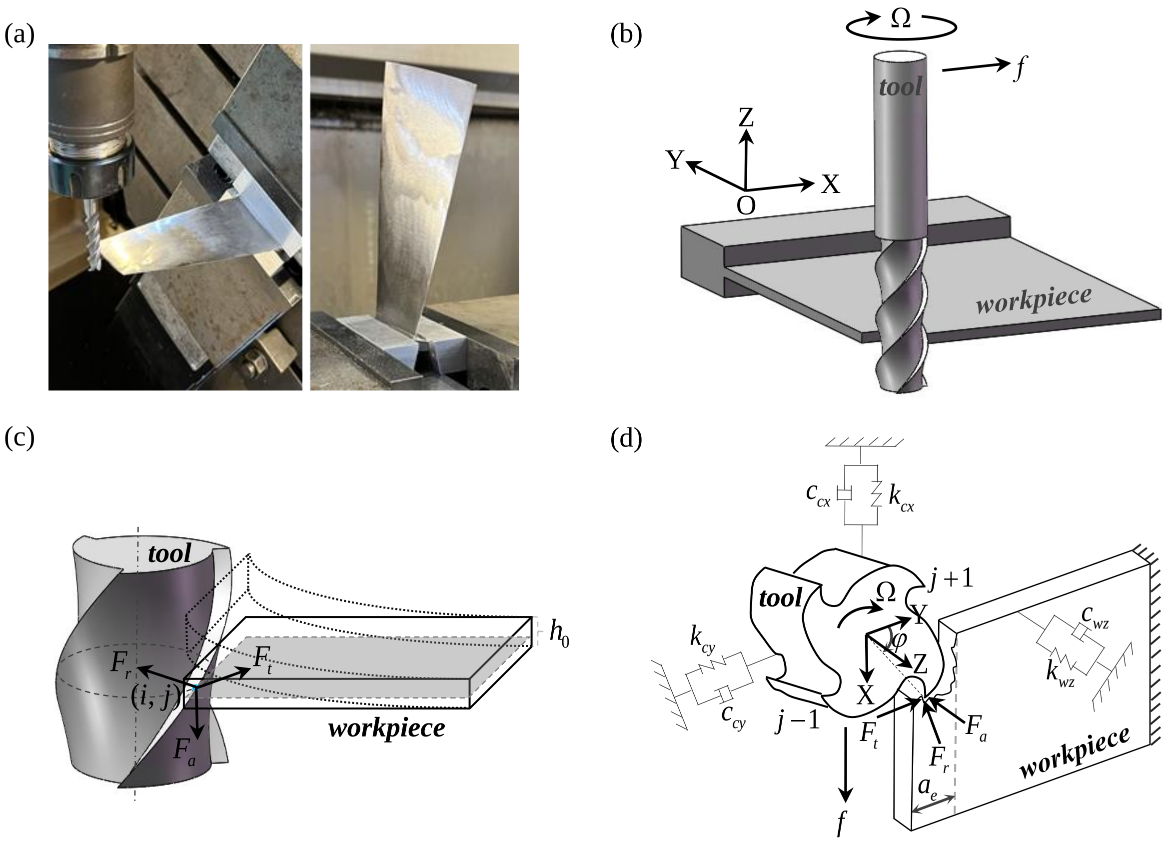

Figure 1. Dynamic interactions between the tool and the workpiece in trimming of thin-walled structures; (a) a typical example of trimming a compressor blade; (b) kinematics of the process; (c) cutting forces generated during the process; (d) physical model of the process where the tool and the workpiece supported three Kelvin-Voight pairs in *X*, *Y* and *Z* directions. To analyze the cutting forces of the tool, the workpiece is discretized into N_A number of slices along the *Z*-direction and the ***i***-th element of the workpiece is depicted by shaded area. The direction of the cutting forces on the tool, i.e. tangential F_t, radial F_r and axial F_a, components (i, j) are shown, where (i, j) represents the contact parts of the ***j***-th tooth and the ***i***-th element of the workpiece. One state of the workpiece vibration along the *Z*-direction is described by dashed lines.

The dynamic interactions occurring during the process can be derived from the Newton's second law, which in the fully nonlinear case can be represented in the matrix form using the generalized co-ordinates $\mathbf{q}$ as

$$\mathbf{M}(\mathbf{q})\ddot{\mathbf{q}}+\mathbf{C}(\mathbf{q})\dot{\mathbf{q}}+\mathbf{K}(\mathbf{q})\mathbf{q}=\mathbf{F}(\mathbf{q},\dot{\mathbf{q}}), \tag{1}$$

which after applying the simplifying assumptions (i) – (iv) can be reduced to its linearized matrix form given below:

$$\mathbf{M}\ddot{\mathbf{q}}+\mathbf{C}\dot{\mathbf{q}}+\mathbf{K}\mathbf{q}=\mathbf{F}(\mathbf{q},\dot{\mathbf{q}}). \tag{2}$$

Assuming that the nonlinear force, $\mathbf{F}(\mathbf{q},\dot{\mathbf{q}})$, for the steady state milling is a periodic function of time, $\mathbf{F}(t)=\mathbf{F}(t+T_r)$, is governed by the rotation speed of the tool with period T_r, the dynamics of the trimming process can be described in the familiar form for the manufacturing community by Eq. (3)

$$\mathbf{M}\ddot{\mathbf{q}}(t)+\mathbf{C}\dot{\mathbf{q}}(t)+\mathbf{K}\mathbf{q}(t)=\mathbf{F}(t), \tag{3}$$

where $\mathbf{M}=diag(m_{cx} \quad m_{cy} \quad m_{wz})$, $\mathbf{C}=diag(c_{cx} \quad c_{cy} \quad c_{wz})$ and $\mathbf{K}=diag\left(k_{cx} \quad k_{cy} \quad k_{wz}\right)$ are modal mass, damping and stiffness matrices, respectively, where the subscript c and w represent tool and workpiece, respectively. $\ddot{\mathbf{q}}(t)=[\ddot{x}_c(t) \quad \ddot{y}_c(t) \quad \ddot{z}_w(t)]^T$, $\dot{\mathbf{q}}(t)=[\dot{x}_c(t) \quad \dot{y}_c(t) \quad \dot{z}_w(t)]^T$ and $\mathbf{q}(t)=\left[x_c(t) \quad y_c(t) \quad z_w(t)-z_0-h_0/2\right]^T$ are the relative acceleration, velocity and displacement vectors between the tool and the workpiece at the time t, and $x_c(0)=0$, $y_c(0)=0$, $z_w(0)=z_0+h_0/2$, where z_0 is the distance between the workpiece bottom and the tool bottom at the initial time and h_0 is the thickness of the workpiece. $\mathbf{F}(t)=[F_x(t) \quad F_y(t) \quad -F_z(t)]^T$ is the force vector at the time t, $F_x(t)$, $F_y(t)$ and $F_z(t)$ are the cutting forces acting on the tool. Eq. (3) is nonlinear due to the cutting force and will be modeled in detail later on.

According to [64, 65], the milling process with helical angle cutters can be modeled as the simultaneous processes of cutting with a number of single-point cuts. In Figure 1(c), the workpiece is discretized into N_A number of slices along the *Z*-axis. Each slice are treated as single point oblique cutting which has an inclination angle of β (helix angle of the tool). The tangential force $F_t(t,i,j)$, radial force $F_r(t,i,j)$ and axial force $F_a(t,i,j)$ on cutting element ($i=1$, $j=1$) at time t are calculated as follow:

$$\begin{bmatrix} F_t(t,i,j) \\ F_r(t,i,j) \\ F_a(t,i,j) \end{bmatrix}=\left\{\begin{bmatrix} K_t \\ K_r \\ K_a \end{bmatrix} h(t,i,j)+\begin{bmatrix} K_{te} \\ K_{re} \\ K_{ae} \end{bmatrix}\right\}\Delta a, \tag{4}$$

where $\Delta a=h_0/N_A$ is the cutting depth of each slice; N_A denotes the number of axial discretization slices of the contact parts ($i=1,\cdots,N_A$) and N denotes the number of teeth ($j=1,\cdots,N$); $h(t,i,j)$ is the chip thickness of cutting element (i, j) at time t; and K_t, K_{te}, K_r, K_{re}, K_a, K_{ae} are the cutting force coefficients and edge force coefficients of tangential, radial and axial, respectively.

As shown in Figure 1(d), the milling resultant force in the *X*, *Y*, and *Z*-directions at time t can be expressed from the tangential, radial, and axial elemental forces and is shown as follow:

$$\begin{bmatrix} F_x(t) \\ F_y(t) \\ F_z(t) \end{bmatrix}=\sum_{i=1}^{N_A}\sum_{j=1}^{N}\left\{g(\varphi_{t,i,j})\begin{bmatrix} -\cos(\varphi_{t,i,j}) & -\sin(\varphi_{t,i,j}) & 0 \\ \sin(\varphi_{t,i,j}) & -\cos(\varphi_{t,i,j}) & 0 \\ 0 & 0 & 1 \end{bmatrix}\begin{bmatrix} F_t(t,i,j) \\ F_r(t,i,j) \\ F_a(t,i,j) \end{bmatrix}\right\}, \tag{5}$$

$$g(\varphi_{t,i,j})=\begin{cases} 1 \ \left(\text{if } \varphi_{st}<\operatorname{mod}(\varphi_{t,i,j},\ 2\pi)<\varphi_{ex}\right) \\ 0 \ (\text{otherwise}) \end{cases}, \tag{6}$$

$$\begin{cases} \varphi_{st} = \arccos\left(\frac{2a_e}{D} - 1\right), \ \varphi_{ex} = \pi \ (down\ milling) \\ \varphi_{st} = 0, \ \varphi_{ex} = \arccos\left(1 - \frac{2a_e}{D}\right) \ (up\ milling) \end{cases}, \tag{7}$$

where the $g(\varphi_{t,i,j})$ is a switch function to determine whether the infinitesimal cutting flute is involved in cutting or not. $\varphi_{t,i,j}$ is the instantaneous rotation angle of the cutting element (i, j) at time t. The start angle and the exit angle are φ_{st}, φ_{ex} respectively. a_e is width of cut, and D is the diameter of the tool.

3 Instantaneous rotation angle, chip thickness and time delay

Due to the large overhang of the workpiece, the stiffness of the workpiece is very low (refer to Table 1). Compared with the common vibration magnitude ranging from a few micrometers to tens of micrometers, the vibration amplitude of the workpiece in such trimming process could reach several millimeters, which is comparable to the workpiece thickness. In such case, the effect of workpiece vibration on the cutter-workpiece engagement needs to be taken into consideration.

In Figure 2(a), the motion track of the workpiece along the *Z*-direction at different times is illustrated where the positions of the workpiece at time t_0, t_1 and t_2 are also depicted. The location of the workpiece along the *Z*-direction is changing over time so that the cutter-workpiece engagement area becomes state-dependent. For a milling tool with N number of tooth rotating at spindle speed Ω rpm (revolution per minute), the instantaneous rotation angle of cutting element (i, j) at time t can be expressed as follow:

$$\varphi_{t,i,j} = \frac{2\pi\Omega}{60}t + \frac{(j-1)2\pi}{N} - \frac{2\tan\beta}{D}\left(z_w(t) - \frac{h_0}{2} + (i-1)\Delta a\right). \tag{8}$$

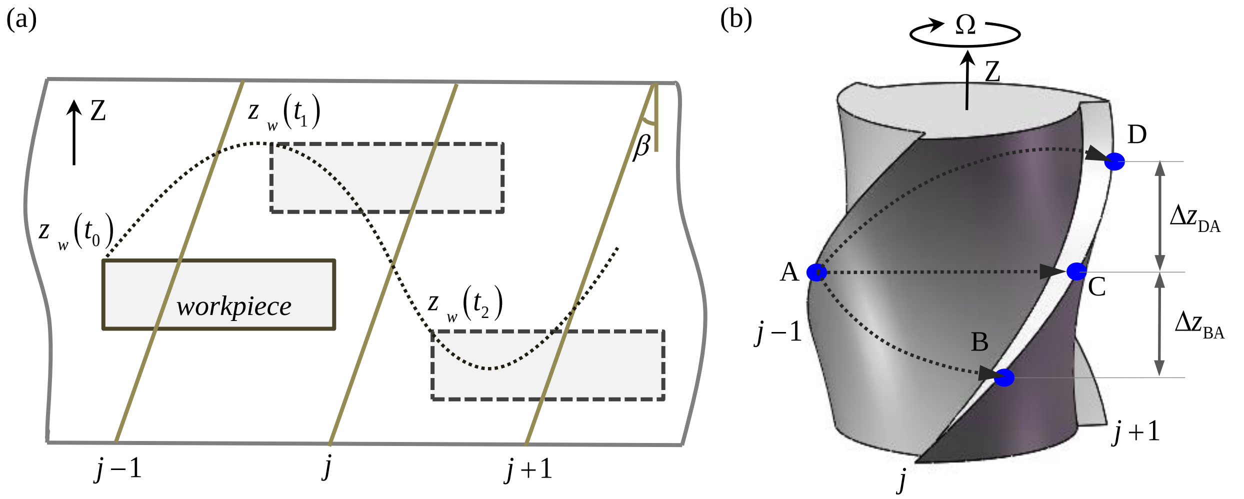

Figure 2. State-dependent instantaneous rotation angle $\varphi_{t,i,j}$ and time delay $\tau(t)$; (a) The tool circumference is expanded where a schematic diagram showing the vibration track of the workpiece along the *Z*-direction and the positions of the workpiece at three different times is presented. Due to the workpiece vibration, the contact parts of workpiece and tool along the *Z*-direction is time-varying. (b) Set point A as the cutting element $(i, j-1)$, due to the workpiece vibration, the corresponding cutting element (i, j) may be point B, C or D. Thus, the time interval between the current and previous teeth is changed, which means time delay is state-dependent and time-varying.

The instantaneous uncut chip thickness at the time t consists of two parts, i.e., the static part contributed by the feed motion and the dynamic part by the vibration of the tool, respectively. The variable uncut chip thickness can be expressed as follow:

$$h(t,i,j) = f\tau(t)\sin(\varphi_{t,i,j}) + \left[\sin(\varphi_{t,i,j}) \quad \cos(\varphi_{t,i,j})\right]\begin{bmatrix} x_c(t) - x_c(t-\tau(t)) \\ y_c(t) - y_c(t-\tau(t)) \end{bmatrix}, \tag{9}$$

where f is the feed rate, $\tau(t)$ is the time delay between the current and previous teeth at time t; $x_c(t-\tau(t))$, $y_c(t-\tau(t))$ are the tool vibrations in *X*, *Y*-directions at time $t-\tau(t)$, respectively.

Although the expression of the chip thickness $h(t,i,j)$ has been obtained from Eq. (9), the time delay $\tau(t)$ remains undetermined. In Figure 2(b), set point A as the cutting element $(i, j-1)$, if the vibration of the workpiece in *Z*-direction is neglected, the cutting element (i, j) is C, and the time delay is equal to tooth period T. However, when the workpiece vibration in *Z*-direction is considered, the cutting element (i, j) may be B, C or D, and the time interval between the current and previous teeth is changed. Thus, the time delay $\tau(t)$ may decrease, increase or remain unchanged. The state-dependent time delay can be modeled by Eq. (10) as shown below:

$$\begin{cases} \Delta z_w(t) = z_w(t) - z_w(t-\tau(t)) \\ \Delta\varphi(t) = \dfrac{2\tan\beta}{D}\Delta z_w(t) \\ \tau(t) = T + \dfrac{\Delta\varphi(t)}{2\pi}TN \end{cases}, \quad (10)$$

where $\Delta z_w(t)$ is the regenerative vibration of the workpiece, $\Delta\varphi(t)$ is the rotation angle variation between previous and current teeth caused by the workpiece vibration. According to Eq. (10), the time delay $\tau(t)$ can be rewritten as follow:

$$\tau(t) = T + \frac{2\tan\beta}{D}\left(z_w(t) - z_w(t-\tau(t))\right)\frac{TN}{2\pi}. \quad (11)$$

Substituting Eq. (11) into Eq. (9), the expression of chip thickness $h(t,i,j)$ can be rewritten as follow:

$$\begin{cases} f_t^{'} = f_t\left(1 + \left(z_w(t) - z_w(t-\tau(t))\right)\dfrac{N\tan\beta}{\pi D}\right) \\ h(t,i,j) = f_t^{'}\sin(\varphi_{t,i,j}) + \left[\sin(\varphi_{t,i,j}) \quad \cos(\varphi_{t,i,j})\right]\begin{bmatrix} x_c(t) - x_c(t-\tau(t)) \\ y_c(t) - y_c(t-\tau(t)) \end{bmatrix} \end{cases}, \quad (12)$$

where f_t is the nominal feed per tooth, $f_t^{'}$ is the actual feed per tooth. From Eq. (11), we can conclude that time delay depends not only on process parameters and tool geometry, but also on the vibration state. Moreover, time delay in trimming model is related to the regenerate effect of the workpiece vibration. The expression of the time delay, Eq. (11), is implicit so that we propose to calculate it by an iterative method. And from Eq. (12), due to the effect of time-varying time delay, the actual feed per tooth is not equal to the nominal feed per tooth f_t, and it is also changing due to the regenerate effect of the workpiece vibration.

To compute complex and interwoven nonlinear relationships between chip thicknesses and generated cutting forces, dynamical responses and time delay need to be evaluated in the sequence shown in Figure 3. This demonstrates that time delay is state-dependent, and can also affect the dynamic response.

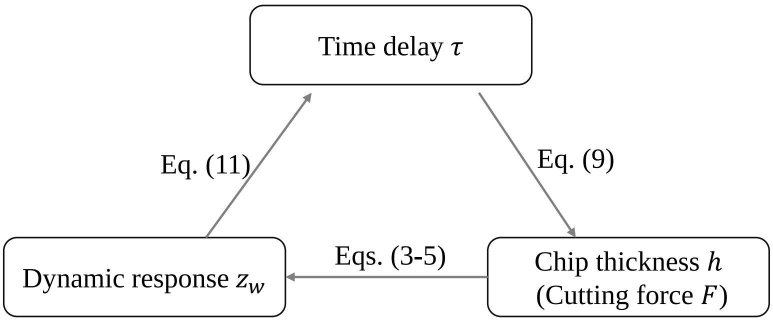

Figure 3. Sequential relationships between time delay, dynamic response and chip thickness. Dynamic response z_w affects time delay τ as described in Eq. (11), time delay affects uncut chip thickness h captured by Eq. (9) and uncut chip thickness affects dynamic response by Eqs (3-5).

The dynamic model of trimming process has a strong nonlinearity hence no suitable linearization method is readily available to analyze its stability efficiently, so that the time-domain numerical simulation method is adopted. The time-domain simulation process is based on the scheme proposed in [19]. For a given spindle speed and width of cut, the simulation time duration t_{end} is equal to the time 120 revolutions. Time increment Δt is calculated from Eq. (13) to ensure that the tooth period is divided into integer interval.

$$\Delta t = T / \mathrm{ceil}\left(T / \Delta t_0\right), \tag{13}$$

where 'ceil(λ)' is the function that takes as input a real number λ and gives as output the nearest integer greater than or equal to λ, and $\Delta t_0 = 1\times10^{-6}$ s.

Time delay $\tau(t)$ is calculated by an iterative search method and the procedure is explained in Appendix A. The milling forces are calculated by Eq. (5) and the dynamic displacements of the tool in *X* and *Y*-directions and the workpiece in *Z*-direction can be obtained by using the explicit Euler method by integrating the Eq (3). Subharmonic sampling strategy proposed by Schmitz et al. [20] combined with a new stability metrics Eq. (14) is used to detect different milling states, e.g., stability and milling bifurcation phenomenon.

$$M_n = \frac{\sum_{i=2}^{N_s} \left| z_{sn}(i) - z_{sn}(i-1) \right|}{N_s}, \tag{14}$$

where z_{sn} is the vector of z_w displacements sampled once every n tooth period, and N_s is the length of the z_{sn} vector. In order to avoid the effect of free vibration, we have truncated the output signals z_w to remove the first 67%.

When compared with the conventional stiffness of the milling systems, the stiffness of the workpiece in this study is very low (refer to Table 1), hence the vibration amplitude of the workpiece in trimming process can reach 1~2 millimeters rather than a few micrometers or tens of micrometers.

Therefore, the improved stability metrics is proposed, the order of magnitude of the vibration displacements z_w is changed by $z_s = z_w / 10^{\eta}$ before calculating M_n, where η is a positive integer, and η is set to 2 in this study. The flow chart of the algorithm for constructing the stability lobe diagram is shown in the **Appendix B**, where $\Delta\Omega$ and a_e are the interval value of spindle speed and width of cut, respectively.

4 Numerical simulation and experimental validation

The proposed state-dependent dynamic model of trimming and numerical algorithm with improved stability metrics will be validated with simulations and experiments in this section. The workpiece is made of Aluminum Alloy 7075 and as 100 mm × 60 mm × 2 mm thin-walled plate with 80 mm overhang. The stiffness is low in *Z*-direction while strong enough in *X* and *Y*-direction. To focus on the effect of state-dependent time delay and instantaneous rotation angle caused by workpiece vibration, a single tooth ($N = 1$) tool is adopted with diameter $D = 8$ mm, helix angle $\beta = 45^{\circ}$ and overhang $L = 20$ mm to ensure enough stiffness of the tool. The tool originally had two teeth but one of the teeth is removed by grinding wheel to avoid disturbances, e.g., tool runout.

4.1 Identification of dynamic parameters

The identification experiment of cutting force coefficients was carried out similar to that in Ref [66]. In order to avoid the effect of cutting vibration and bottom edge cutting on cutting force, the thin-walled plate with 4 mm overhanging length was cut by side milling with 3.5 mm width of cut. The cutting forces were measured by a dynamometer with the sampling frequency was set to 20 kHz. The identified cutting coefficients parameters are K_a=481 N/mm^2 and K_{ae}=2.0 N/mm.

The experimental modal test was performed on the workpiece with impact hammer, accelerometer, and data acquisition system. Two different points on the workpiece are measured. The distance between the two points along the *X*-direction is 10mm and the connecting line between the two points is parallel to the *X*-direction. Modal parameters including modal mass, natural frequency, damping ratio and stiffness calculated by rational fraction polynomial fitting algorithm are shown in Table 1, and the measured and fitted FRFs are compared in Figure 4. It is seen that the modal curves of the two points are almost the same, which indicates that the modal parameters of the two positions are basically the same. The data of Measurement-1 is used to calculate the stability lobe diagram. As the stiffness along the *X*-direction of the thin-walled structure changes gradually, we used a narrow area of the workpiece to carry out the simulations and experiments so that the stiffness variation along the workpiece edge is small. This is confirmed by the modal data of Measurement-1 and of Measurement -2, which are almost the same as can be see in Figure 4 and Table 1.

Table 1. Identified modal parameters of the experimental milling system.

Mode	Order	Frequency (Hz)	Mass (kg)	Damping ratio (%)	Stiffness (N/m)
Measurement-1	1st	243.12	0.0084	0.8720	1.9707×10^4
	2nd	755.75	0.0138	0.2187	3.1093×10^5
Measurement-2	1st	243.05	0.0086	1.0249	2.007×10^4
	2nd	755.79	0.0174	0.2445	3.9161×10^5

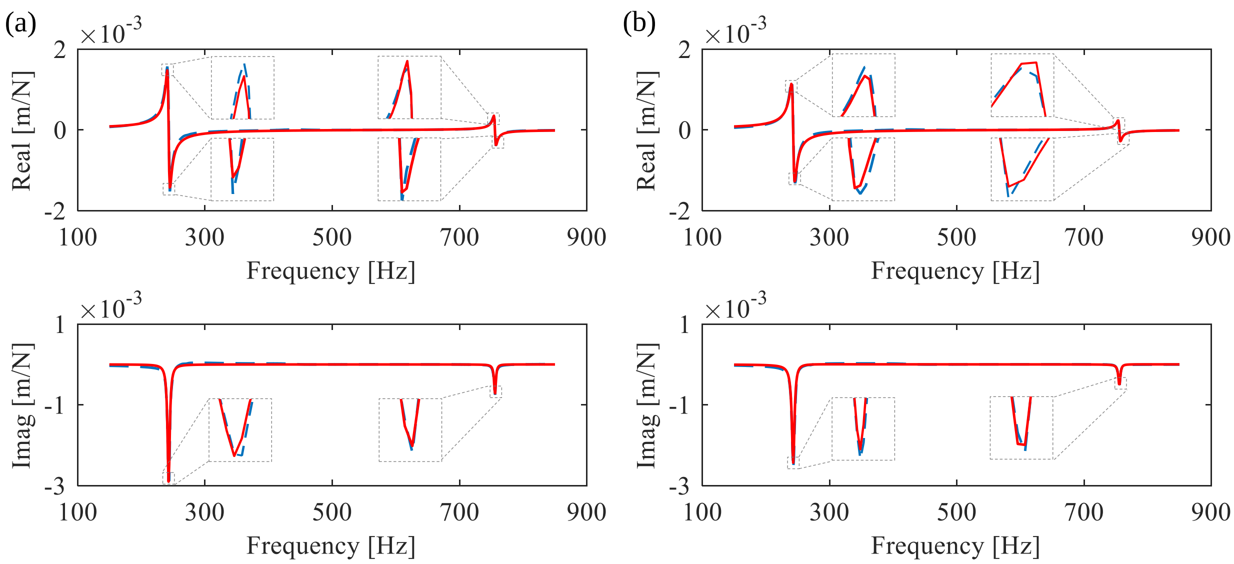

Figure 4. FRF of the workpiece in *Z*-direction. The blue dash lines and red solid lines represent the measured and fitted results, respectively. Data of two different points on the workpiece is shown in (a) and (b). The distance between the two points along the *X*-direction is 10mm and the connecting line between the two points is parallel to the *X*-direction. The modal curves of the two points are almost the same, which indicates that the modal parameters of the two positions are basically the same. The experimental modal tests are conducted 3 times on each point and the set of data of measured frequency response have been averaged in ModalView software.

4.2 Prediction of stability charts

Since the dynamic response z_w depends on uncut chip thickness, uncut chip thickness depends on time delay and time delay depends on dynamic response, the dynamic model of trimming process exists complex nonlinear coupling relationships. In order to analyze the stability property of the trimming process, we set cutting conditions with up milling, $f_t = 0.03$ mm to draw the stability lobe diagram. The range of spindle speed is 3000 to 6300 rpm with the step of 100 rpm and radial width is 1.0 to 5.0 mm with the step of 0.1 mm. Stability solution presented in the last part of Section 3 is used to predict stability and bifurcation types. First, the simulation time duration t_{end} is divided equally with time increment Δt. Then, time delay, cutting forces and vibration displacements are calculated by Eq. (11), Eq. (5) and Eq. (3) for each time step, respectively. The vibration displacement of the workpiece z_w is selected to calculate the stability metrics M_n by Eq. (14). Last, the subharmonic sampling strategy is used to analyze the dynamic behaviors of milling process. This procedure is carried out for every combination of spindle speed and width of cut within the given range, specifically from 3000 to 6300 rpm and from 1.0 to 5.0 mm. The computed stability lobe diagram is shown in Figure 5(a), where blank and blue areas indicate stable and chatter regions respectively. Hopf bifurcations are marked by red dot and period-2 bifurcations by blue circles. The peak-to-peak (PTP) diagram proposed by Smith and Tlusty [21] is also plotted in Figure 5(b). The boundaries of the two-lobe diagrams are roughly the same, which shows the validity of the improved stability metrics.

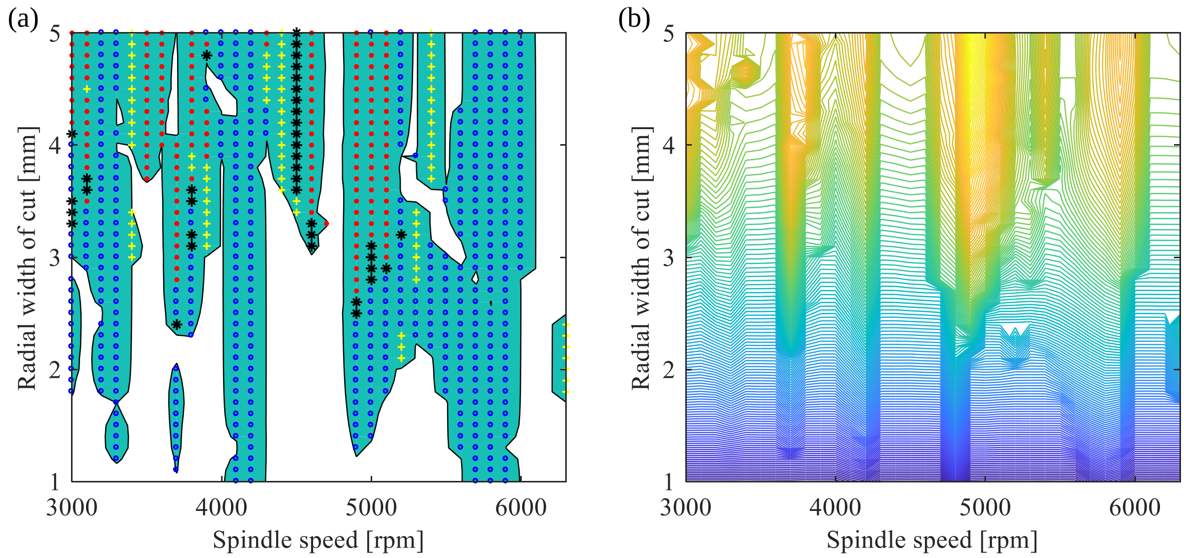

Figure 5. Example results of dynamic stability for the trimming process; (a) stability lobe diagram plotted using time-domain numerical simulation with the improved stability metrics; (b) Peak-Po-Peak (PTP) diagram plotted using the cutting force in *Z*-direction.; In the panel (a), the blank area is the stable area and the blue area is the chatter area. Some unstable points such as Period-2 (blue circle ‘o’), period-3 (yellow plus sign ‘+’), period-4 (black asterisk ‘*’), and secondary Hopf or high order period-n (red dot ‘.’) are marked with different symbols and colors. The stable boundaries of the two-lobe diagrams calculated by different methods are roughly the same, which shows the validity of the improved stability metrics.

For stable trimming process (such as $\Omega = 6100\,\text{rpm}$, $a_e = 3.0\,\text{mm}$), the workpiece vibration is periodic with tooth period (forced vibration only), the motion trajectories of the workpiece as well as the corresponding 1/revolution-sampled points (‘•’ pitch-label) is plotted in Figure 6(a). Only a single group of points is observed in the Poincaré map for once per tooth sampling which is shown in Figure 6(b). Figure 6 indicates that the axial height difference of the workpiece vibration between current and previous teeth is zero so that time delay calculated by Eq. (11) converges to a constant value, which is seen in Figure 7.

Instantaneous rotation angle $\varphi_{t,i,j}$ is a linear function of time if the workpiece vibration are neglected. However, in this study, the instantaneous rotation angle $\varphi_{t,i,j}$ depends on the vibration displacement of workpiece which is time-varying so that the instantaneous rotation angle changes nonlinearly. As the chip thickness and cutting force are closely related to the instantaneous rotation angle, these values are also changed at different time rather than phase shifts. In Figure 8, the instantaneous rotation angle $\varphi_{t,i,j}$ of the cutting element ($i=1$, $j=1$) and the Z-direction cutting force of the tool at different time are plotted. Comparing with the case that workpiece is rigid, the cutting force with considering the workpiece vibration changes at different time. The start and end time of the engagement between the cutter and the workpiece is different and t_1 is less than t_2 (t_1 and t_2 are the cutting time when the workpiece is regarded rigid and flexible, respectively.), which indicates that the state-dependent rotation angle $\varphi_{t,i,j}$ caused by the workpiece vibration changes the actual engagement time in each tooth period.

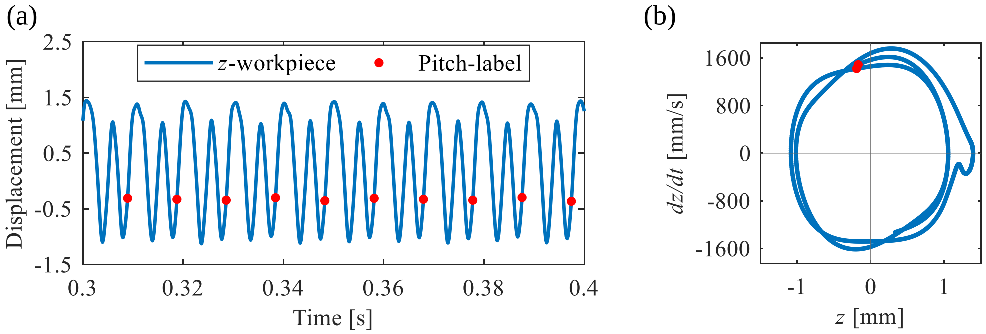

Figure 6. Stable trimming behaviour obtained for $\Omega = 6100$ rpm and $a_e = 3.0$ mm; (a) time history of workpiece vibration displacement in Z-direction and pitch label displacement 1/rev; (b) phase portrait and Poincaré map (red point).

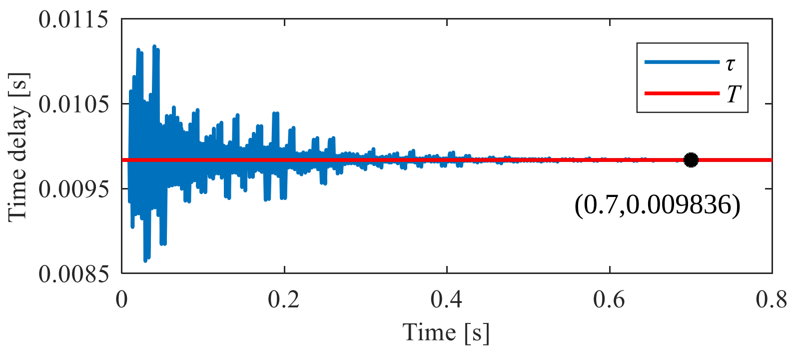

Figure 7. Simulated time delay and tooth period for $\Omega = 6100$ rpm and $a_e = 3.0$ mm. For stable trimming, the time delay converges to the tooth period $T = 0.009836$ s.

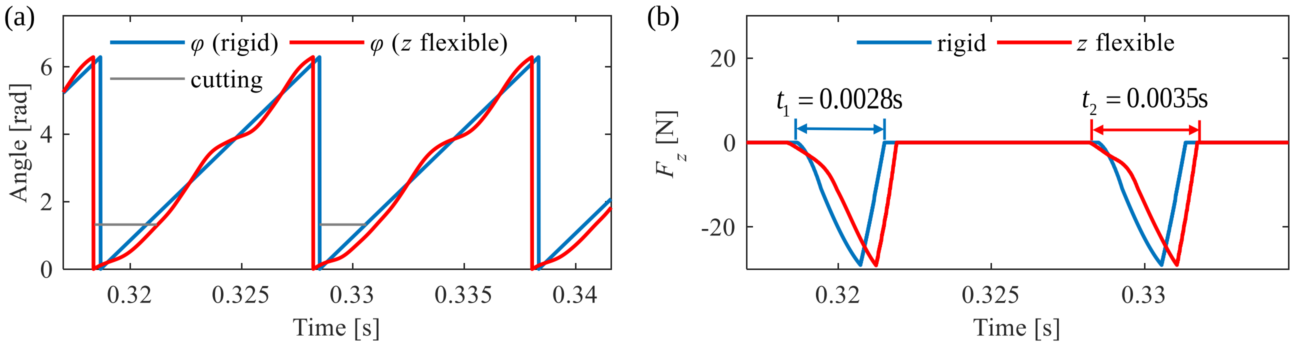

Figure 8. Comparison of the instantaneous rotation angle and cutting force between flexible and rigid workpieces with $\Omega = 6100$ rpm and $a_e = 3.0$ mm; (a) the instantaneous rotation angle φ of the cutting element ($i=1$, $j=1$) at different time. When workpiece vibration is considered, φ changes nonlinearly, and the engagment time of tool-workpiece is also shown by 'cutting'; (b) the cutting force of the tool in *Z*-direction at different time. t_1 and t_2 are the cutting duration when workpiece is regarded rigid or flexible, respectively, where t_2 is 25% longer than t_1 .

For the period-*n* bifurcation, the motion trajectories of the workpiece vibration repeat every *n* tooth periods, and the sampled points appear at n distinct locations in the Poincaré map. Taking period-2 bifurcation trimming (such as $\Omega = 4100$ rpm, $a_e = 3.5$ mm) as an example, the cutting force of the tool in *Z*-direction as well as the corresponding 1/revolution-sampled points ('•' pitch-label) is plotted in Figure 9(a). The Poincaré map of the workpiece vibration displacement for once per tooth period sampling is shown in Figure 9(b), which indicates that period-2 bifurcation occurs.

In order to analyze the characteristics of period-2 bifurcation in the proposed model, the state-dependent time delay is shown in Figure 10, the instantaneous rotation angle and chip thickness of the cutting element ($i=1$, $j=1$) at different time are plotted in Figure 11. In period-2 bifurcation trimming, the time delay is time-varying and its maximum change is nearly 8% compared with the tooth period. The variation period of the time delay is consistent with the vibration period of the workpiece. Similarly to the stable trimming, the instantaneous rotation angle changes nonlinearly in period-2 bifurcation trimming, but its period has changed. Comparing the uncut chip thicknesses with (h_2) and without (h_1) considering the workpiece vibration, we find that the phase of h_1 and h_2 is different, and the cutting thickness h_1 does not change completely smoothly in one of the tooth periods. It is noted that the sharp change of h_2 in Figure 11(b) is reasonable because of the sudden change of the time delay at the corresponding time node.

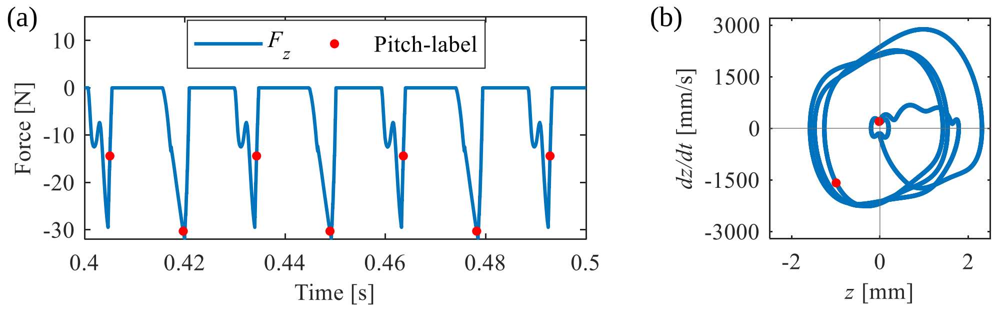

Figure 9. Period-2 bifurcation with $\Omega = 4100$ rpm and $a_e = 3.5$ mm; (a) the cutting force of tool in *Z*-direction and pitch label cutting force 1/rev; (b) phase portrait and Poincaré map (red point).

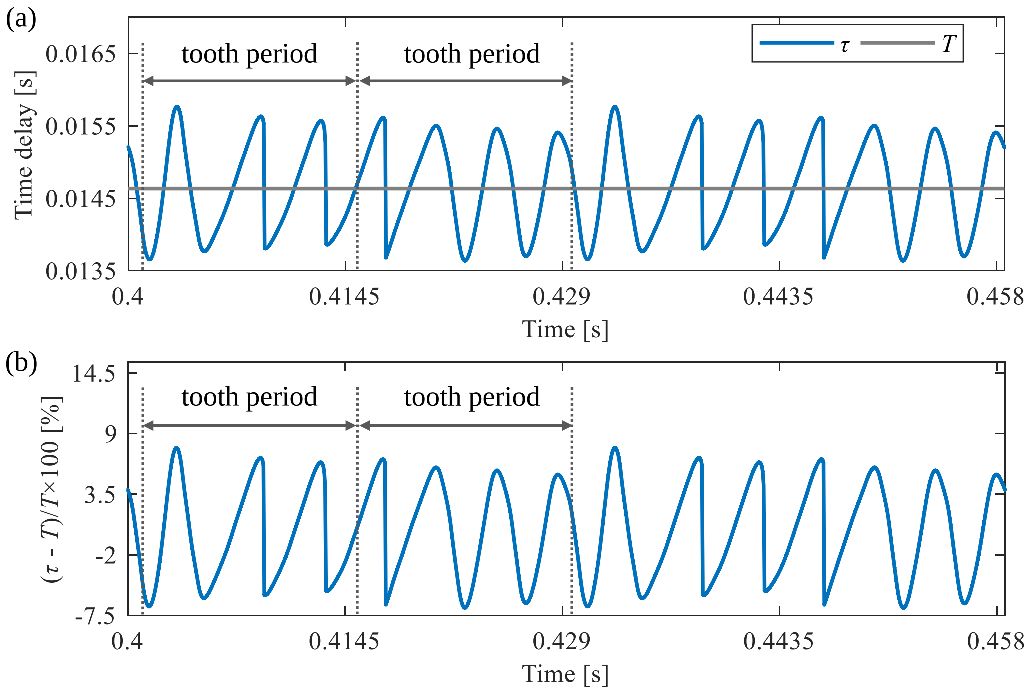

Figure 10. Simulated time histories for time delay, tooth period and change rate with $\Omega = 4100$ rpm and $a_e = 3.5$ mm; (a) For period-2 bifurcation trimming, the time delay is time-varying, and the maximum and minimum values are 0.01578 s and 0.01356 s, respectively. The tooth period is 0.01463 s. (b) Use the equation $(\tau - T)/T \times 100$ to calculate the change rate, and the maximum value is nearly 8%.

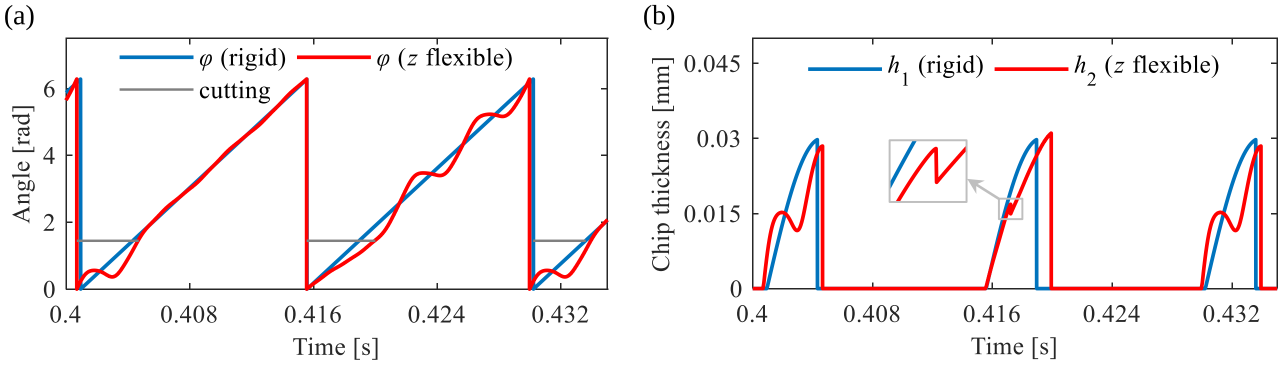

Figure 11. Comparisons between state-dependent and independent dynamics for $\Omega = 4100$ rpm and $a_e = 3.5$ mm; (a) the instantaneous rotation angle φ of the cutting element ($i=1, j=1$) at different time; (b) the instantaneous chip thickness of the cutting element ($i=1, j=1$) at different time. When the workpiece vibration is considered, φ changes nonlinearly, and the engagement duration of tool-workpiece is also shown by 'cutting'. h_1 is the static cutting thickness without considering the workpiece vibration, h_2 is the dynamic cutting thickness.

4.3 Discussion on engagement conditions and stability analysis

As explained in Section 3.2, the actual cutting duration will be changed at stable trimming process when workpiece vibration is taken into account. In order to further investigate this phenomenon, we have analyzed the change rate trend of cutting duration at the same spindle speed and different width of cut or at different spindle speeds and the same width of cut. The results are shown in Figure 12(a) and (b). In Figure 12(a), for low spindle speeds (such as $\Omega = 3500$ rpm, $\Omega = 4500$ rpm), with the increase of width of cut, the change rate of cutting duration decreases. However, for high spindle speeds such as $\Omega = 6100$ rpm, $\Omega = 6200$ rpm, with the increase of width of cut, the change rate of cutting duration increases first and then decreases. In Figure 12(b), when width of cut a_e is set to 1.5 mm, with the increase of spindle speed, the change rate of cutting duration also increases. And when the width of cut a_e is set to 2.0 or 2.5 mm, with the increase of spindle speed, the change rate of cutting duration only fluctuates slightly, which indicates that the change of spindle speed has little effect on cutting duration at these widths of cut.

The same strategy is adopted to analyze the variation trend of the change rate of time delay at period-2 bifurcation trimming process and the results are shown in Figure 12(c) and (d). In Figure 12(c), with the increase of width of cut, the maximum change rate of time delay also increases for spindle speeds $\Omega = 4100$ rpm and $\Omega = 5900$ rpm. However, for the spindle speeds, $\Omega = 4200$ rpm and $\Omega = 5800$ rpm, the maximum change rate of time delay remains basically unchanged with the increase of width of cut. These four curves are far apart from each other along the vertical axis, which shows that the spindle speed has a relatively big effect on the maximum change of time delay. In Figure 12(d), when the width of cut a_e is set to 1.7, 2.1 or 2.5 mm, with the increase of spindle speed, the maximum change rate of time delay also increases. These three curves are relatively steep, which also shows that the spindle speed has a relatively big effect on the maximum change of time delay. Since these three curves are almost close to each other along the vertical axis excepting the cutting parameter ($\Omega = 5500$ rpm, $a_e = 1.7$ mm), it shows that the width of cut has little effect on the maximum change of time delay within the spindle speed range of 5500 to 5900 rpm.

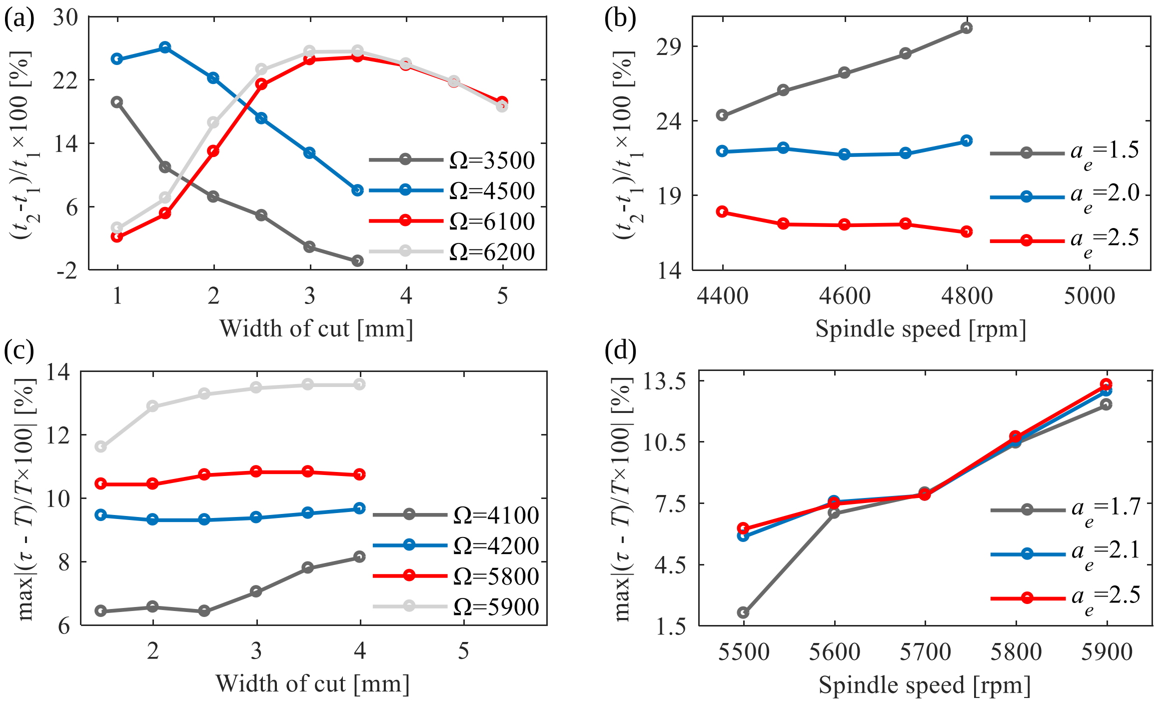

Figure 12. Change rate of cutting time and time delay under different cutting parameters. t_1 and t_2 are the cutting time when the workpiece is regarded as rigid and flexible respectively. τ and T are the time delay and tooth period respectively. (a) The change rate of cutting time at the same spindle speed and different width of cut. (b) The change rate of cutting time at the same width of cut and different spindle speed. (c) The maximum change rate of time delay at the same spindle speed and different width of cut. (d) The maximum change rate of time delay at the same width of cut and different spindle speed.

As has been explained at the beginning of Section 4, to focus more on the effect of state-dependent and time-varying time delays caused by workpiece vibration, the stiffness of the tool in our experiment is designed to be very high. This effectively changes the problem from 3 DOF (three degrees-of-freedom) to 1 DOF (one degree-of-freedom), where only flexibility of the workpiece is in the *Z*-direction. In another words, when state-dependent and time-varying time delays are not considered, vibration in *Z*-direction can be neglected as the system stiffness becomes high resulting that all the cutting parameters in the stability lobe diagram are stable.

Let us examine now the stability lobe diagram corresponding to the following set of cutting parameter represented by points A(6100 rpm, 2.5 mm), B(6100 rpm, 3.5 mm), C(6200 rpm, 2.5 mm), D(6200 rpm, 3.0 mm) E(4100 rpm, 3.3 mm), F(4200 rpm, 3.0 mm), G(4200 rpm, 3.5 mm), as shown in Figure 13(a). And the related experimental results are presented in Section 4.4.

In order to assess a difference between the stability lobe diagrams calculated with the classic approach without considering the state dependent time delay, we superimposed these two lobe diagrams, which is shown in Figure 13(b). The red curve represents the classic lobe diagram with 2 DOF (two degrees-of-freedom), where the dynamics of the tool in *X* and *Y*-directions are considered. The black curve marks the stability borders for our approach having 3 DOF with the state-dependent and time-varying time delay, where the dynamics of the tool in *X* and *Y*-directions and the workpiece in *Z*-direction are considered. Four simulated results, marked as points P1 (4600 rpm, 3.5 mm), P2 (5900 rpm, 1.5 mm), P3 (6300 rpm, 1.6 mm), P4 (7100 rpm, 2.1 mm), were used to probe the computed stability lobe diagrams. In Figure 13(b), P1, P2 and P3 are in the chatter area for 3 DOF model but they are stable according to 2 DOF model. In contrast, P4 is a stable point for 3 DOF model but it exhibits chatter in 2 DOF prediction. The simulated displacement time histories for points P1 to P4 are presented in **Appendix C**.

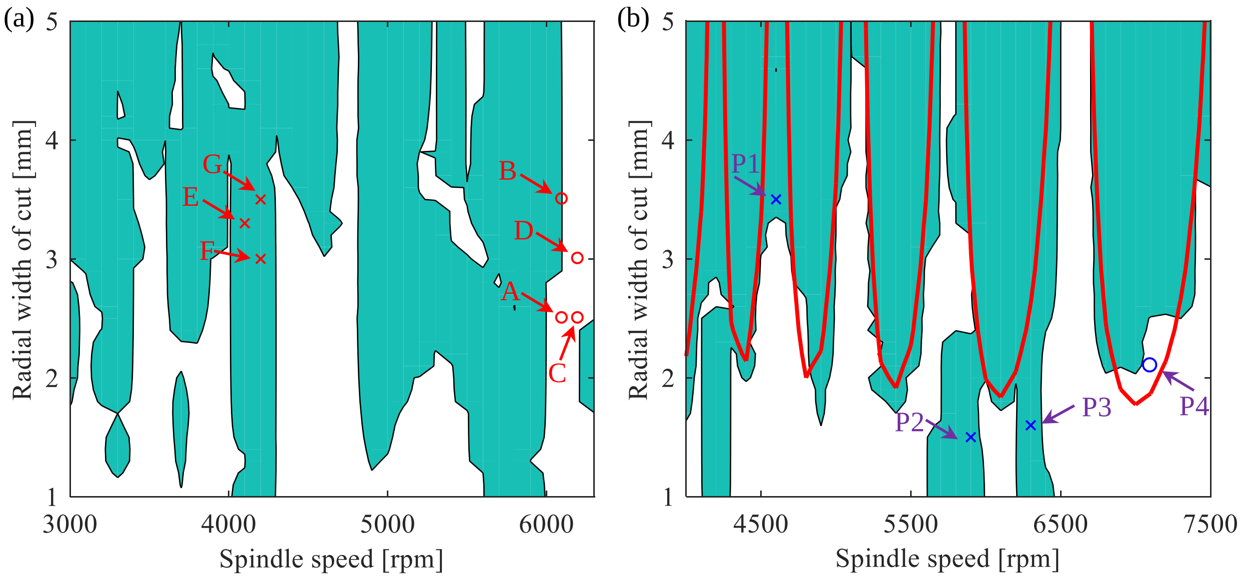

Figure 13. Stability lobe diagrams for three different models and test points obtained for a chosen set of cutting parameters given in brackets; (a) 1 DOF with state-dependent and time-varying time delay marking important points A(6100 rpm, 2.5 mm), B(6100 rpm, 3.5 mm), C(6200 rpm, 2.5 mm), D(6200 rpm, 3.0 mm), E(4100 rpm, 3.3 mm), F(4200 rpm, 3.0 mm) and G(4200 rpm, 3.5 mm); Points E, F, G are period-2 bifurcations; (b) classic 2 DOF (red curves) and the 3 DOF with state-dependent and time-varying time delay (color areas). The blank and color areas mark stable and chatter regions respectively. Four typical points P1 (4600 rpm, 3.5 mm), P2 (5900 rpm, 1.5 mm), P3 (6300 rpm, 1.6 mm), P4 (7100 rpm, 2.1 mm) are also shown.

4.4 Experimental studies

In this work the experiments were conducted to calibrate the developed mathematical model and provide some insight into its validation. The trimming tests are carried out on the five-axis machining center (Mikron UCP800) and the experimental setup is shown in Figure 14. A rotating dynamometer is used to record the dynamic milling force and an accelerometer is attached on the workpiece to measure the vibration acceleration signal. The Keyence laser displacement sensor is used to measure the vibration amplitude of the workpiece.

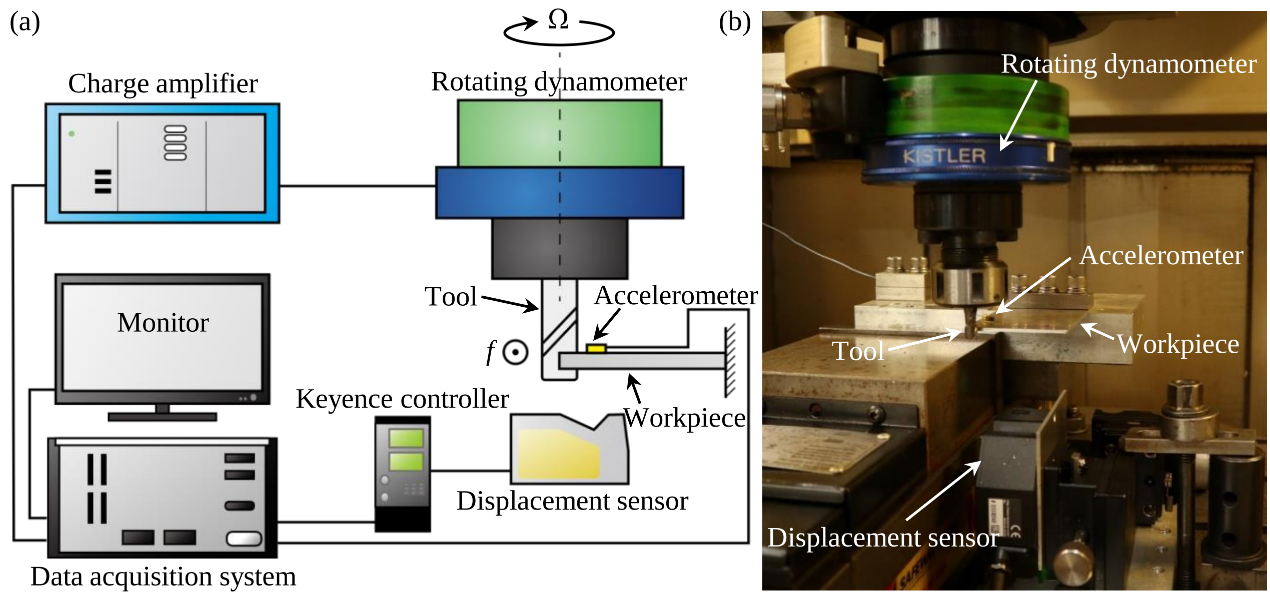

Figure 14. Experimental set-up for investigating the dynamics of trimming thin-walled structures; (a) schematic diagram of experimental set-up; (b) photograph showing sensor locations. A rotating dynamometer is used to record the dynamic milling force of tool. Accelerometer and Keyence laser displacement sensors are used to measure the acceleration and displacement of the workpiece respectively.

For stable trimming ($\Omega = 6100$ rpm, $a_e = 3.0$ mm, we used the same stable parameters as in the simulation), the acceleration of the workpiece vibration as well as the corresponding 1/revolution-sampled points ('•' pitch-label) is plotted in Figure 15(a), and the corresponding FFT spectrum is shown in Figure 15(b). It can be seen that the signal in stable state only has the tooth passing frequency and its harmonics, and the dominant frequencies 915 Hz, 508.4 Hz are 9, 5 multiplication of the tool passing frequency, respectively. A comparison of the measured and simulated displacements is shown in Figure 16, where a good agreement of the main waveforms is evident but there is a space for a better correlation. Specifically, higher harmonics in time histories obtained from simulation and experiment results differ, which may be attributed to identification errors of cutting force coefficients and modal parameters.

The FFT spectra of measured displacement in points A (6100 rpm, 2.5 mm), B (6100 rpm, 3.5 mm), C (6200 rpm, 2.5 mm), D (6200 rpm, 3.0 mm) are shown in Figure 17. Since the frequencies are multiples of the tooth passing frequency, these points are all stable.

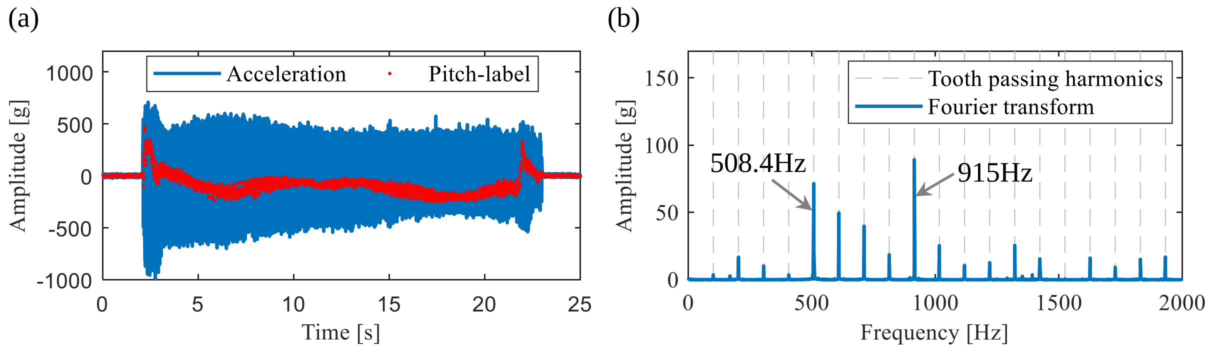

Figure 15. Measured acceleration for $\Omega = 6100$ rpm and $a_e = 3.0$ mm; (a) time histories of the acceleration and the corresponding 1/revolution-sampled points ('•' pitch-label); (b) FFT spectrum of the acceleration signal and the frequencies are integral multiplication of the tooth passing frequency. These results show that the trimming process under this cutting parameters is stable.

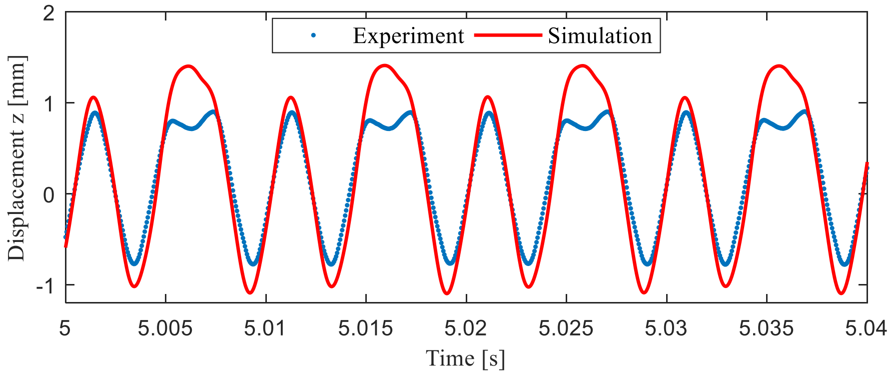

Figure 16. Experimental and simulated workpiece displacement time histories for $\Omega = 6100$ rpm and $a_e = 3.0$ mm. A good agreement is clearly visible for the fundamental waveform with some discrepancies for the higher harmonics. Possible reasons for the difference are potential errors in identification of cutting force coefficients and modal parameters.

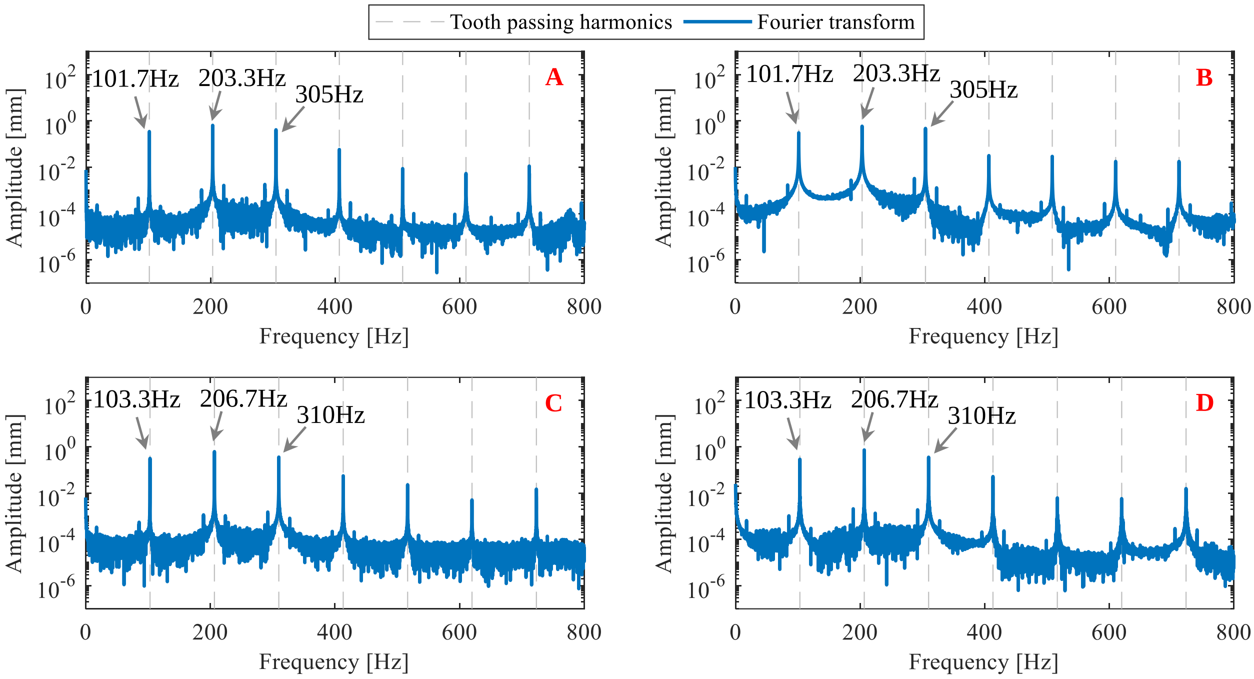

Figure 17. FFT spectra of the measured displacements at different stable points A(6100 rpm, 2.5 mm), B(6100 rpm, 3.5 mm), C(6200 rpm, 2.5 mm), D(6200 rpm, 3.0 mm) in logarithmic scale. These frequencies are multiples of the tooth frequency, indicating that these points are stable.

Taking the cutting parameters $\Omega = 4100$ rpm and $a_e = 3.5$ mm, which is unstable in the simulation, the FFT spectrum of the measured displacement shown in Figure 18(a) indicates that the fundamental frequency 34.17 Hz is a half of the tooth passing frequency 68.33 Hz. The dominant frequencies 205 Hz is 3 multiple of the tool passing frequency, and the frequencies 102.5 Hz and 239.2 Hz are 3 and 7 multiplication, respectively, of the fundamental frequency. The FFT spectrum of the measured acceleration is demonstrated in Figure 18(b), where the dominant frequencies 273.3 Hz is 4 multiplication of the tool passing frequency. The frequencies 102.5 Hz, 307.5 Hz and 512.5 Hz are 3, 9 and 15 multiples, respectively, of the fundamental frequency 34.17 Hz. Due to half of the tooth passing frequency has been discovered in these experimental results, period-2 bifurcation is verified.

The FFT spectra of the measured displacements of points E(4100 rpm, 3.3 mm), F(4200 rpm, 3.0 mm), G(4200 rpm, 3.5 mm) are shown in Figure 19. When $\Omega = 4200$ rpm, the fundamental frequency 35 Hz is a half of the tooth passing frequency 70 Hz, other frequencies are multiplication of 35 Hz.

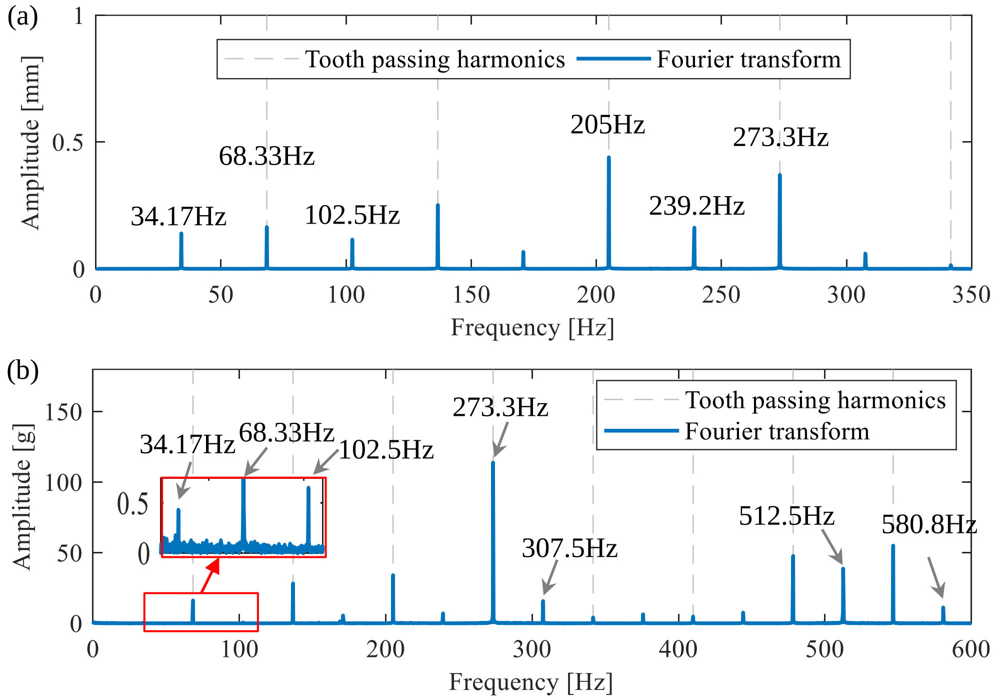

Figure 18. Spectra of workpiece displacement (a) and acceleration (b) for $\Omega = 4100$ rpm and $a_e = 3.5$ mm. The fundamental frequency 34.17 Hz is half of the tooth passing frequency 68.33 Hz and other frequency (such as 102.5 Hz, 239.2 Hz, 307.5 Hz, 512.5 Hz, 580.8 Hz) are integral multiples of the fundamental frequency 34.17 Hz.

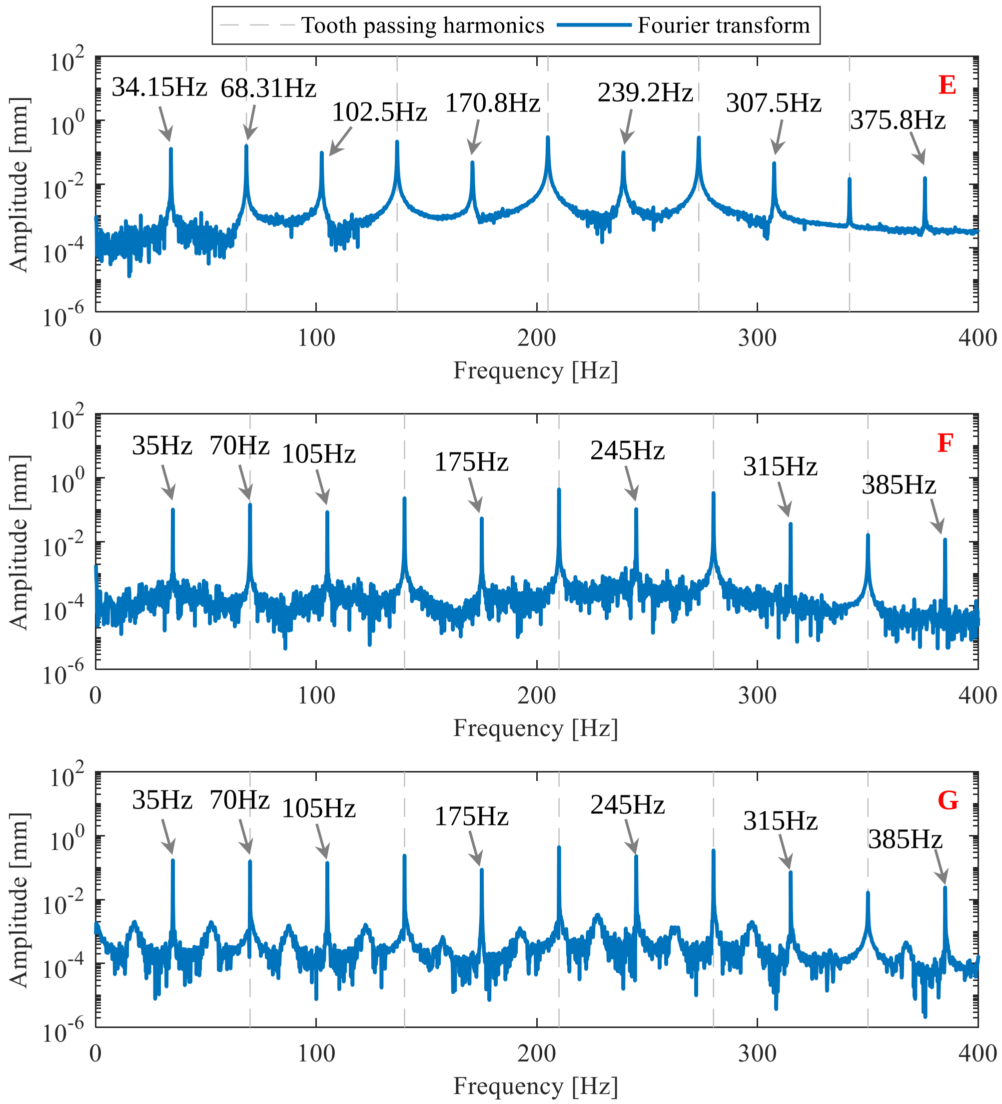

Figure 19. FFT spectra of the measured displacements at different period-2 bifurcation points E(4100 rpm, 3.3 mm), F(4200 rpm, 3.0 mm), G(4200 rpm, 3.5 mm) in logarithmic scale. The fundamental frequency is a half of the tooth passing frequency.

5 Conclusions

This study presents a development of the mathematical model of trimming a thin-walled cantilever workpiece by considering the effect of workpiece vibration along the tool-axis on time delay and instantaneous rotation angle when the helix angle cutters are used. A novel dynamic model accurately describing the dynamics of thin-walled workpiece trimming process is established, where the relay relationship of state-dependent time delay, uncut chip thickness (cutting forces) and dynamic response is clearly figured out. To solve the strongly nonlinear dynamic problem, an iterative method for calculation of the state-dependent time delay and a time-domain numerical algorithm with an improved stability metrics for the prediction of trimming stability are presented.

Simulation results comparing with those of the traditional model show the efficiency of the proposed model. Moreover, the mechanism of period-n instability phenomenon observed in trimming process is fully explained. Both of the simulation and experiment results verified that two states, i.e., period-n instabilities with time-varying time delay and stability states with constant time delay, exist in the thin-walled workpiece trimming process.

Our investigations reveal how the large amplitude vibration of workpiece affects the time delay and stability in the trimming process. The new findings of this study can enhance our understanding of the thin-walled workpiece trimming process. It is expected to help the research community and industry in programming of parameters and even in development of new equipment, such as trimming robot, to improve productivity. For future work, the following questions about thin-walled workpiece trimming may be further explored: high order period-n phenomenon in trimming process by considering the tool runout when multi-tooth milling tool is used; optimization the helix angle of the tool and feed rate, as these factors have a relatively large effect on workpiece vibration amplitude.

CRediT authorship contribution statement

Sen-Lin Ma: Investigation, Methodology, Formal analysis, software, Data Curation, Writing - original draft, Writing - review & editing.

Tao Huang: Investigation, Methodology, Formal analysis, Supervision, Writing - review & editing, Funding acquisition.

Xiao-Ming Zhang: Investigation, Formal analysis, Supervision, Writing - review & editing, Funding acquisition.

Marian Wiercigroch: Investigation, Formal analysis, Writing - review & editing.

Ding Chen: Investigation, Methodology.

Han Ding: Supervision, Project administration, Funding acquisition.

Declaration of Competing Interest

The authors declare that they have no known competing financial interests or personal relationships that could have appeared to influence the work reported in this paper.

Acknowledgments

This work was supported by the National Natural Science Foundation of China (52075205, 92160207, 52090054), National Key R&D Program of China (2020YFA0714900) and Natural Science Foundation of Hubei Province, China (2020CFA077).

Appendixes

A. Algorithm for calculating time delay

Time delay $\tau(t)$ is calculated by an iterative search method and the detailed procedure is shown in Table A1. The input parameters include tooth period T, time node t, time increment Δt, displacement $z_w(t)$, time delay of previous time node $\tau(t-\Delta t)$, tool geometric parameters β D N, and error threshold ε. And the output parameter is Time delay τ. The iterative error τ_{error} and its derivative $d\tau_{error}/d\tau$ is used to judge the iterative direction. Due to the strong nonlinearity of the model, the solution result of the time delay may have multiple solutions. For this, we adopt multiple initial values τ_0 for iterative search, and then compare the obtained results $\tau(t)$ with $\tau(t-\Delta t)$. According to the continuity of the physical process, we select the value closest to $\tau(t-\Delta t)$ as the final value. For the selection of the initial value τ_0, we first set the change range of time delay to be ±20% of the tooth period T ($0.8T \sim 1.2T$), then divide this range into five equal parts, and select the middle four values as the initial values.

Table A1. Algorithm for calculating time delay

Input: tooth period T; time node t; time increment Δt; displacement $z_w(t)$; time delay of previous time node $\tau(t-\Delta t)$; tool geometric parameters β D N; error threshold ε, initial values τ_0.

Output: Time delay τ

Step I:

(0) Set $\tau_{error} = \tau - \left(T + \frac{TN \tan\beta}{\pi D}\left(z_w(t) - z_w(t-\tau)\right)\right)$, $\frac{d\tau_{error}}{d\tau} = 1 + \frac{TN \tan\beta}{\pi D \Delta t}\left(z_w(t-\tau) - z_w(t-\tau+\Delta t)\right)$;

(1) If first tooth period, let $\tau = t$, exit and output τ; Else let $\tau = \tau_0$;

(2) If $t-\tau<0$, let $\tau = t$; Elseif $\tau <= 0$, let $\tau = \Delta t$;

(3) Calculate τ_{error} and $\frac{d\tau_{error}}{d\tau}$, let $\tau_{error0} = \tau_{error}$; If $\tau_{error}\frac{d\tau_{error}}{d\tau} < 0$, let flag = 1; Else let flag = -1;

(4) If $|\tau_{error}| < \varepsilon$ or $\tau_{error0}\tau_{error} <= 0$, exit and output τ;

(5) If flag = = -1, let $\tau = \tau - \Delta t$; Elseif flag = = 1, let $\tau = \tau + \Delta t$;

(6) If $t-\tau<0$, let $\tau = t$; Elseif $\tau <= 0$, let $\tau = \Delta t$;

(7) let $\tau_{error0} = \tau_{error}$ and Calculate τ_{error}, and go to **Step**:4.

Step II:

(0) Set $\Delta\tau = \left|\tau - \tau(t-\Delta t)\right|$;

(1) Calculate $\Delta\tau$ for each iterative search result τ with different initial values τ_0;

(2) Select time delay τ corresponding to the minimum $\Delta\tau$.

B. Flow chart of the algorithm for constructing the stability lobe diagrams

The flow chart of the algorithm for constructing the stability lobe diagram is shown in Figure A1. The input parameters include tool parameters (D, β, N), system modal parameters ($\mathbf{M}$, $\mathbf{C}$, $\mathbf{K}$), cutting force coefficients (K_t, K_{te}, K_r, K_{re}, K_a, K_{ae}) and cutting conditions (Ω, f_t, a_e, h_0, up or down milling). And the output of the algorithm is a stability lobe diagram with different bifurcation types. The procedure of the algorithm is described as follows:

For current given spindle speed and width of cut, time delay, the cutting forces and vibration displacements are calculated by Eq. (9), Eq. (3) and Eq. (1), respectively, in simulation time duration t_{end}. Then, the stability metrics M_n is calculated by Eq. (12) and the stability of the milling process behaviors mapped as stable, period-n bifurcation and Hopf bifurcation. This process needs to be carried out for every spindle speed and width of cut. At the end, the stability lobe diagram is constructed.

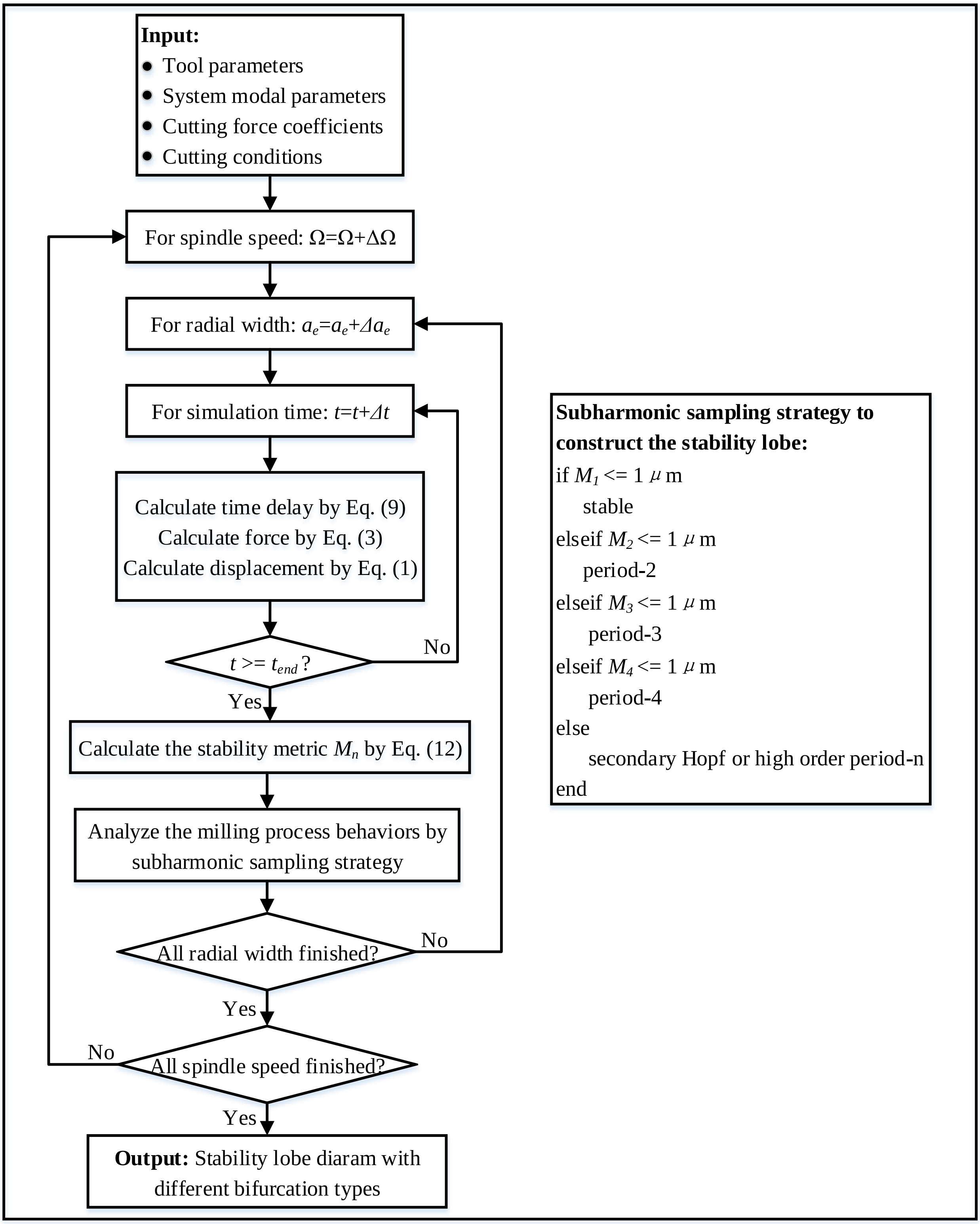

Figure A1. Flow chart of the numerical algorithm to construct the stability lobe diagram. The input parameters include tool parameters, system modal parameters, cutting force coefficients and cutting conditions. And the output result is a stability lobe diagram with different bifurcation types. For given spindle speed and width of cut, we calculate time delay, cutting forces and vibration displacements by Eq. (9), Eq. (3) and Eq. (1), respectively, in the set simulation time duration t_{end} . Then, the stability metrics M_n can be calculated by Eq. (12), and the milling process behaviors can be analyzed by subharmonic sampling strategy.

C. Simulation parameters of stability lobe diagram (Figure 13(b)) and corresponding simulated vibration displacement time histories for P1 to P4

The simulation parameters of the stability lobe diagram shown in Figure 13(b) are assigned as follows: A single tooth ($N=1$) tool with diameter $D=8$ mm, helix angle $\beta=45^{\circ}$ is used. The thickness of the plate is 2 mm which is equal to the cutting depth. The modal parameters of the tool and workpiece are listed in Table A2 and the cutting coefficients parameters are listed in Table A3. Up milling with feed per tooth $f_t=0.03$ mm. The range of spindle speed is 4000 to 7500 rpm with the step of 100 rpm and radial width is 1.0 to 5.0 mm with the step of 0.1mm.

Table A2. Modal parameters of the milling system.

Mode	Frequency (Hz)	Mass (kg)	Damping ratio (%)	Stiffness (N/m)
Workpiece (Z)	243.12	0.0084	0.8720	1.9707×10^{4}
Tool (X)	768.90	0.6859	0.6823	1.6009×10^{7}
Tool (Y)	775.33	0.6526	0.9137	1.5576×10^{7}

Table A3. Cutting coefficients parameters.

K_t (MPa)	K_r (MPa)	K_a (MPa)	K_{te} (N/mm)	K_{re} (N/mm)	K_{ae} (N/mm)
1128	395	195	26.3	39.1	4.3

The simulated displacement time histories of four typical points P1 (4600 rpm, 3.5 mm), P2 (5900 rpm, 1.5 mm), P3 (6300 rpm, 1.6 mm), P4 (7100 rpm, 2.1 mm) of Figure 13(b) are shown in Figure A2 to Figure A5, respectively. P1, P2 and P3 are chatter points in 3 DOF, but stable points in 2 DOF, P4 is a stable point in 3 DOF, but chatter point in 2 DOF.

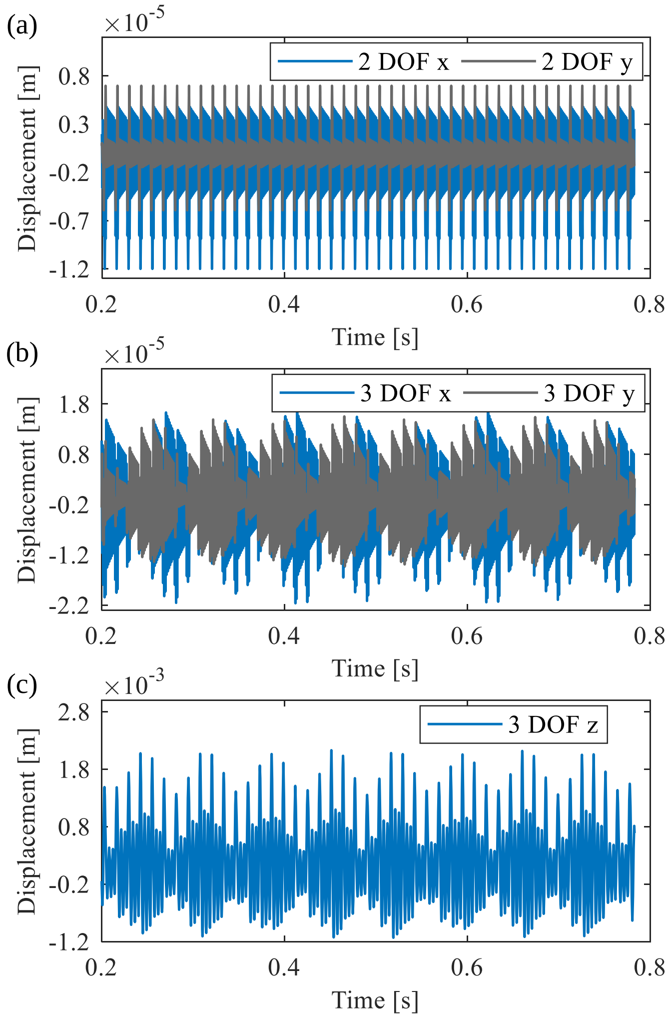

Figure A2. Simulated displacement time histories for P1 (4600 rpm, 3.5 mm), which is a stable point in 2 DOF, but chatter point in 3 DOF.

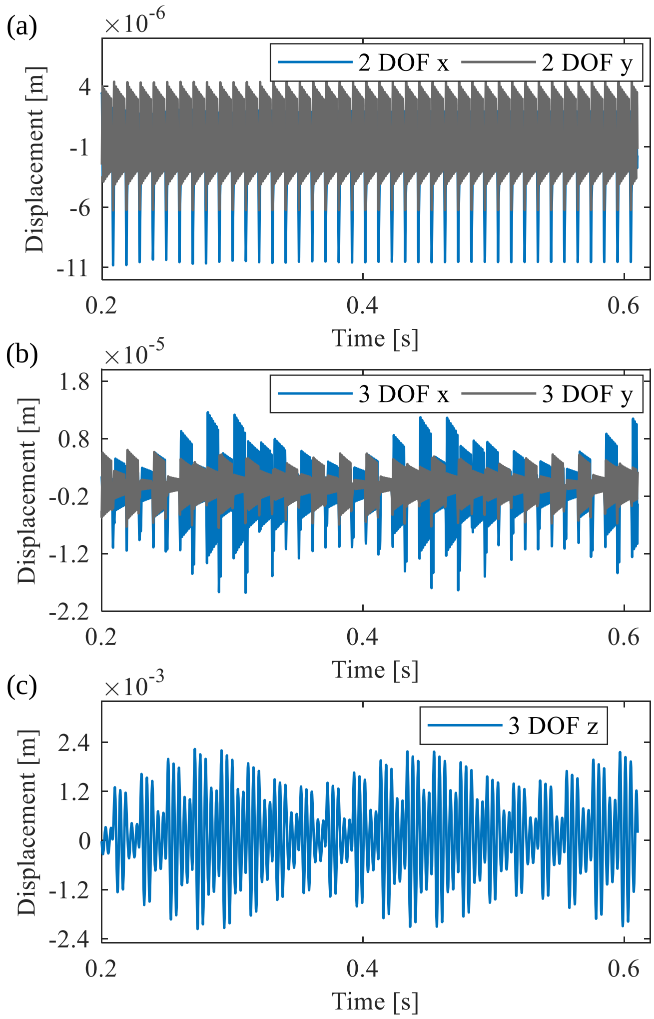

Figure A3. Simulated displacement time histories for P2 (5900 rpm, 1.5 mm), which is a stable point in 2 DOF, but chatter point in 3 DOF.

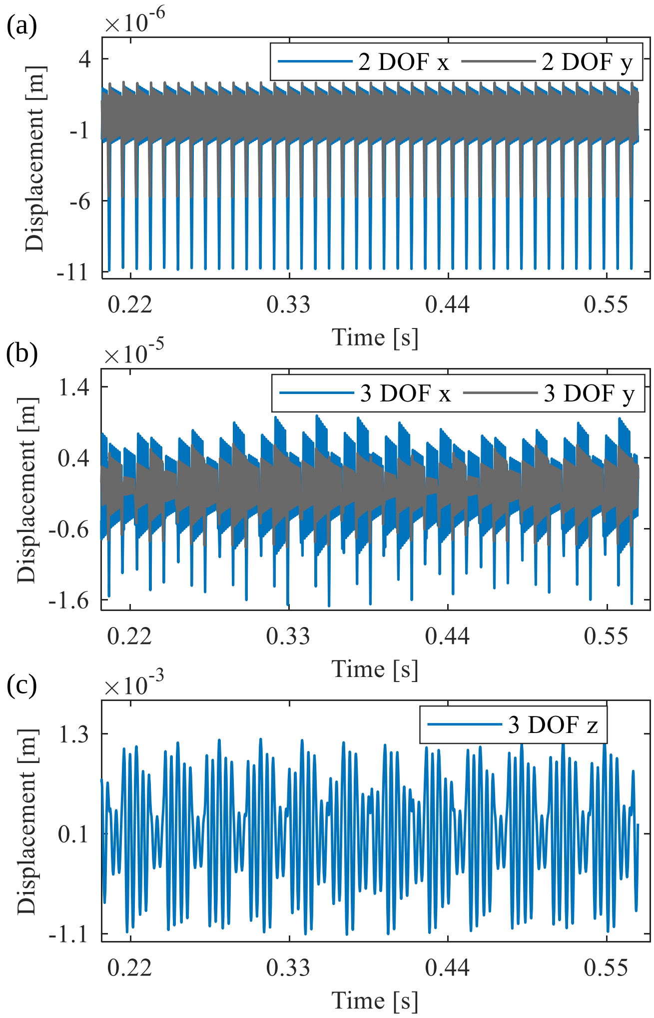

Figure A4. Simulated displacement time histories for P3 (6300 rpm, 1.6 mm), which is a stable point in 2 DOF, but chatter point in 3 DOF.

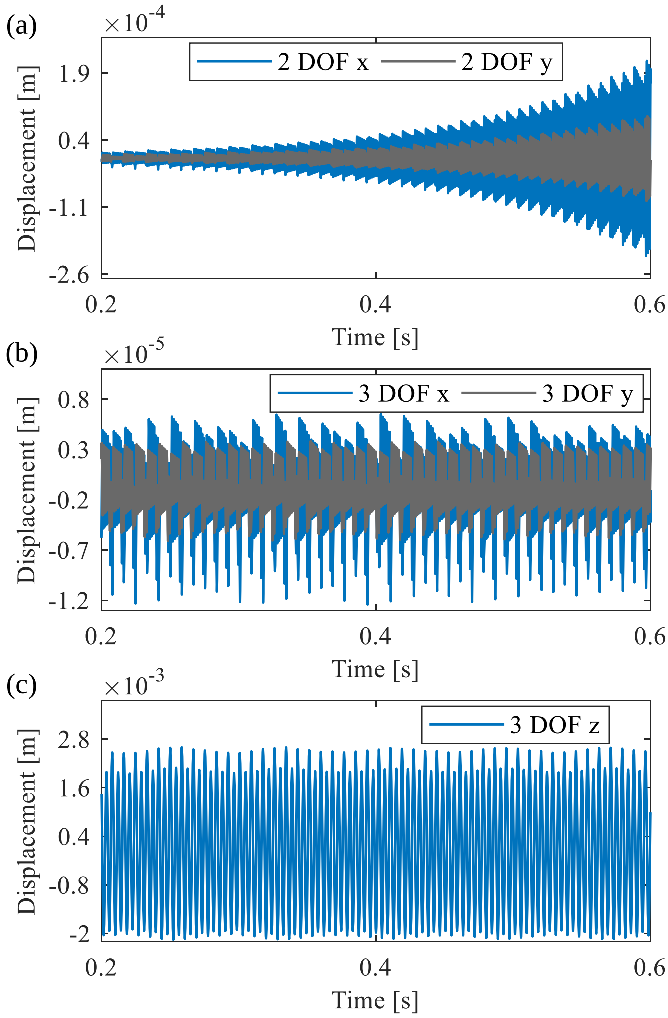

Figure A5. Simulated displacement time histories for P4 (7100 rpm, 2.1 mm), which is a chatter point in 2 DOF, but stable point in 3 DOF.

References

[1] M. Wan, X. Liang, Y. Yang, W. Zhang, Suppressing vibrations in milling-trimming process of the plate-like workpiece by optimizing the location of vibration absorber, Journal of Materials Processing Technology 278 (2020) 116499.

[2] G. Liu, J. Dang, W. Ming, Q. An, M. Chen, H. Li, High-quality machining of edges of thin-walled plates by tilt side milling based on an analytical force-based model, Journal of Manufacturing Science and Engineering 141 (2019) 61008.

[3] G. Liu, J. Dang, C. Li, W. Ming, Q. An, M. Chen, Investigation on the vibration and machined surface quality in tilt side milling of thin-walled plates, The International Journal of Advanced Manufacturing Technology 103 (2019) 2287-2300.

[4] J. Qiu, R. Ge, An improved stability lobe and turning chatter characteristic investigation, International Journal of Mechanical Sciences 149 (2018) 338-348.

[5] Y. Liu, Z. Liu, Q. Song, B. Wang, Development of constrained layer damping toolholder to improve chatter stability in end milling, International Journal of Mechanical Sciences 117 (2016) 299-308.

[6] Z. Fu, X. Zhang, X. Wang, W. Yang, Analytical modeling of chatter vibration in orthogonal cutting using a predictive force model, International Journal of Mechanical Sciences 88 (2014) 145-153.

[7] M. Wiercigroch, E. Budak, Sources of nonlinearities, chatter generation and suppression in metal cutting, Philosophical Transactions of the Royal Society of London. Series A: Mathematical, Physical and Engineering Sciences 359 (2001) 663-693.

[8] Y. Yan, J. Xu, M. Wiercigroch, Regenerative chatter in a plunge grinding process with workpiece imbalance, The International Journal of Advanced Manufacturing Technology 89 (2017) 2845-2862.

[9] Y. Yan, J. Xu, M. Wiercigroch, Regenerative and frictional chatter in plunge grinding, Nonlinear Dynamics 86 (2016) 283-307.

[10] S.D. Merdol, Y. Altintas, Multi frequency solution of chatter stability for low immersion milling, Journal of Manufacturing Science and Engineering 126 (2004) 459-466.

[11] Y. Altintas, E. Budak, Analytical prediction of stability lobes in milling, CIRP annals 44 (1995) 357-362.

[12] L. Cao, X.M. Zhang, T. Huang, H. Ding, Derived nodes approach for improving accuracy of machining stability prediction, Journal of Vibration and Acoustics 140 (2018) 31017.

[13] T. Huang, X.M. Zhang, H. Ding, A novel approach with smallest transition matrix for milling stability prediction, Nonlinear Dynamics 90 (2017) 95-104.

[14] T. Huang, X.M. Zhang, X.J. Zhang, H. Ding, An efficient linear approximation of acceleration method for milling stability prediction, International Journal of Machine Tools and Manufacture 74 (2013) 56-64.

[15] Y. Ding, L. Zhu, X. Zhang, H. Ding, A full-discretization method for prediction of milling stability, International Journal of Machine Tools and Manufacture 50 (2010) 502-509.

[16] J. Niu, Y. Ding, L. Zhu, H. Ding, Runge－Kutta methods for a semi-analytical prediction of milling stability, Nonlinear Dynamics 76 (2014) 289-304.

[17] W. Li, L. Wang, G. Yu, An accurate and fast milling stability prediction approach based on the Newton-Cotes rules,

International Journal of Mechanical Sciences 177 (2020) 105469.
[18] N.D. Sims, The self-excitation damping ratio: a chatter criterion for time-domain milling simulations, Journal of Manufacturing Science and Engineering 127 (2005) 433-445.
[19] A. Honeycutt, T.L. Schmitz, A new metrics for automated stability identification in time domain milling simulation, Journal of Manufacturing Science and Engineering 138 (2016) 74501.
[20] A. Honeycutt, T.L. Schmitz, Milling stability interrogation by subharmonic sampling, Journal of Manufacturing Science and Engineering 139 (2017) 41009.
[21] S. Smith, J. Tlusty, Efficient simulation programs for chatter in milling, CIRP Annals Manufacturing Technology 42 (1993) 463-466.
[22] H.Z. Li, X.P. Li, X.Q. Chen, A novel chatter stability criterion for the modelling and simulation of the dynamic milling process in the time domain, The International Journal of Advanced Manufacturing Technology 22 (2003) 619-625.
[23] M.L. Campomanes, Y. Altintas, An improved time domain simulation for dynamic milling at small radial immersions, Journal of Manufacturing Science and Engineering 125 (2003) 416-422.
[24] L. Zhongqun, L. Qiang, Solution and analysis of chatter stability for end milling in the time-domain, Chinese Journal of Aeronautics 21 (2008) 169-178.
[25] Y. Yan, J. Xu, M. Wiercigroch, Estimation and improvement of cutting safety, Nonlinear Dynamics 98 (2019) 2975-2988.
[26] Y. Yan, M. Wiercigroch, Dynamics of rotary drilling with non-uniformly distributed blades, International Journal of Mechanical Sciences 160 (2019) 270-281.
[27] Y. Yan, J. Xu, M. Wiercigroch, Modelling of regenerative and frictional cutting dynamics, International Journal of Mechanical Sciences 156 (2019) 86-93.
[28] Z. Zhang, H. Li, X. Liu, W. Zhang, G. Meng, Chatter mitigation for the milling of thin-walled workpiece, International Journal of Mechanical Sciences 138-139 (2018) 262-271.
[29] D. Wang, M. Löser, S. Ihlenfeldt, X. Wang, Z. Liu, Milling stability analysis with considering process damping and mode shapes of in-process thin-walled workpiece, International Journal of Mechanical Sciences 159 (2019) 382-397.
[30] X. Dang, M. Wan, W. Zhang, Y. Yang, Chatter analysis and mitigation of milling of the pocket-shaped thin-walled workpieces with viscous fluid, International Journal of Mechanical Sciences 194 (2021) 106214.
[31] A.R. Yusoff, N.D. Sims, Optimisation of variable helix tool geometry for regenerative chatter mitigation, International Journal of Machine Tools and Manufacture 51 (2011) 133-141.
[32] Z. Dombovari, G. Stepan, The effect of helix angle variation on milling stability, Journal of Manufacturing Science and Engineering 134 (2012) 51015.
[33] X. Zhang, J. Zhang, B. Pang, D. Wu, X. Zheng, W. Zhao, An efficient approach for milling dynamics modeling and analysis with varying time delay and cutter runout effect, The International Journal of Advanced Manufacturing Technology 87 (2016) 3373-3388.
[34] J. Niu, Y. Ding, L. Zhu, H. Ding, Mechanics and multi-regenerative stability of variable pitch and variable helix milling tools considering runout, International Journal of Machine Tools and Manufacture 123 (2017) 129-145.

[35] D. Zhan, S. Jiang, J. Niu, Y. Sun, Dynamics modeling and stability analysis of five-axis ball-end milling system with variable pitch tools, International Journal of Mechanical Sciences 182 (2020) 105774.

[36] N.D. Farahani, Y. Altintas, Chatter stability of serrated milling tools in frequency domain, Journal of Manufacturing Science and Engineering 144 (2021) 31013.

[37] P. Bari, Z.M. Kilic, M. Law, P. Wahi, Rapid stability analysis of serrated end mills using graphical-frequency domain methods, International Journal of Machine Tools and Manufacture 171 (2021) 103805.

[38] F. Tehranizadeh, K. Rahimzadeh Berenji, E. Budak, Dynamics and chatter stability of crest-cut end mills, International Journal of Machine Tools and Manufacture 171 (2021) 103813.

[39] X. Tang, F. Peng, R. Yan, Z. Zhu, Z. Li, S. Xin, Nonlinear process damping identification using finite amplitude stability and the influence analysis on five-axis milling stability, International Journal of Mechanical Sciences 190 (2021) 106008.

[40] Z. Li, O. Tuysuz, L. Zhu, Y. Altintas, Surface form error prediction in five-axis flank milling of thin-walled parts, International Journal of Machine Tools and Manufacture 128 (2018) 21-32.

[41] Y. Sun, S. Jiang, Predictive modeling of chatter stability considering force-induced deformation effect in milling thin-walled parts, International Journal of Machine Tools and Manufacture 135 (2018) 38-52.

[42] G. Totis, T. Insperger, M. Sortino, G. Stépán, Symmetry breaking in milling dynamics, International Journal of Machine Tools and Manufacture 139 (2019) 37-59.

[43] J. Niu, J. Jia, R. Wang, J. Xu, Y. Sun, D. Guo, State dependent regenerative stability and surface location error in peripheral milling of thin-walled parts, International Journal of Mechanical Sciences 196 (2021) 106294.

[44] Q. Song, X. Ai, J. Zhao, Design for variable pitch end mills with high milling stability, The International Journal of Advanced Manufacturing Technology 55 (2011) 891-903.

[45] V. Sellmeier, B. Denkena, Stable islands in the stability chart of milling processes due to unequal tooth pitch, International Journal of Machine Tools and Manufacture 51 (2011) 152-164.

[46] M. Wan, W. Zhang, J. Dang, Y. Yang, A unified stability prediction method for milling process with multiple delays, International Journal of Machine Tools and Manufacture 50 (2010) 29-41.

[47] A. Comak, E. Budak, Modeling dynamics and stability of variable pitch and helix milling tools for development of a design method to maximize chatter stability, Precision Engineering 47 (2017) 459-468.

[48] T. Hayasaka, A. Ito, E. Shamoto, Generalized design method of highly-varied-helix end mills for suppression of regenerative chatter in peripheral milling, Precision Engineering 48 (2017) 45-59.

[49] A. Otto, S. Rauh, S. Ihlenfeldt, G. Radons, Stability of milling with non-uniform pitch and variable helix Tools, The International Journal of Advanced Manufacturing Technology 89 (2017) 2613-2625.

[50] S. Jiang, D. Zhan, Y. Liu, Y. Sun, J. Xu, Modeling of variable-pitch/helix milling system considering axially varying dynamics with cutter runout offset and tilt effects, MECHANICAL SYSTEMS AND SIGNAL PROCESSING 168 (2022) 108674.

[51] S. Seguy, T. Insperger, L. Arnaud, G. Dessein, G. Peigné, On the stability of high-speed milling with spindle speed variation, The International Journal of Advanced Manufacturing Technology 48 (2010) 883-895.

[52] S. Sastry, S.G. Kapoor, R.E. DeVor, Floquet theory based approach for stability analysis of the variable speed face-

milling process, Journal of Manufacturing Science and Engineering 124 (2002) 10-17.

[53] E. Al-Regib, J. Ni, S. Lee, Programming spindle speed variation for machine tool chatter suppression, International Journal of Machine Tools and Manufacture 43 (2003) 1229-1240.

[54] A. Yilmaz, R.E. AL, J. Ni, Machine tool chatter suppression by multi-level random spindle speed variation, Journal of Manufacturing Science and Engineering 124 (2002) 208-216.

[55] M. Zatarain, I. Bediaga, J. Muñoa, R. Lizarralde, Stability of milling processes with continuous spindle speed variation: Analysis in the frequency and time domains, and experimental correlation, CIRP Annals 57 (2008) 379-384.

[56] S. Sébastien, D. Gilles, A. Lionel, I. Tamás, Control of chatter by spindle speed variation in high-speed milling, Advanced Materials Research 112 (2010) 179-186.

[57] G. Jin, H. Qi, Z. Li, J. Han, Dynamic modeling and stability analysis for the combined milling system with variable pitch cutter and spindle speed variation, Communications in Nonlinear Science and Numerical Simulation 63 (2018) 38-56.

[58] C. Wang, X. Zhang, R. Yan, X. Chen, H. Cao, Multi harmonic spindle speed variation for milling chatter suppression and parameters optimization, Precision Engineering 55 (2019) 268-274.

[59] X.H. Long, B. Balachandran, B.P. Mann, Dynamics of milling processes with variable time delays, Nonlinear Dynamics 47 (2006) 49-63.

[60] B. Pritam, L. Mohit, W. Pankaj, Improved chip thickness model for serrated end milling, CIRP Journal of Manufacturing Science and Technology 25 (2019) 36-49.

[61] A. Comak, Y. Altintas, Dynamics and stability of turn-milling operations with varying time delay in discrete time domain, Journal of Manufacturing Science and Engineering 140 (2018) 101013.

[62] T. Insperger, G. Stepan, F. Hartung, J. Turi, State dependent regenerative delay in milling processes., Long Beach, California USA, 2005, pp. 5138-5147.

[63] D. Bachrathy, G. Stépán, J. Turi, State dependent regenerative effect in milling processes, Journal of Computational and Nonlinear Dynamics 6 (2011) 41002.

[64] H.Z. Li, W.B. Zhang, X.P. Li, Modelling of cutting forces in helical end milling using a predictive machining theory, International Journal of Mechanical Sciences 43 (2001) 1711-1730.

[65] H. Li, X. Li, Modelling and simulation of chatter in milling using a predictive force model, International Journal of Machine Tools and Manufacture 40 (2000) 2047-2071.

[66] M.Y. Tsai, S.Y. Chang, J.P. Hung, C.C. Wang, Investigation of milling cutting forces and cutting coefficient for aluminum 6060-T6, Computers and Electrical Engineering 51 (2016) 320-330.